Characterisation of a C elegans strain presenting with a mitochondrial contact site and cristae organizing system (MICOS) subunit deficiency

DK Sejo

orcid.org/0000-0002-1654-5844

Dissertation accepted in partial fulfilment of the requirements for the degree *Master of Science in Biochemistry* at the North-West University

Supervisor: Dr M Pretorius

Assistant Supervisor: Dr A Jordaan

Graduation December 2022

24251984

Ke tsaya chono e go leboga kemonokeng ya losika segolo bogolo bomme ba: **Neo** le **Ruth** ka tshusumetso e kgolo e lo nnileng le yone mo go ageng monna yo o ke leng ene gompieno. Go malome **Reuben** ke lebogela tsela ya thuto e o mpontshiteng yone ke sa le yo monnye.

Tzanzo le **Kagoentle** ke lebogela gonna gwa lona mo botshelo jwa me, this is dedicated to you both.

Ke tseye le chono e go leboga rre yo ntsetseng **Tlhokomelang** le barolong borra **Sejo** ba ba tshelang le botlhe ba ba ithobaletseng bo Mojanaga o mmatau o nthua o thibela, o kgopo e Masepa. Namane tsa tholo tse dijang mogope di o lala, kgaratlha mmeko moholo dijelang motho sebakeng. Tholo e dinaka di maripa setlhatlhoga dithota le dithotana. Ke leboga le baTswening borra **Ratuludi** ba ba tshelang le ba ba ithobaletseng, baTswening bo ke naiwa mmeleng ma-kopong ga ke naiwe, baTswening bo rammopa le kgomo ba bopa le modisa wa tsone, magadimana ntweng ba ereng baja ba sa gadime.

Kwa bofelong ke leboga ditsala tsame **Tshepo** le **Mosala** ka kemonokeng e e tsepameng.

ACKNOWLEDGEMENTS

I would like to express my gratitude to the following people and institutions for the significant contribution towards the success of this project.

My supervisor **Dr Marianne Pretorius** for her guidance, patience, and support throughout the course of this study. I am grateful for the level of professionalism and compassionate understanding when I was struggling with some of the work, most importantly your valuable inputs that contributed significantly to the completion of this project.

Prof Francois Van der Westhuizen for his assistance in acquiring import permits for the nematodes, genotyping training, and his overall involvement in the *C. elegans* group.

My assistant supervisor **Dr Anine Jordaan** for her assistance with transmission electron microscopy sample preparations and image acquisition.

Dr Gerhard du Preez for his assistance in setting up the *C. elegans* laboratory as well as his desire to always help when needed.

Prof Zander Lindeque for his guidance, time and valuable input throughout the metabolomics part of this study.

The NWU Postgraduate bursary for financial contribution towards this study.

I would also like to thank my colleagues in the mitochondrial laboratory for their assistance and support, with special gratitude to **Belinda Fouche** for her help with Oroboros experiments.

ABSTRACT

Mitochondrial architecture varies remarkably from one tissue to another, and aberrations in mitochondrial architecture are associated with several dysfunctions. This indicates that mitochondrial function and architecture are intertwined. Existing literature has contributed significantly to our current understanding of the role mitochondria play in ATP production, and apoptosis. However, our understanding of how mitochondria attain their definite shape to perform their routine functions is less clear. The inner mitochondrial morphology is characterized by cristae which undergo membrane bending at cristae junctions. The cristae can be lamellar, tubular, or triangular in astrocytes. Moreover, cristae structure is associated directly with mitochondrial function. High energy-demanding tissues such as neurons and skeletal muscles show mainly lamellar cristae, suggesting a large planer membrane area is essential to accommodate the respiratory chain complexes. While the mitochondrial contact site and cristae organizing system (MICOS) plays a critical role in the formation of cristae, the mechanism of cristae formation is a sophisticated process that has not yet been fully elucidated.

The aim of this study was to characterize a *Caenorhabditis elegans* (*C. elegans*) strain presenting with a MICOS subunit (Mic27) deficiency. The mutant *C. elegans* strain (VC1196) harbours a mutation in *moma-1* gene which is an ortholog of mammalian *APOOL*. Existing literature suggests that coordination of the MICOS complex with respiratory complexes and lipids establishes the inner membrane architecture as an assembly of Mic27 and Mic10 is highly dependent on mitochondrial lipid cardiolipin and respiratory complexes. Thus, the results obtained in this study support the initially stated hypothesis as the VC1196 knockout deficient in the MICOS subunit showed aberrant cristae morphology, decreased mitochondrial oxidative phosphorylation (OXPHOS) enzyme activity and, respiration as well as poor scores in phenotypic assays. The pronounced disease phenotype in the VC1196 strain re-ported in this study illustrated its usefulness as a mitochondrial disease model for future studies in this field.

Key words: C. elegans, Lipidomics, MICOS, Mitochondrial mutations, OXPHOS, ROS.

Contents

List of figures

List of tables

List of equations

List of symbols, units, and abbreviations

	Symbols
~	Approximately
A	Alpha
B	Beta
Δ	Delta
Δp	Proton motive force
ΔpH	Proton gradient
	Units
%	Percentage
°C	Degrees Celsius
µg	Microgram
µl	Microliter
µm	Micrometre
µM	Micromolar
pb	Base pairs
Da	Dalton
kDa	Kilodalton
L	Litre
M	Metre
M	Molar
m/z	Mass to charge ratio
mg	Miligram
min	Minute
ml	Millilitre
mm	Millimetre
ng	Nanogram
nmol	Nanomole
pH	Potential of hydrogen
ppm	Parts per million
v/v	Volume of solute per volume of solvent

xg	Relative configural force

Abbreviations

Aa

A	Adenine
AA	Amino acids
ACN	Acetonitrile
ADP	Adenosine-5’-diphosphate
ATP	Adenosine-5’-triphosphate

Bb

BCA	Bicinchoninic acid
BSA	Bovine serum albumin
BSTFA	N, O-bis(trimethylsilyl)trifluoroacetamide

Cc

C	Cytosine
Ca2+	Calcium ion
CaCl2	Calcium chloride
Cat.no	Catalogue number
C.elegans	Caenorhabditis elegans
CGC	Caenorhabditis genetic centre
CI	Chemotaxis index
CI	Complex I (NADH: ubiquinone oxidoreductase)
CII	Complex II (succinate: ubiquinone oxidoreductase)
CIII	Complex III (ubiquinol: cytochrome c oxidoreductase)
CIV	Complex IV (cytochrome c oxidase)
CJs	Cristae junctions
CO2	Carbon dioxide
CoA	Coenzyme A
CuSO4.5H2O	Copper (II) sulphate pentahydrate
CV	Complex V (ATP synthase) or coefficient of variance (depending on the context)
Cyt c	Cytochrome c

Dd

DAFF	Department of agriculture and fisheries
DICP	2,6-Dichloroindophenol sodium salt hydrate
DMSO	Dimethyl sulfoxide
DNA	Deoxyribonucleic acid
ds	Double stranded
DTNB	5,5' Dithio-bis[-2-nitobenzoic acid)

Ee

E. coli	*Escherichi a coli*
EDTA	Ethylenediaminetetraacetic acid
EMS	Ethyl methane sulfonate
ER	Endoplasmic reticulum

et al	*et alli (*Latin) and others
EtBr	Ethidium bromide
ETC	Electron transport chain
	Ff
FA	Fatty acids
$FADH_2$	Flavin adenine dinucleotide
FUDR	5-fluoro-2-deoxyuridine
	Gg
GC-TOF/MS	Gas chromatography time of flight mass spectrometry
G	Guanine
GFP	Green flourecent protein
GTPase	Guanosine triphosphatase
	Hh
H	Hydrogen
H	Hour(s)
HCL	Hydrogen chloride
H_2O	Water
H_2O_2	Hydrogen peroxide
CH_3	Methyl group
HSP	Heat shock proteins
	Ii
IMM	Inner mitochondrial membrane
IMS	Inner mitochondrial space
IS	Internal standard
	Kk
K_2HPO_4	di-potassium hydrogen phosphate
KH_2PO_4	Potassium phosphate monobasic
	Ll
LB	Luria broth
L	Litre
LDH	Lactate dehydrogenase
LS	Leigh syndrome
	Mm
mg	Miligram
MgCl2	Magnesium chloride
Min	Minutes
mL	Millilitre
mm	Millimetre
mM	Millimolar
MRC	Mitochondrial respiratory chain
mRNA	messenger ribose nucleic acid
	Nn
NaCl	Sodiun chloride

NADH	Nicotinamide adenine nucleotide
NaN3	Sodiun azide
NaOCL	Sodiun hypochloride
	Oo
OAA	Oxaloacetate
OCR	Oxygen consumption rate
OMM	Outer mitochondrial membrane
OXPHOS	Oxidative phosphorylation
	Pp
PCR	Polymerase chain reaction
pH	Potential of hydrogen
PO	Propylene oxide
pmol	Picomole
P-value	Significant value
	Qq
QH-	Ubiquinol; reduced coenzyme Q
qPCR	Quantitative PCR
	Rr
RC	Respiratory chain
Redox	Reduction-oxidation
RNA	Ribose nucleic acid
ROS	Reactive oxygen species
rpm	Revolution per minute
	Ss
SD	Standard deviation
SOP	Standard operating procedure
	Tt
TCA	Tricarboxylic acid cycle
Tm	Melting temperature
	UV
UV	Ultraviolet
	Vv
V	Volts
	Ww
WT	Wild type

1. CHAPTER ONE

Chapter summary

This chapter gives an overview of the dissertation. Introduction to the inner and outer structure of the mitochondria is given as well as the linkage with the MICOS complex.

1.1. Introduction

Mitochondria are highly specialized organelles present in almost all eukaryotic cells (Roger *et al*., 2017). These dynamic organelles possess a sophisticated and distinctive architecture that is characterized by the inner mitochondrial membrane (IMM) and outer mitochondrial membrane (OMM) (Khosvari *et al.*, 2020). In addition, the former is further compartmentalized into two regions: the (1) inner boundary membrane (IBM) and (2) inner cristae membrane (ICM). Mitochondria are involved in synthesis of haem, steroids, amino acids (AA), phospholipids and iron sulphur clusters (Hamza *et al*., 2012). In higher eukaryotes, mitochondria play a pivotal role in calcium signalling and apoptosis (Hajnóczky *et al.*, 2003). In order to perform these functions, the mitochondria must establish and maintain the ultrastructure that determines the function of these organelles (Cserép *et al*., 2018). The IBM of normal mitochondria is characterized by fenestrated laminar and tubular cristae with cristae junctions creating pores, intercristae, and intermembrane spaces (Huynen *et al.*, 2016). Contrary to this, aberrant mitochondria are characterized by cristae membranes which are organized in concentric circles resembling an onion-like structure (Bornhövd *et al*., 2006).

Hoppins *et al.* (2011) proposed that formation of the filamentous structure within the IMM of budding *Saccharomyces cerevisiae* mitochondria is facilitated by the MICOS complex. A recent study revealed that a core subunit (Mic60) physically interacts with various IM and OM proteins thereby establishing a contact site (Stoldt *et al*., 2019). Moreover, this study also showed that MICOS subunits of both human and yeast form intricately arranged clusters within the IMM, frequently confined in opposing distribution bands that can adopt a helical order. The sub-complex containing Mic10 plays a crucial role in stabilizing cristae junctions and has membrane-bending attributes which shape cristae junctions (Callegari *et al.*, 2019). This is indicative that the MICOS complex is crucial for IM morphogenesis.

In addition to the above, previous studies also link Optic Atrophy 1 (OPA1) (Yamaguchi *et al*., 2008) and F_1F_0-ATP synthase (Davies *et al*., 2012) as other crucial factors for mitochondrial cristae ultrastructure. The OPA1 localizes in the IM where it regulates mitochondrial cristae structure and

fusion (Yamaguchi *et al*., 2008; Cogliati *et al.*, 2013). Furthermore, OPA1 exists as a virtually stoichiometric mix of soluble intermembrane space (IMS) localized short (S-OPA1) and IM-anchored long (L-OPA1) forms (Ishihara *et al.*, 2006).

The MICOS complex is at the centre of mitochondrial morphology management as it plays a pivotal role in the formation, maintenance and stabilization of mitochondrial cristae (Eramo *et al*., 2019). This protein complex consists of at least seven subunits in mammalian cells: Mic10, Mic13, Mic19, Mic25, Mic26, Mic27 and Mic60 (Ott *et al*., 2015; Huynen *et al*., 2016). Many of these subunits have orthologs in *C. elegans* and other eukaryotes (reviewed in Munoz-Gomez *et al*., 2015). The MICOS strain under investigation (VC1196) harbours a mutation in *moma-1* gene, an ortholog of *APOOL* which encodes Mic27 and has a Mic27 deficiency. Mic27 and Mic26 are cooperatively required for the integrity of F_1F_0-ATP synthase and integration of F_1 into the monomeric F_1F_0-ATP synthase (Weber *et al.*, 2013). The nematodes, *C. elegans* contains many genes that have functional counterparts in humans which makes it an extremely useful model for human diseases (The *C. elegans* sequencing consortium 1998). The primary aim of this study was to characterise a *C. elegans* strain presenting with a MICOS subunit deficiency (Mic27). In addition, the study further consisted of five objaectives which included (1) genotyping using PCR, (2) detection of mitochondrial ultrastructure using transmission electron microscopy (TEM), (3) measuring oxygen consumption rate (ORC) in intact nematodes using Oroboros instrument, (4) measuring enzyme activity using crude nematode mitochondria, and (5) phenotipical charactirization.

1.2. Dissertation outline

This MSc dissertation is presented in chapter format as per the requirements of North-West University (NWU). The study is organized into five chapters with literature cited listed at the end of chapter 5.

Chapter 2: summarizes existing literature on mitochondrial research, the OXPHOS system as well as mitochondrial diseases with focus on MICOS subunit deficiency particularly in the nematode *C. elegans*. This section of the dissertation also provides the research rational, problem statement and the aims and objectives.

Chapter 3: provides in depth information about the methodologies and data analyses that were employed to achieve the aims and objectives of this study. All the reagents used as well as suppliers are listed.

Chapter 4: provides a summary of the results and discussion in the context of literature.

Chapter 5: provides the conclusions of the study as well as possible future perspectives. A list of full references follows imediately after chapter five.

2. CHAPTER TWO: LITERATURE REVIEW

Chapter summary

This chapter gives a detailed overview of the general mitochondrial dynamics, functions, arrangement of different constituents and machineries involved in this vital organelle responsible for a variety of functions including energy production, cellular metabolism. Furthermore, this chapter links the mitochondrial contact site and cristae organizing system (MICOS) to mitochondrial dynamics. This multiprotein complex (MICOS) is associated with the formation and maintenance of mitochondrial cristae, which are integral structures that harbours the complexes of the respiratory chain and F_1F_0-ATP synthase. The MICOS is located at cristae junctions which are narrow openings that connect the cristae membranes to the inner membrane boundary (IMM), and it forms contact with the outer mitochondrial membrane (OMM). Better understanding of MICOS can be a useful tool to unravel mitochondrial related disorders which is imperative in diagnosis and treatment for patients. Moreover, details of the disease model (*Caenorhabditis elegans*) that is utilized to study the aberrations in MICOS is given. The utility of this nematode in mitochondrial research is embedded in the extremely conserved nature of mitochondrial morphology, composition and function across evolution.

2.1. The mitochondrion

The mitochondrion (plural mitochondria) is a membrane-bound organelle that is found in the cytoplasm of eukaryotic cells (Garcia *et al*., 2019). This organelle plays a pivotal role in the generation of cellular energy in the form of adenosine triphosphate (ATP). In addition, the mitochondrion generates heat, stores calcium for cell signalling activities and mediates cell growth and death. The size of a mitochondrion ranges from 0.5 to 10 µm and is typically round (Garcia *et al*., 2019). Moreover, mitochondrial mass per cell differs broadly; for instance, liver cells and muscles cells comprise of hundreds or even thousands of mitochondria (Garrett and Grisham, 2013; Chinnery and Hudson., 2013).

Mitochondrial diseases are group of various chronic, often genetically heritable disorders that are characterized by failure of the mitochondria to produce enough ATP for the body to function properly (Yi and Doug., 2016). Mitochondrial diseases can be present at birth but, can also occur at any age and are becoming clinically prominent worldwide (Chinery and Hudson., 2013; Rackham and Filipovska., 2014). Moreover, mitochondria contribute fundamentally to the cohort of inborn errors of metabolism with an estimated prevalence of 1 in 5000 people across a lifetime (Schaefer *et al*., 2004; Yi and Doug., 2016). High energy demand organs such as the heart, brain and skeletal muscles are frequently affected by mitochondrial diseases (Horvarth *et al*., 2009). Parkinson's

disease (PD) for example, which is a second most common neurodegenerative disorder affecting 2-3% of the global population over 65 years (Poewe *et al*., 2017), is linked with loss of dopaminergic neurons and a subsequent depletion of dopamine at the striatum (Kashimori *et al*., 2016). Diminished mitochondrial function, toxic accumulation of ROS and altered cristae morphology are pathological hallmarks of a variety of human diseases including diabetes and PD (Shoffner *et al*., 1993; Baloyannis *et al*., 2006; Van Laar *et al*., 2016).

2.1.1. Mitochondrial morphology and structure

Mitochondria are known as the powerhouse of eukaryotic cells, mitochondria contain approximately 1500 and 1000 different proteins in humans and yeast, respectively (Sickmann *et al*., 2003; Reinders *et al*., 2006 and Calvo *et al*., 2006). Moreover, mitochondria have unique replication and transcription machineries, making them the only autonomous organelles in eukaryotic cells to display such high-level architecture (Ramachandran *et al*., 2016). Specific mitochondrial functions like calcium signaling (Rizzuto *et al*., 2009), production of energy via the electron transport chain (ETC) (Garrett and Grisham, 2013) and the biosynthesis of cofactors, lipids and amino acids (Becker *et al*., 2008) have been discovered over the years. Furthermore, mitochondria are significant components for cellular metabolism regulation, haem synthesis, and programmed apoptosis in addition to energy production (Chinnery and Hudson., 2013).

Mitochondrial structure is categorized by dual membranes. One membrane surrounds the other where the OMM separates the mitochondrion from the cytosol and the IMM defines the matrix as depicted in figure 2-2 (A). The tricarboxylic acid cycle (TCA) enzymes in the matrix utilize pyruvate and fatty acids as substrates to drive ATP production by OXPHOS. TCA cycle intermediates activate the ETC to drive protons out of the matrix across the IMM leading to a proton gradient that is utilized by ATP synthases to generates ATP within the matrix (igure 2-2 (B). ETC and ATP synthase complexes are located in the invaginations of the inner membrane known as cristae figure 2-2 (C) (Bohnert *et al*., 2015).

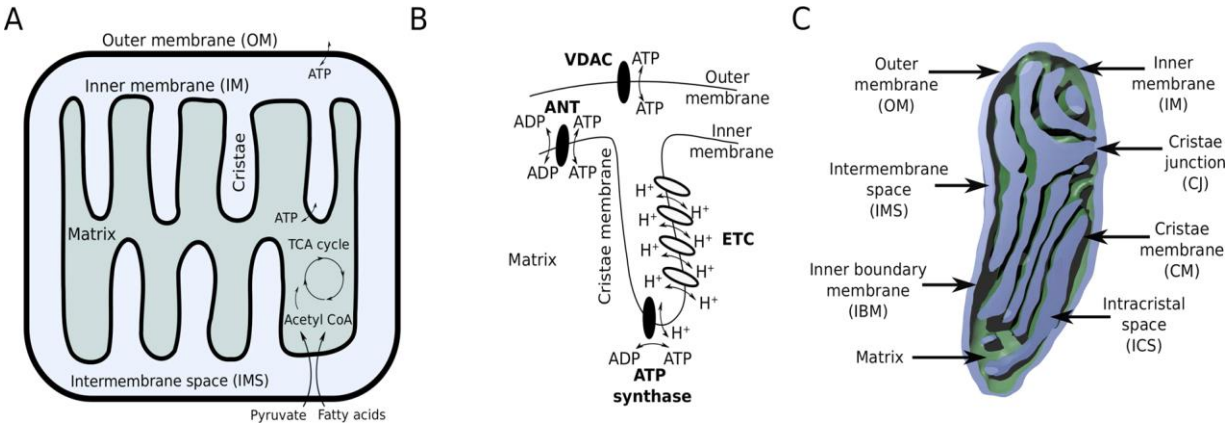

Figure 2-1: Detailed schematic representation of mitochondrial dynamics. (A) The OM separates the mitochondria from the cytosol, the matrix which carries TCA cycle enzymes is enclosed by the IM. (B) Depicts cristae morphology and protein localization that facilitates production of ATP. (C) Comprehensive physiological annotation of mitochondrion with both inner and outer membrane separated by intermembrane space. Image adapted from (Garcia *et al*., 2019).

The actual mitochondrial morphology exhibits a large heterogeneity on metabolic conditions and is linked with diverse physiological conditions and their explicit subcellular energy demands (Perkins and Ellisman., 2011). Typically, mitochondria display a lamellar and tubular cristae composition within the brain (Perkins *et al*., 2001). Proteins of the outer mitochondrial membrane are incorporated, depending on the contents of their secondary structure, α-helix proteins are primarily recognized and introduced by translocase of the outer membrane (TOM) and/ the mitochondrial import (MIM) complex (Vogtle *et al*., 2009). Conversely, proteins containing β-barrels are introduced by TOM and integrated utilizing the sorting and assembly machinery (SAM). Interestingly, mitochondria can form an endoplasmic reticulum (ER)- mitochondrial encounter structure (ERMES) to physically interact and communicate with ER (Wiedemann and Pfanner., 2017).

2.1.2. Electron Transport Chain (ETC)

A chain of electron carriers operates together to transfer electrons from donor to acceptor such as oxygen (O_2) to establish the electron transport chain (ETC) (Willey *et al*, 2014). Molecules involved in ETC includes nicotinamide adenine dinucleotide (NAD^+), NAD phosphate ($NADP^+$) (NAD can be in a hydroquinone form), cytochrome, coenzyme Q, flavin adenine dinucleotide (FAD), flavin mononucleotide (FMN), haem and non-haem proteins as depicted in figure 2.3 below. These electron carriers vary in their chemical nature and the manner in which they carry electrons (Garrett and Grisham, 2013; Willey *et al*, 2014). NADH contains a nicotinamide ring

which accepts two electrons and one proton from a donor, flavin proteins bear two electrons and two protons and the coenzyme Q (coQ)/ ubiquinone transports two electrons and two protons.

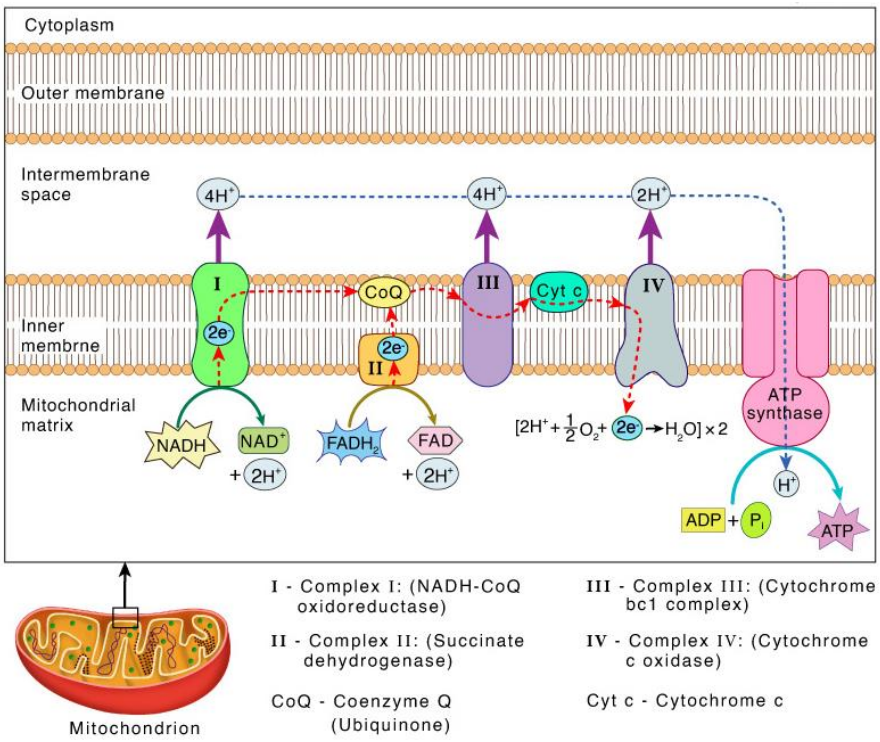

Figure 2-2: Schematic flow of electron transport chain. The transfer of electrons from donors to acceptors via redox reaction is clearly shown as well as how protons are pumped into the intermembrane space. The protons in the intermembrane space creates a proton gradient thereby resulting in the generation of ATP which is facilitated by ATP synthase. https://www.sciencefacts.net/electron-transport-chain.html.

The ETC is situated at cristae membranes (Rea *et al*., 2007; Willey *et al*, 2014) and comprises four protein complexes (I-IV), complex I, III and IV are the proton pumps. Ineffective electron transfer through various ETC subunits and ineffective transfer of carriers (ubiquinone, cytochrome c) through the inner membrane of mitochondria can result in the production of superoxide (Reinecker *et al*., 2009). A variety of mutations that compromise mitochondrial functionality led to pathological, life-shortening diseases (Wallace., 2005). Rea *et al* (2007) investigated the contribution of partial mitochondrial ETC inhibition to the life extension phenotype of *C. elegans.* Disturbance in components of mitochondrial ETC complexes and their inter-complex electrons carriers can extend lifespan of the nematodes from 20% to 200% (Feng *et al*., 2001). However, not all mitochondrial mutations that interrupt the ETC in *C. elegans* extend the nematode lifespan (Rea *et al*., 2007). Some can shorten the lifespan of nematodes and two prominent examples are mev-

1(kn1) and gas-1(fc21) which are both life shortening mutations and affect complex II and I, respectively (Kayser *et al.*, 2004).

2.1.3. Mitochondrial fusion and fission

Mitochondria can exist as vastly interrelated networks and not just as isolated organelles, frequently shifting between these two conditions by maintaining equilibrium among opposing fusion and fission forces (Byrne *et al*., 2019). Mitochondrial fusion is a physical process of merging the outer and inner mitochondria membranes of two originally distinct mitochondria and, mitochondrial fission is the process by which the mitochondria segregate into two separate organelles (Bohnert *et al*., 2015). This transition between fission and fussion states is pivotal for standard mitochondrial functioning in the maintenance of cellular bioenergetics (Ono *et al*., 2001). Mitochondrial fission is highly dependent on dynamin related protein 1 (Drp1). Mitochondrial fusion abnormalities have been associated with variety of human neuropathies like dominant optic atrophy (Zanna *et al*., 2007) and Charcot-Marie-Tooth disease (Cartoni *et al*., 2010), while mitochondrial fission defects are implicated in neurodegenerative diseases like Alzheimer's (Cho *et al*., 2009) and Parkinson's (Deng *et al*., 2008). Dynamin-related GTPases play a pivotal role in regulating mitochondrial dynamics. These proteins possess intrinsic abilities to reorganize membrane structures in a GTP hydrolysis-dependent manner thus resulting in mitochondrial membrane reorganization (Youle and van der Bliek., 2012).

In addition, fusion permits impaired mitochondria to alleviate stress by mixing their contents as a form of efficient complementation, diluting oxidized proteins and accumulated mitochondrial DNA mutations. Conversely, fission is desired to build new mitochondria, but it also contributes significantly to quality control by enabling the removal of damaged mitochondria by budding off deteriorating components for targeted breakdown via mitophagy or autophagy (Twig *et al*., 2008). Disturbances in fusion and fission homeostasis are detrimental to mitochondrial function and health (Kanazawa *et al*., 2008).

Remodelling and deformation of biological membranes is linked to several proteins (Danne *et al*., 2017). Affectors of inner mitochondrial remodelling includes proteins like ATP-synthase (Muhleip *et al*., 2016), OPA1 (Frezza *et al*., 2006) and members of the recently identified mitochondrial complex such as Mic60 and Mic10 (Bohnert *et al*., 2015; Hessenberger *et al*., 2017; Eramo *et al*., 2019). Mitochondrial fusion is orchestrated by mitofusin 1 and 2 together with OPA1 in humans (Kanazawa *et al*., 2008). Mitofusin proteins form dimeric interactions across the OMM, tethering adjacent mitochondria and inducing fusion through GTP hydrolysis (Escobar-Henrigues and

Anton., 2013). In addition, the dynamin-like GTPase OPA1 is crucial for inner IMM fusion as well as internal cristae structure maintenance (Olichon *et al*., 2006).

The functional ortholog of OPA1 in *C. elegans* is called *eat-3* (Kanazawa *et al*., 2008; Byrne *et al*., 2019). This gene, like its human counterpart, has GTPase activity and microtubule binding activity. *Eat-3* is involved in numerous processes, including nematode larval development, mitochondrial fusion and response to superoxide (Byrne *et al*., 2019). A study performed by (Barrera *et al*., 2016), showed that OPA1 is indispensable for mitochondrial fusion but dispensable for formation of cristae junctions (CJs). Conversely, (Byrne *at al*., 2019) analysed mitochondrial dynamics using *C. elegans* to determine how disruptions in fusion/fission process influence organelle homeostasis and found that it alters mitochondrial morphology. The *C. elegans eat-3* mutants have small brood-sizes and generally grow slower compared to *C. elegans* mutants with defects in other mitochondrial fusion and fission proteins (Kanazawa *et al*., 2008).

2.1.4. Role of mitochondria in cellular respiration

The mitochondrial respiratory chain (RC) consists of four multimeric, membrane-bound complexes used to complete oxidation of fats, sugars, and proteins to produce ATP (Lemarie and Grimm., 2011). Each of these substrates can be catabolised to acetyl-CoA which delivers the acetyl group to the TCA cycle where it is oxidized for the production of energy. Sugars undergo glycolysis in the cytosol to enter the mitochondria as pyruvate, where pyruvate dehydrogenase plays a pivotal role in the conversion to acetyl-CoA (reviewed by Bartlett and Eaton., 2003). Fatty acids are converted to acetyl-CoA inside the mitochondria by β-oxidation, while several enzymes exist for conversion of specific amino acids into acetyl-CoA, pyruvate or directly into TCA intermediates. Cellular respiration occurs when there is conversion of energy from reducing equivalents like flavin adenine dinucleotide–($FADH_2$) and nicotinamide adenine dinucleotide (NADH) into ATP which can be used by the cell (Hoeks *et al*., 2012). Complex I, complex II and complex IV are the three proton pumping complexes of the ETC ((Maechler *et al*., 2006; Lemarie and Grimm., 2011; Sousa *et al*., 2018).

As seen in figure 2-3 below which gives an annotation of the ETC bioenergetics, the phosphorylation of ADP to ATP by complex V with the aid of proton gradient is the final step of oxidative phosphorylation (Osellame *et al*., 2012). To optimize transport of electrons during respiration, these RC enzymes result in the formation of large supermolecule assemblies known as respirosomes which are located in the cristae membranes thus making cristae the main oxidative phosphorylation site (Boekema and Braun., 2006).

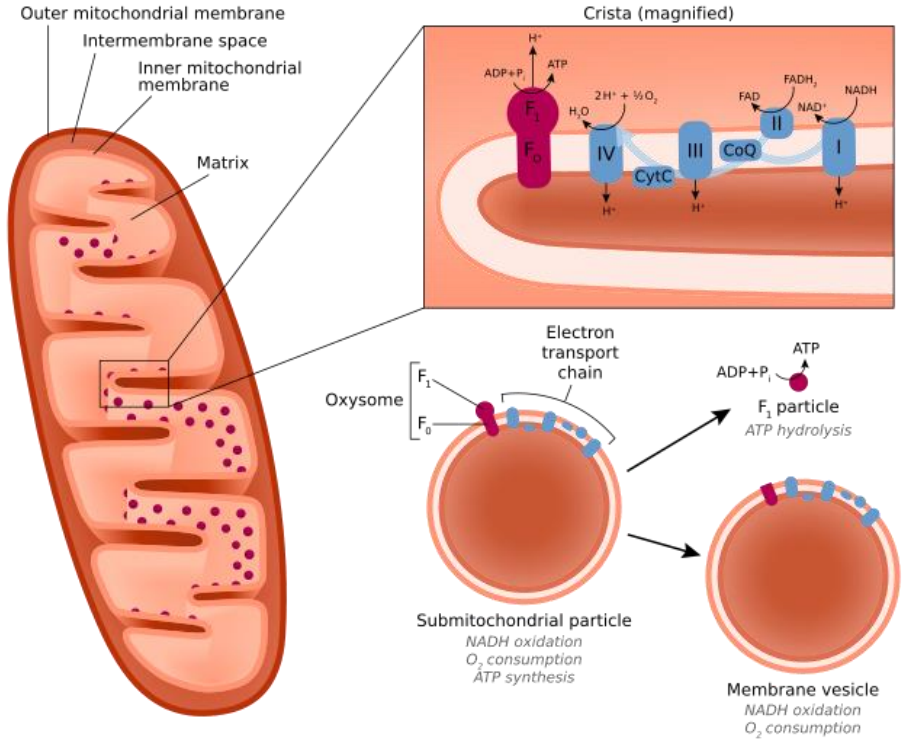

Figure 2-3: Electron transport chain bioenergetics. The four respiratory complexes and ATP-synthase are indicated as well as their electron/proton pathways. NADH supplied by the TCA cycle is converted to NAD+ to drive oxidative phosphorylation. The transport of electrons through the respiratory chain complexes results in pumping of protons into the cristae lumen. Adapted from Osellame *et al*., 2012).

Mitochondrial respiration which is utilized to build a P^+ gradient across the cristae surface area is supported by oxygen (Osellame *et al*., 2012). The P^+ gradient drives the synthesis of ATP, protein import, and transfer of calcium and ion exchangers. The regulation of OXPHOS is facilitated by cellular calcium signalling so that Ca^{2+} ion transfer signals into the mitochondrial matrix and increase energy demand and drives increased energy provision by OXPHOS through upregulating the TCA cycle limiting enzymes (Raffaello *et al*., 2016). Failure in bioenergetics often results in fatal cellular function, particularly in nerve and muscle cells. Moreover, excessive Ca^{2+} uptake in mitochondria is pivotal in the heart and brain muscles where prolonged unphysiological Ca^{2+} influx increases, and when combined with oxidative stress, might lead to pathological transformation (Boekema and Braun., 2006).

2.1.5. Inner mitochondrial membrane composition

Mitochondria possess two membranes that divide them into four sub compartments, namely, OMM, inner boundary membrane (IMB), IMM and matrix (Kozjak-Pavlovic., 2016). Machineries that mediate transportation of proteins and metabolites or control mitochondrial morphology are found

in both the membranes. The IMM comprises two distinct domains, namely: (1) cristae membrane which are joined by small tubular cristae junctions and (2) IBM (Vogel *et al*., 2006). The IBM is adjacent to the OMM, and the cristae membrane represents IBM invaginations that extend into the matrix space. Cristae aid in normal mitochondrial functioning (Eramo *et al*., 2019; Colina-Tonorio *et al*., 2020). These lamellar invaginations are connected to the outer membrane boundary by cristae junctions (Munoz-Gomez *et al*., 2015; Kozjak., 2017; Baker *et al*., 2019), where the MICOS complex is located. There are several factors that influence cristae morphology, for example, membrane potential and lipid composition alter formation of mitochondrial cristae (Ghochani *et al.*, 2010).

The mitochondrial matrix serves as the innermost mitochondrial compartment and is characterized by a pH of 7.9 to 8. This pH drives the production of ATP through the trans-membrane electrochemical gradient it creates (Rizzuto *et al*., 2012). Several processes including DNA replication, transcription, translation, and other enzymatic reactions take place in the mitochondrial matrix (Kukat *et al*., 2015). The biosynthetic reactions of the TCA cycle also take place in the mitochondrial matrix. Reactions are catalysed by specific enzymes and as a result the matrix contains a high protein density (up to 500 mg/ml) (Kühlbrandt., 2015). The IMM forms projections, termed cristae, that expand deeply into the mitochondrial matrix and serve as the primary biological energy conversion site in all non-photosynthetic eukaryotes (Perkins *et al.*, 1997). Mitochondrial cristae normally adopt a tubular and lamellar morphology; however, the size, number, distribution and shape of mitochondrial cristae is impacted by diverse physiological and pathological conditions (Cogliati *et al.*, 2016). A typical example is in aged nematodes, which are characterized by lack of cristae junctions and enlarged mitochondrial cristae (Brandt *et al*., 2017). Although the mitochondrial cristae ultrastructure has been described decades ago (Kukat *et al*., 2015; Munoz-Gomez *et al*., 2015; Kozjak., 2017), mechanisms and function of mitochondrial cristae remodelling remain elusive.

2.1.6. Mitochondrial cristae dynamics

Mitochondrial cristae were discovered over six decades ago by the Romanian cell biologist George Palade using electron microscopy (Palade., 1953). Mitochondrial cristae contain an important multiprotein complex (MICOS) and are the main site of OXPHOS which is crucial for the production of cellular energy (Anand *et al.*, 2021). According to existing literature, the cristae morphology considered globally is tubular or lamellar invaginations formed by IBM projections into the mitochondrial matrix (Rabl *et al.*, 2009). The process is facilitated by a variety of interacting partners including, the relatively recently described mitochondrial contact site and

cristae organizing system (MICOS) complex, dimeric F_1F_0-ATP synthase and OPA1 (Harner *et al*., 2016).

One of the core MICOS subunits (Mic60) is located in the IMS and forms contact sites with several outer membrane proteins, including sorting and assembly machinery (SAM) (Bohnert *et al*., 2015). Cristae morphology and biogenesis is regulated by ATP synthase dimerization, moreover, ATP synthase instigates the positive curvature that leads to the formation of cristae sheets at the tip (Rabl *et al.*, 2009). Oligomerization of OPA1 narrows cristae junctions and facilitates dimerization of ATP synthase (Patten *et al.*, 2014). According to existing literature (Ott *et al*., 2015), MICOS is essential for cristae stability. The inner MICOS complex interacts with outer membrane SAM to yield the mitochondrial intermembrane space bridging complex (MIB).

Mitochondria can constantly shift between existing as an isolated organelle and highly interconnected networks via a balance between the opposing processes of fusion and fission (Ono *et al*., 2001). This transition is important for mitochondrial function in the maintenance of optimal cellular bioener-getics, in regulating cellular stress response, and intercellular Ca2+ signalling. The mutant strain (VC1196) used in this study harbours a mutation in the *moma-1* gene which is an ortholog of mammalian *APOOL* encoding a MICOS subunit Mic27. Normal lamellar or tubular mitochondrial cristae are orderly arranged under normal conditions (Davies *et al*., 2012). However, the size, number and distribution of mitochondrial cristae differ significantly under diverse physiological and pathological conditions (Mannella., 2006; Cogliati *et al*., 2013; Cogliati *et al*., 2016).

2.1.7. Import of nuclear-encoded proteins

Mitochondria comprise of approximately 1000 proteins. A total of 99% of these proteins are nuclear encoded and are synthesized as precursor proteins in the cytosolic ribosomes prior to import into mitochondria (Dolezal., 2006). There are two main groups of targeting signals that are recognized by receptors on the surface of mitochondria as indicated in figure 2-4. The first group of mitochondrial targetting sequences are the amino terminal extensions of precursors, and the second group contains a variety of precursor proteins and targeting signals (Horvath *et al*., 2015). These signals are responsible for directing precursors to their functional destination in the mitochondrial sub-compartments.

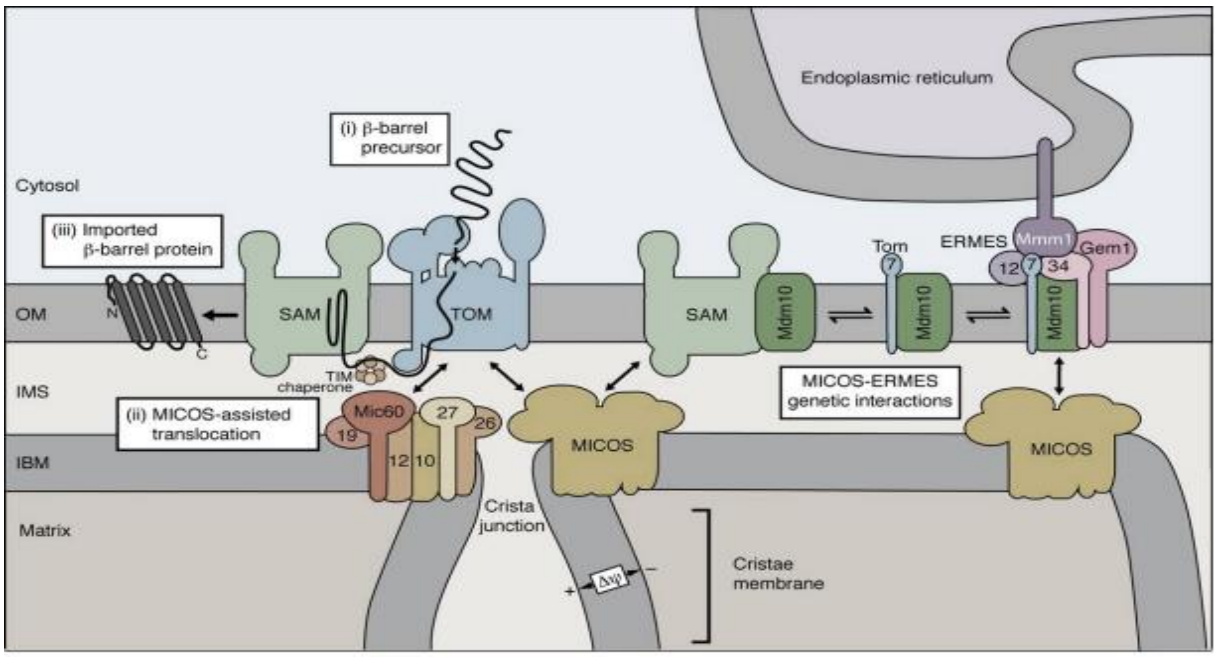

Figure 2-4: Import of nuclear encoded proteins. Import of nuclear encoded proteins is regulated by TOM whereas β-barrel proteins are integrated into OM with the aid of SAM. Interaction of MICOS with SAM and TOM further stimulates biogenesis of β-barrel proteins. Image adapted from (Horvath *et al*., 2014).

Mitochondrial genome encoded proteins do not utilise mitochondrial import pathways, and these proteins are predominantly subunits of the OXPHOS machinery (Schmidt *et al*., 2010). Conversely, import of nuclear encoded proteins can occur in five main pathways which all employ the TOM complex (Horvath *et al.*, 2015).

2.1.7.1. Presequence pathway

This pathway is used by ~60% of all mitochondrial precursor proteins and involves the transfer of cleavable precursors/preproteins from the TOM complex to the presequence translocase of the inner membrane (TIM23) complex (Dolezal., 2006; Neupert & Herrmann., 2007; Schmidt *et al*., 2010). Synthesis of preproteins occurs in the amino-terminal presequence that form positively charged amphipathic α-helices (Habib *et al*., 2007). Presequence translocase-associated motor (PAM) plays a pivotal role in importing hydrophobic preproteins into the matrix (Gentle *et al*., 2004). In addition, preproteins designed for the inner membrane encompass a hydrophobic sorting signal behind the positively charged matrix-targeting signal. The matrix signal is proteolytically removed for both matrix- translocated and inner membrane sorted proteins by mitochondrial processing peptidase (MPP) (Mossmann *et al*.,2011).

2.1.7.2. Carrier pathway

This pathway is used to import proteins of IMM containing an internal targeting signal, which is not removed during import but remains part of the mature mitochondrial protein (de Marcos-Lousa *et al*., 2006). The major substrates of this pathway are the hydrophobic metabolite carriers of the IMM (Schmidt *et al*., 2010). In addition, the hydrophobic proteins are imported via the TOM complex, chaperone complexes and the TIM22 complex. The substrates are bound to small TIM chaperones to be further translocated to the carrier translocase Tim22 complex (Curran *et al*., 2004).

2.1.7.3. Oxidative folding pathway

Oxidative folding is a sophisticated process that involves the interplay between conformational folding, formation of disulphide bonds and isomerization (Fischer *et al*.,2013). The relationship between these three reactions is insignificant, since redox and reshuffling rates are modulated by effective concentrations of thiolate anions as well as reactivity and accessibility of both disulphide and cysteine bonds (Welker *et al*., 2000). The discovery of many oxidized, disulphide-containing intermembrane space proteins changed the narrative of the oxidative folding pathway (Vogtel *et al*., 2012; Horvath *et al*., 2015). It was previously assumed that the mitochondrial intermembrane space is the reducing environment (Chacinska *et al*., 2004). The discovered system was termed (MIA) for mitochondrial intermembrane space import and assembly (Horvath *et al*., 2015). It functions by accepting preproteins after their translocation through TOM.

2.1.7.4. Outer membrane transport pathway

The OMM comprises two categories of transmembrane proteins, which are proteins with α-helical transmembrane segments and β-barrel proteins (Hohr *et al*., 2015). The former is estimated to be encoded by 20-30% of genes in most organisms and the latter is estimated to be encoded only by 2-3% of the genes in gram negative bacteria (Imai *et al*., 2011). In addition, the import of β-barrel proteins involves TOM complex, SAM complex of OMM and intermembrane space chaperones (Kojer *et al.*, 2012).

2.1.7.5. Integration of α-helical outer membrane proteins

The integration of α-helical proteins comprises several other pathways that are not yet fully understood (Schmidt *et al*., 2010). The mitochondrial import (MIM) complex plays a pivotal role in facilitating the insertion of some α-helical proteins into the OMM, particularly multispanning OMM proteins and proteins with an amino-terminal membrane anchor (Papic *et al.*, 2011). The TOM receptors are involved in multi-spanning protein recognition prior to their integration by the MIM complex (Horvath *et al.*, 2015).

2.2. Overview of MICOS complex

The MICOS complex (previously known as MINOS, MitOS/MIB) is a large, hetero-oligomeric protein complex that is located in the cristae junctions, which are tubular structures measuring 12-40nm in diameter that demarcate the cristae from the rest of the IBM (Huynen *et al*., 2016; Rampelt *et al*., 2017). Mitochondrial cristae are projections of the IMM that house OXPHOS machinery that produces the bulk of cellular ATP (Eramo *et al*., 2020). The MICOS complex is important for the maintenance of cristae structure, inner-outer mitochondrial membrane contact site formation, and regulation of protein import and organization of respiratory complexes (Huynen *et al*., 2016; Li *et al*., 2015; Eramo *et al*., 2020; Stephan *et al*., 2020).

The MICOS complex engages with the OMM as it extends across the intermembrane space through the SAM (Wiedenman *et al*., 2003). SAM consists of a core sam50 protein and Metaxins1/2/3 and its association with the MICOS is termed mitochondrial inner membrane space bridging complex (MIB) (Ott *et al*., 2012). MICOS-MIB, cristae junctions and architecture can be disrupted by depletion of core MICOS-MIB subunits. These alterations lead to cristae abnormalities and impaired mitochondrial ATP production (Darshi *et al*., 2010). In addition, deletion of key MICOS subunits results in the loss of cristae junctions and detachment of elongated cristae into the mitochondrial matrix (Hashimi., 2019).

2.2.1. Structural organization of MICOS subunits

The MICOS complex has been characterized as a large multiprotein complex that is essential for IMM architecture (Hoppins *et al*., 2011; Munoz-Gomez *et al*., 2015; Kozjak.,2017; Eramo *et al*., 2019). A variety of studies have been previously performed on yeast species to gather information on this complex in pursuit to unravel mitochondrial dysfunctions. The annotation in figure 2-5 is an indication of the human MICOS and interacting parters. The IMM is indicated on the left (2-5 a) clearly showing all important components of the mitochondrial ultrastructure and the MICOS are indicated on 2-5 b with all the subunits.

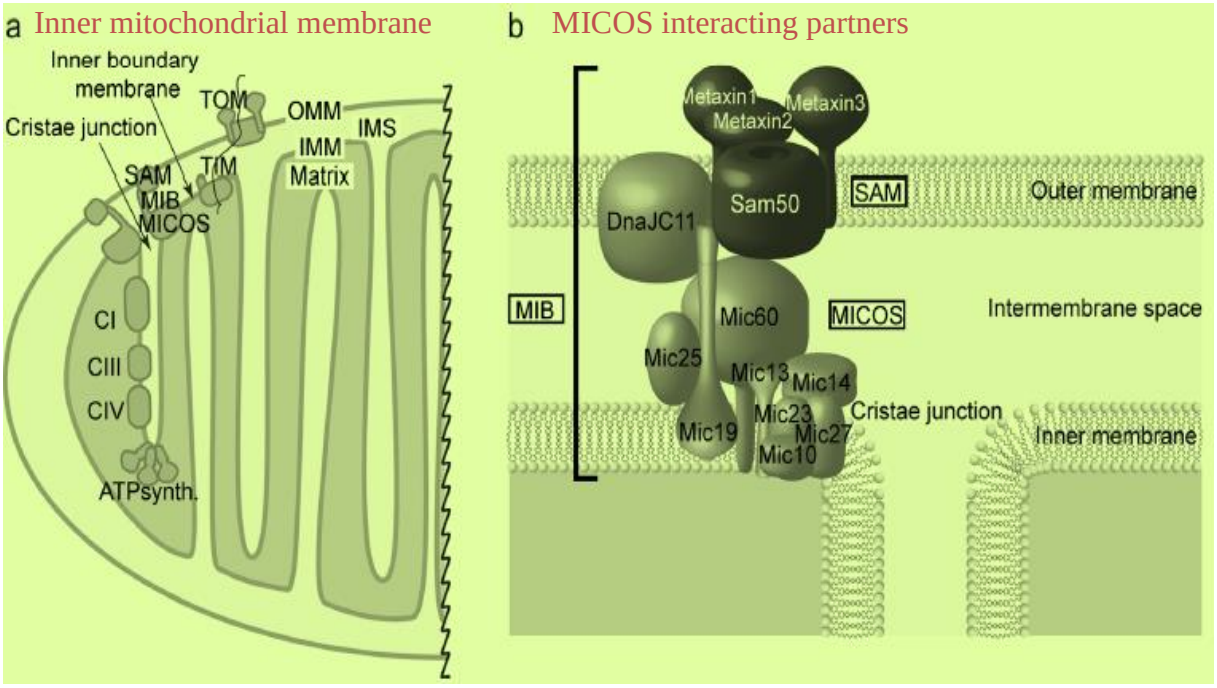

Figure 2-5: Schematic representation of the human MICOS and interacting partners. (Adapted from Kozjak., 2017). The interacting MICOS partners are shown on part (2-5 b) of figure 2-5 above, the IMM containing, cristae membrane, ETC complexes as well as ATP synthase are shown in 2-6 a.

The MICOS complex consists of six and seven subunits in yeast (Hoppins *et al*., 2011; Munoz-Gomez *et a*l., 2015) and human (Kozjak.,2017; Eramo *et al*., 2019), respectively. The subunits are termed 'Mic plus a number' (table 2-1) which is based on the molecular weight of each subunit in kDa (Hoppins *et al*., 2011; Munoz-Gomez *et al*., 2015; Kozjak.,2017; Eramo *et al*., 2019). Core subunits (Mic10 and Mic60) are linked with other peripheral proteins and protein complexes to form mature MICOS. Loss of the Mic60 subunit decreases MICOS subunits and is thus harmful to cristae architecture (Eramo *et al*., 2019). Table 2-1 shows the subunits of MICOS and other essential components, their proposed functions and genes in mammalian cells (reviewed in Eramo *et al*., 2019). This study followed the uniform nomenclature of MICOS complex formation that was proposed by Pfanner. (2014).

Table 2-1: Components of MICOS-MIB and their proposed function in mammals

Protein name	Human gene	MICOS-MIB function
Mic60/mitofilin	*IMMT*	Core subunit required for cristae morphology
Mic19	*CHCHD3*	Homologue[1] of Mic25, responsible for MICOS-MIB stability through N-terminal myristoylation.
Mic25	*CHCHD6*	Homologue of Mic19 with a role in Mic60 stabilization and cristae morphology
Mic13	*QIL1*	Bridges and stabilizes the mic 60 and Mic10 subcomplexes to form the mature MICOS
Mic10	*MICOS 10*	Core of Mic10 subcomplexes, oligomer with Mic60 upholding normal cristae morphology.
Mic26	*APOO*	Paralogue[2] of Mic27, stabilizing Mic10 sub complex and cristae morphology
Mic27	*APOOL*	Paralogue of Mic26, stabilising Mic10 sub complex and cristae morphology.
Sam50	*SAAMM50*	Core of sam50 and regulates cristae morphology
Metaxin1/2/3	*MTX1/2/3*	Helps stabilize cristae architecture.
dnajc11	*DNAJC11*	Upholds normal cristae morphology.
armc1	*ARMC1*	Controls mitochondrial distribution in the cell.

[1] Genes that are inherited in two species by a common ancestor, these genes can be similar in sequence, however, similar sequences are not necesarily homologous (Willey et al. 2014).
[2] Homologous genes that developed through duplication, these genes code for proteins with similar but not identical functions (Eramo *et al*., 2019).

2.2.1.1. Mic60/*IMMT*

Mic60 (encoded by *IMMT* gene) was the first described component of the MICOS. It was identified as a heart muscle protein (HMP) due to its abundance in cardiac tissues (Tateo *et al.*, 1994; Odgren *et al*., 1996). In addition, Odgren and colleagues disclosed that Mic60 was exclusively found in the mitochondria, consisting of an N-terminal mitochondrial target sequence and a coiled-coil region exposed to the IMS. However, evidence emerged later that proved Mic60 is a transmembrane protein of the IMM thus was renamed mitofilin based on its structure and localization (Gieffers *et al*., 1997).

Mic60 (AKA mitofilin) is a core subunit of the MICOS complex, and forms contact between the inner and outer membranes (Hessenberger *et al*., 2017). In addition, Mic60 displays membrane shaping activity as it plays a pivotal role in deforming liposomes into thin membrane tubules. Existing literature shows the interaction of Mic60 and Mic19 in the formation of a MICOS subcomplex (Pfanner *et al*., 2014; Guarani *et al.*, 2015; Eramo *et al*., 2019) however, the molecular mechanism of interaction remains an active area of research.

According to existing literature, the mechanism controlling cristae shape is a result of the physical interaction of two MICOS subunits (Mic60 and Mic19) with optic atrophy (OPA1) (Barrera *et al*., 2016; Darshi *et al*., 2010). Interestingly, experiments performed by Barrera *et al (2016)* showed elevated Mic60 levels and decreased apoptosis efficiency as a result of OPA1 depletion.

2.2.1.2. Mic10/MICOS10

The core of the MICOS complex comprises both Mic10 and Mic60, and their deletion causes virtually complete loss of cristae junctions and cristae shape similar to onion ring like slices (Hoppins *et al.*, 2011; Kondadi *et al*., 2020). Structurally, Mic10 exist as a hairpin-like inner membrane protein consisting of two transmembrane domains connected by a short loop that carries a positive charge, the loop is important for targeting Mic10 precursors which is nuclear encoded like all MICOS subunits into the IMM (Bohnert *et al.*, 2015). The termini are both visible to the intermembrane space (Von der Malsburg *et al*., 2011). Barboot *et al*., (2015) revealed that the molecular function of Mic10 in promoting cristae junction formation is via the ability to change membrane morphology *in vivo* and *in vitro*. Thus, Mic10 loss is linked to massive CJs loss as well as aberrant cristae structure.

The two transmembrane domains contain glycine motifs which mediate helix-helix interactions within the lipid bilayers (Russ and Engelman., 2000). Oligomerization of Mic10 via its transmembrane segments is facilitated by these glycine rich motifs and it plays a crucial role in the stability of cristae junctions (Barbot *et al*., 2015). A study conducted in yeast by Bohnert *et al*. (2015), revealed strong expansion and deformation of cristae membranes and CJs as a result of Mic10 overexpression. This is indicative that Mic10 can remodel the IMM autonomously of MICOS subunits.

In addition, Guarani and colleagues verified that overexpressed Mic10 fails to restore its interaction with sorting and assembly machinery component (SAMM) 50 and other subunits of the MICOS complex (Guarani *et al*., 2015). SAM50 is also an important protein that plays a role in the maintenance of mitochondrial cristae structure and proper assembly of respiratory chain complexes (Ott *et al*., 2012).

2.2.1.3. Mic19/*CHCHD3*

Mic19 (encoded by *CHCHD3* gene in humans) is 26-kDa a large protein encompassing a coiled-coil-helix (CHCH) consisting of two CX9C cystein motifs and an amino terminal myristoylation domain followed by a DUF737[3] (Darshi *et al*., 2010). Mic19 is contained in IMM and was primary recognised in the screen for novel substrates of cAMP-dependent protein kinase (Schauble *et al*., 2007). Moreover, Mic19 plays a pivotal role in the MICOS-MIB stability through N-terminal myristoylation (Ott *et al.,* 2015). The homeostasis of Mic60 and Mic19 are vital for the integrity of the mammalian MICOS complex (Li *et al.,* 2015). In addition, Mic19 as a peripheral protein is essential for routine functioning of MICOS in the maintenance of inner membrane architecture (Sakowska *et al.,* 2015). Some studies done in *Saccharomyces cerevisiae* revealed that the MICOS consist of two independent sub-complexes that are bridged together by Mic19 which other experiments determines position and number of cristae junctions holding the fold of the inner membrane in place (Friedman *et al*., 2015).

Depletion of Mic19 leads to elevated levels of Dynamin related protein (Drp1) and a decrease in OPA1 levels (Kozjak-Pavlovic., 2017; Darshi *et al*., 2010). Drp1 plays a pivotal role in mediating mitochondrial fission through oligomerization into membrane-associated tubular structures, and its loss induces muscle wasting and weakening (Favaro *et al*., 2019). Moreover, Mic19 depletion is also associated with aberrant cristae morphology as well as levels of MICOS components with the exclusion of Mic25 (Ott *et al*., 2015). Mic19 binds to Mic60 though the CHCH domain of Mic60, while Mic19 N-myristoylation motif is required for amino-terminus recruitment to the OMM, both

[3] Domain of unknown function

CHCH and myristoylation are imperative for mitochondrial localization and import (Darshi *et al*., 2010). Additional interaction cohorts of Mic19 include OPA1 and heat shock protein (Hsp) 70, the latter is essential for ATP synthase activity (Darshi *et al*., 2011) and functions of the former were discussed in section 2.1.3.

2.2.1.4. Mic25/*CHCHD6*

Mic25 (encoded by *CHCHD6)* is a paralog of Mic19 and a homolog of Mic60 (Munoz-Gomez *et al.,* 2015; An *et al*., 2012). It was identified in a screen for novel cellular stress response markers, since it is downregulated post genotoxic stress (An *et al*., 2012). Similar to the Mic19 structure, Mic25 also exhibits an amino terminus myristylation site, followed by DUF737 domain and carboxyl terminal domain consisting of two CX9C motifs. However, a prominent variation between these two subunits is functions they perform. Mic25 plays a crucial role in Mic60 stabilization and cristae morphology (Eramo *et al*., 2019; Munoz-Gomez *et al*., 2015; An *et al*., 2012). Surprisingly, its depletion has no effect on any MICOS or MIB complex subunit and has no effect on cristae morphology, although depletion results in mitochondrial elongation (Ott *et al*., 2015).

Ding *et al*. (2015) reported the extent of Mic25 knockout on cristae. The impact on the mitochondria can be detected by fewer cristae junctions and lower cristae density. A study conducted by Li *et al*. (2015) further elucidated the interplay of both Mic25 and Mic19 on the overall MICOS structure. Simultaneous depletion of these two subunits has equivalent phenotypes to Mic19 depletion alone, and this indicative of the paramount role of Mic19 in maintenance of cristae morphology (Li *et al*., 2015).

2.2.1.5. Mic13/*QILI*

Mic13 (encoded by *QIL1)* is an important bridging subunit of the MICOS complex, linking and stabilizing the core subunits (Mic60 and Mic10) of the MICOS (Guarani *et al*., 2016; Guarani *et al*., 2015). Loss of this subunit leads to accumulation of Mic60 and degradation of Mic10, thus destabilizing the mature MICOS complex (Guarani *et al*., 2016; Guarani *et al*., 2015). Alterations influenced by loss of Mic13 are characterized by destabilized cristae, defective mitochondrial respiration and aberrant mitochondrial morphology (Bódis *et al*., 2019).

Mutations in Mic13 are prevalent in mitochondrial encephalopathy with liver dysfunction (Guarani *et al.,* 2016). Symptoms include cerebellar atrophy, neurological impairment, lack of voluntary movement, microcephaly, muscle hypotonia and urinary excretion of 3-methylglutaconic acid in Individuals affected (Godiker *et al*., 2018). Conversely, Guarani *et al.* (2016) showed that absence

of *QIL1* is associated with disassembly of MICOS, mild cytochrome c oxidase defect, sensitivity to glucose withdrawals and aberrant cristae in patients' fibroblasts.

2.2.1.6. Mic26/*APOO*

Mic26 (encoded by *APOO*) is a paralogue of Mic27 and is responsible for stabilizing the Mic10 subunit and maintaining cristae morphology (Koob *et al*., 2015). The Mic26 and Mic27 subunits are indispensable for integration and stability of the remaining MICOS subunits. Furthermore, they hold an apoliprotein O-like lipid binding domain, and Mic27 has been shown to bind specifically to cardiolipin *in vitro* (Weber *et al*., 2013). According to existing literature, the mammalian Mic26 exist in three diverse isoforms: (I) a non-glycosylated 22 kDa mitochondrial protein, (II) an endoplasmic reticulum (ER)/Golgi-resident form and (III) a glycosylated and secreted 55 kDa protein (Koob *et al*., 2015). Mic26 interacts physically with numerous MICOS complex subunits (Mic60, Mic27 and Mic10) and spans the inner mitochondrial membrane. Overexpression of Mic26 induces mitochondrial fragmentation, promotes formation of reactive oxygen species (ROS) and results in impaired mitochondrial respiration (Koob *et al*., 2015). Conversely, downregulation of Mic26 induces a decreases mitochondrial oxygen consumption, but has no effect on the level of ROS and mitochondrial network morphology. Mutations in Mic26 are often prevalent in mitochondrial myopathy with lactic acidosis, cognitive impairment and autistic features (Beninca *et al*., 2021).

2.2.1.7. Mic27/*APOOL*

Mic27 (encoded by *APOOL*) is a paralogue of Mic26, and it plays a crucial role in mitochondrial cristae architecture (Weber *et al*., 2013). Expression of these paralogues in mammalian cells is highly coordinated, indicating a functional relationship among the two proteins (Koob *et al*., 2015). However, functions they perform in the MICOS complex vary since lack of Mic27 in yeast is associated with stronger phenotypes of cristae aberrations than Mic26 (Von der malsburg *et al.*, 2011). The precise functions of these two paralogues have not been fully elucidated, but recent studies shows that the interplay of MICOS complex and F_1F_0-ATP synthase is crucial for determining cristae architecture through Mic27 and Mic10 (Eydt *et al.*, 2017).

Mic27 and Mic26 are required cooperatively for the integrity of F_1F_0–ATP synthase complex and integration of F_1 subunits into the monomeric F_1F_0–ATP synthase, although the mechanism behind this requirement is unknown (Anand *et al.,* 2020). Moreover, these two subunits are indispensable for integration and stability of the remaining MICOS subunits. Mic27 and Mic26 contain an apoliprotein O-like lipid binding domain, and Mic27 has been shown to bind specifically to cardiolipin *in vitro* (Weber *et al*., 2013). Hoppins *et al*. (2011) showed that MICOS subunit

members have a strong negative genetic interaction with cardiolipin synthesis pathway enzymes which further suggests that cardiolipin and MICOS play a role in the maintenance of mitochondrial function.

A complexome profiling study conducted by Weber *et al.* (2013) revealed that Mic27 is a protein of the mitochondrial membrane facing the intermembrane space. Overexpression of Mic27 is characterized by mitochondrial fragmentation, reduced oxygen consumption rate (ORC) and aberrant cristae morphology. Conversely, its downregulation leads to impaired mitochondrial respiration as well as aberrant cristae morphology (Von der Malsburg *et a1FOl.*, 2011).

2.3. Mammalian MICOS, MIB complex and other interacting partners

The mammalian MICOS displays a higher degree of complexity and specificity compared to the yeast counterpart. Although a variety of the MICOS subunits have been previously described in both humans and yeast (Hoppins *et al*., 2011; An *et al*., 2012; Pfanner *et al.*, 2014; Hashimi., 2019), other MICOS subunits and interacting partners still need to be elucidated to aid medical scientists in disease diagnosis.

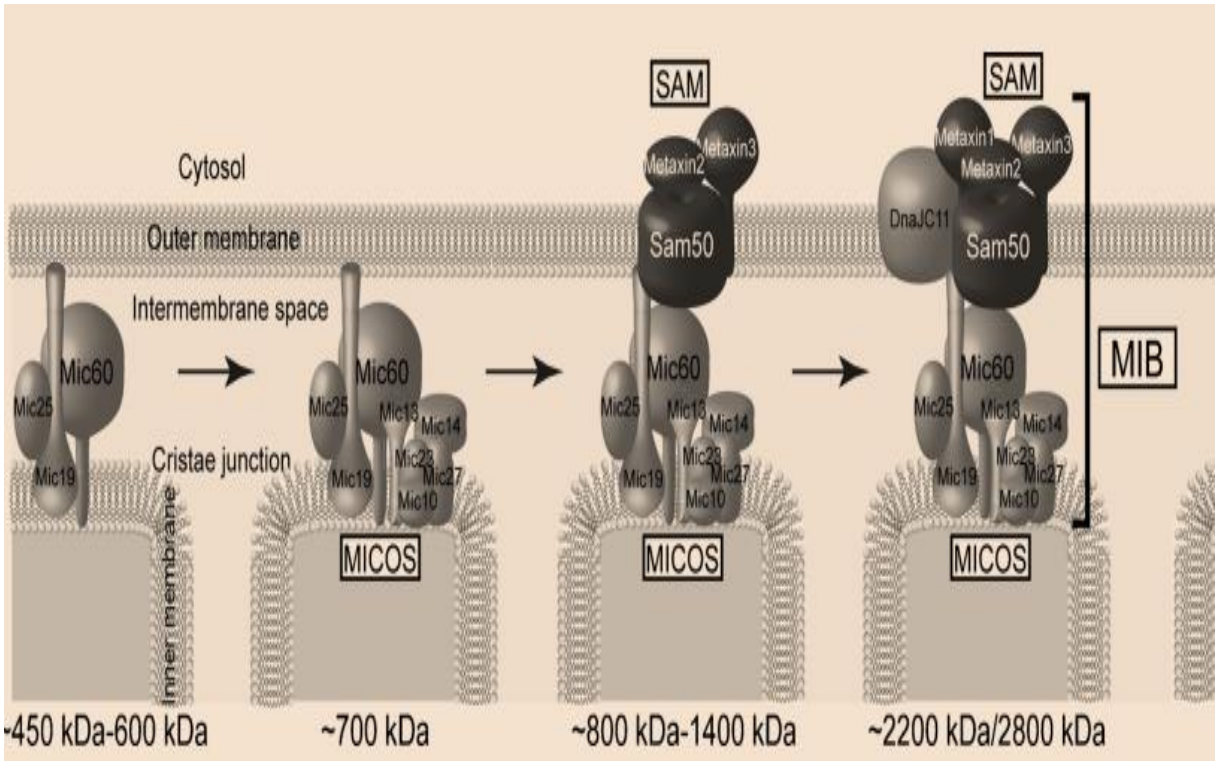

Figure 2-6: Assembly pathway of MICOS-MIB and other interacting complexes. (Adapted from Kozjak-Pavlovic., 2016). This pathway illustrates how the MICOS associates with SAM complex of the outer membrane to form MIB complex which connects the inner and outer membrane.

The MICOS complex is ~700 kDa in mass (Kozjak-Pavlovic., 2017) as depicted in figure 2-6 above. The full-sized MIB complex has been described to be more than 2 MDa (Huynen *et al*., 2015). The MIB complex is formed by the interaction of MICOS with the SAM complex of the OMM (Pfanner *et al*., 2004; Ott *et al*., 2015). The assembly of MIB potentially reflects diverse assembly stages. According to existing literature, the inner membrane MICOS complex interacts with the outer SAM complex to form the MIB (Ott *et al*., 2015). In addition to these findings, Ott *et al*., (2015) as found three main complex forms: (1) the membrane bridging subcomplex containing additional sorting and assembly machinery component 50 (SAMM50), metaxin 2 (MTX2) and MTX3, (2) MICOS complex containing all subunits, and (3) complete MIB with additional MTX1 and DNAJC11. The interaction between MICOS and MIB complexes plays an essential role as a signalling hub to allow for communication between the mitochondrial interior and the rest of the cell (Eramo *et al*., 2019). Moreover, these interactions and machineries involved in microtubule transport facilitate coordinated movement of the whole mitochondrion within the cell, possibly indicating direct mitochondrial transport to distinct subcellular locations for targeted energy production (Eydt *et al*., 2017). However, the stoichiometry of known and novel subunits and subcomplexes must be investigated to fully disclose and delineate the part played by each of these proteins in mitochondrial and MIB complex organization (Kozjak-Pavlovic., 2016).

2.4. Involvement of MICOS in OXPHOS regulation

Mitochondrial OXPHOS assembly is a sophisticated process that involves regulation of two evolutionarily distinct gene expression machineries: the circular mtDNA genome and nuclear genome (Tang et al., 2020). The former encodes 13 structural subunits of complex I, III, IV and V, 22 tRNA and two rRNA (Rackham and Filipovska., 2014; Tang *et al*., 2020). The nDNA then encodes supplementary genes required for mtDNA maintenance, replication, transcription, translation, post-translational modification, transport and assembly exclusively (Reinecker *et al*., 2009). Furthermore, regulatory mechanisms like activators that facilitate mitochondrial translation with the import of nuclear-encoded mitochondrial proteins as well translational plasticity are required for fine-turning protein synthesis to the nascent assembly of OXPHOS complexes (Tang *et al.*, 2020).

Assembly and functionality of the OXPHOS system is regulated by mitochondrial cristae structure (Baker *et al*., 2019). MICOS and OPA1 are among the large protein families that shape and regulate cristae dynamics (Cogliati *et al*., 2016; Baker *et al*., 2019). The former plays a pivotal role in inner membrane architecture and the latter controls remodelling of cristae during apoptosis.

The ETC and OXPHOS systems are integrated processes that bring about energy generation in the form of ATP (Lauridsen *et al*., 2019). Glucose is metabolised to pyruvate under aerobic conditions in the cytosol by glycolysis, and pyruvate is transported into the mitochondrial matrix where it is converted to acetyl coenzyme A (acetyl CoA). Additionally, fatty acids are esterified to fatty acyl CoA which undergoes β-oxidation to form acetyl CoA that feeds into the TCA cycle to generate reduced electron carriers, flavin and nicotinamide adenine dinucleotides ($FADH_2$ and NADH) (Goetzman and Prochownik., 2018).

The OXPHOS system is composed of 92 structural subunit genes, 79 of the genes are encoded by the nuclear genome and the other 13 are encoded by the mitochondrial genome. Complex I (NADH: ubiquinone oxidoreductase) consists of 44 subunits, namely 14 enzymatic principal subunits divided equally amongst both genomes, the remaining 30 subunits are nDNA encoded accessory subunits essential for maintenance of complex stability (Garrett and Grisham. 2013). Complex II (succinate: ubiquinone oxidoreductase) consists of subunits entirely encoded by nDNA. Complex III (ubiquinol: cytochrome c oxidoreductase) consists of 11 subunits of which 10 is encoded by nDNA and 1 by mtDNA. Complex IV (cytochrome c oxidase) consists of 3 subunits encoded by the mtDNA and 11 subunits encoded by the nDNA. Lastly, complex V (F0F1-ATP synthase) consists of 17 nDNA and 2 mtDNA encoded subunits (Wang *et al*., 2001; Vogel *et al*., 2006; Mick *et al*., 2011; Chinnery and Hudson., 2013).

A variety of diseases are linked to defects in the oxidative phosphorylation system, including neurodegenerative (Maynard *et al*., 2015; Desler *et al*., 2017), age related diseases in adults (Thomsen *et al*., 2018) and human metabolic diseases (Bhatti *et al.*, 2017). Moreover, impaired mitochondrial function such as reduced OXPHOS, enhanced generation of reactive oxygen species (ROS) and low ATP production are the major causes of many metabolic disorders (Bhatti *et al*., 2017).

2.5. Interplay of MICOS complex and phospholipids

MICOS functions as a principal determinant of the IMM assembly as it coordinates lipids and respiratory complexes to establish the IMM structure (Friedman *et al*., 2015). The biosynthetic enzymes of the IMM component known as cardiolipin (CL) display robust genetic connections with MICOS components, demonstrating that they work together and/ cooperate to maintain mitochondrial function (Hoppins *et al.*, 2011; Friedman *et al.*, 2015). In addition, phosphatidylethanolamine and mitochondria specific cardiolipin which are non-bilayer-forming phospholipids influence properties of the inner membrane by interacting with protein complexes and inducing the curvature of the membrane thus promoting fusion (Acehan *et al*., 2010).

Cardiolipin is a signature phospholipid of mitochondrial membranes and is implicated in vital mitochondrial processes and in OXPHOS in particular (Claypool and Koehler., 2012). The formation of cardiolipins is facilitated by two phosphatidyl-glycerol molecules connected by an extra glycerol moiety and holds an anionic charge. In addition, cardiolopin make up about 10% of phospholipids and are found in several part of the mitochondria (Osman *et al*., 2011). Several diseases including Barth syndrome (Schlame and Ren. 2006) and cardiac arrest (Saini-Chohan *et al*., 2009) are linked to cardiolipin deficiency. The former is characterized by reduced concentration and altered cardiolipin composition, moreover, patients often have variable clinical findings, including cardiac arrest, myopathy, neutropenia and growth reduction (Schlame and Ren., 2006). The latter is characterized by significant reduction of cardiolipin (Saini-Chohan *et al*., 2009)

Other functions like ADP/ATP stabilization carried by cardiolipin are completed by individual lipid species. Conversely, numerous functions are based on communal traits of these phospholipids, like their non-bilayer properties and conical shape (Gohil *et al*., 2005). Moreover, phospholipids are imperative for ordinary cristae architecture and mitochondrial function.

2.6. Implication of MICOS complex in human disease

Significant understanding into the regulation of gene expression in mitochondrial genomes has come from mutated genes that encode mitochondrial proteins leading to dysfunction in the mitochondria which is the causative agent of a variety of human diseases (Vafai and Mootha., 2012; Rackham and Filipovska., 2014). Disorders linked to mutations in the mDNA are becoming clinically prominent and are associated with many diseases in humans (Longley *et al*., 2005). A variety of mitochondrial diseases primarily result from mutations in either nuclear genes whose gene products locate to the mitochondrion, or genes encoded by the mtDNA (Haas *et al*., 2007). Moreover, secondary mitochondrial dysfunction can result from pharmacological agents or a host of other genetic disorders. A variety of neurological and muscular diseases are caused by mutations in the mtDNA (Longley *et al*., 2005). Mitochondrial diseases contribute to the cohort inborn errors of metabolism, which is estimated to affect 1 in 5000 people across a lifetime (Schaefer *et al.*, 2004; Falk *et al.*, 2009).

The MICOS is a vital protein complex that assists with the formation, maintenance and stability of mitochondrial cristae (Eramo *et al*., 2019). Loss of Mic60 is detrimental to cristae structure and leads to abnormal mitochondrial phenotypes including concentric cristae rings, swirls, loss of cristae, disconnected cristae tubules and detachment of cristae from the OMM in humans (Li *et al*., 2015). A single deletion of a MICOS subunit decreases the number of cristae junctions and alters the IMM structure to that characterized by extended, stacked and lamellar morphology (Hoppins *et al*., 2011). Cristae shape is essential to modulate the kinetics of chemical reactions and the structure

of protein complexes, thus alterations of mitochondrial cristae affect the structure of the OXPHOS system, resulting in impaired cellular metabolism and growth (Cogliati *et al*., 2016). Although mitochondrial cristae aberrations are associated with a variety of human diseases, it is unclear whether such changes are the primary cause or a contributing factor to disease progression (Eramo *et al*., 2019). However, it remains unclear which mechanisms are involved in cristae aberrations and mitochondrial dysfunction observed in many human diseases, as a result of mutations in MICOS subunit genes. Despite this, human diseases linked to MICOS core subunits and its peripheral interactions are beginning to emerge. The subsections that follow below elucidates a few of the diseases that relate to alterations in the MICOS complex subunits or its other interacting partners.

2.6.1. Parkinson's disease

Parkinson's disease (PD) is a common neurodegenerative movement disorder and was initially described by James Parkinson in the 1800s PD is associated with loss of dopaminergic neurons within the substantia nigra[4] (Darshi *et al*., 2010). Individuals affected with PD display a variety of clinical symptoms including slow movement (bradykinesia), rigidity and movement tremors at rest (Ritz *et al*., 2016). Several developments have been made to characterize the pathology, discriminate clinical signs, and improve therapeutic treatment since recognition of this neurological disorder over two centuries ago (Cieri *et al*., 2017; Delamarre and Maissner, 2017; Tsai *et al*., 2018). However, the exact causes of this disease remain unknown and there is no cure nor available neuroprotective therapies to delay disease progression. Comprehensive understanding of the aetiology of PD progression is imperative in development of novel therapeutics for disease treatment.

Growing evidence implicates Mic60 in the pathogenesis of PD (Van Laar *et al*., 2019). Pathological hallmarks of PD include impaired mitochondrial respiration, morphology and fission/fusion/transport dynamics which are linked to Mic60 (Bose and Beal., 2016). Moreover, Mic60 cooperates with other proteins directly involved in general regulation of mitochondrial dynamic processes including those associated with neurodegenerative diseases like PD (Darshi *et al*., 2010).

Laboratory research and epidemiological studies have been conducted to discover the potential causes of this prevalent disease (Khandhar and Marks, 2007; Delamarre and Maissner, 2017). Existing ideology proposes that a combination genetic preposition and environmental exposure account for variety of PD cases although the underlying mechanism remains elusive (Ritz *et al*.,

[4] Part of the brain that regulates movement

2016). Multiple biological pathways that promote pathogenesis of PD, many of which converge on mitochondrial function, have been identified through epidemiological and genetic studies (Cieri *et al*., 2017).

According to Van Laar and Berman, (2013) mitochondrial dysfunction is a major contributor to pathophysiology of PD, with impaired mitochondrial morphology, respiration and fission/fusion/transport dynamics all linked with PD. The connection between mitochondria and PD is demonstrated by a heritable form of the disease, wherein monogenetic PD-causing alterations in nuclear expressed proteins such as PTEN-induced kinase 1 (PINK1), parkin, LRRK2 and alpha-synuclein have shown to affect mitochondrial function (Sanders *et al*., 2014).

A rare coding variant in the *IMMT* gene coding for Mic60 which is one of the two core subunits of MICOS has been discovered in PD (Tsai *et al*., 2018; Van Laar *et al.*, 2019). These subunits of MICOS also interact with proteins directly involved in the general regulation of dynamic mitochondrial processes as well as those associated with neurodegenerative diseases which places it in a unique position to regulate PD-relevant stress (Tsai *et al*., 2018). According to existing literature, overexpression of Mic60 elevates mitochondrial function and protects against PD related dopamine and rotenone-induced cell arrest in the human neuroblastoma cell lines (SH-SY5Y) (Van Laar *et al*., 2016). A study conducted in PINK1 knockouts Drosophila further disclosed that Mic60 overexpression abrogates mitochondrial aberrations and symptoms associated with PD (Tsai *et al*., 2018).

2.6.2. Diabetes mellitus and obesity

Both obesity and diabetes mellitus are long term disorders affecting millions of people around the globe. These disorders are both considered substantial risk factors for progression of late onset Alzheimer's disease (Baker *et al.*, 2011) and cardiomyopathy (Rigotto and Basso., 2019). Diabetes is a chronic disease comprising an early onset disease denominated type I which results from complete failure of the pancreatic islet β-cells to produce insulin, and a progressive disease denominated type II (T2D) which is characterized by initial elevated insulin secretion thus resulting in islet stress and loss of glucagon (Rigotto and Basso., 2019). Type I diabetes requires exogenous insulin administration for survival and the type II diabetes is treated often by prescribed medication, while the conditions may differ between individuals based on lifestyle and diet.

The fundamental origin of obesity is energy imbalances between calories consumed and used as a result of elevated intake of food rich in energy and reduced physical activity (Rigotto and Basso. 2019). According to Liesa and Shirihai. (2013), the hallmarks of obesity include decreased mitochondrial number and impaired mitochondrial structure and function in tissues. Aberrations in

mitochondrial structure and MICOS subunits in diabetic and obese patients have been implicated in metabolically active tissues of individuals such as skeletal muscle, liver, fat and heart (Wilcox., 2005).

The skeletal muscle plays a pivotal role in glycolysis and OXPHOS for energy production and accounts for ~ 60-70% of insulin-stimulated post-prandial uptake of glucose (Wilcox., 2005). Over 80% of the total mitochondrial mass in skeletal muscles is made up of the cristae which exhibits high plasticity to meet energy demands (Nielsen *et al*., 2017). Mic60 is identified as a crucial MICOS subunit that helps the skeletal muscles to perform their routine functions. Dillon *et al*, (2019) analysed Mic60 transcripts in skeletal muscles and found that it is increased by exercise following an extended period of bedrest. Conversely, a reduction in mitochondrial function in obese and diabetic individuals is linked to loss of cristae (Kelley *et al*., 2002). Another study conducted by Baseler *et al*, (2011) showed a reduction in Mic60 in hearts of diabetic mice while transgenic cardiac-specific Mic60 overexpression normalizes cristae structure and mitochondrial energy output and weakens the cardiac dysfunction induced by diabetes.

2.6.3. Barth syndrome

Barth syndrome is a rare X-linked autosomal recessive condition caused by mutations in the *Tafazzin* gene, an acyltransferase in the mitochondria that responsible for generating essential cardiolipin which is enriched predominantly in the IMM (Schlame and Ren., 2006). Clinical symptoms of affected patients include reduced concentration and altered cardiolipin composition. Ikon and Ryan, (2017) revealed a reduced cardiolipin from cultured fibroblasts and tissue samples of affected individuals, which is linked to loss of cristae structure and mitochondrial dysfunction. Moreover, the mitochondrial phenotype characterized by onion-like structure observed in MICOS deficient models is also common in skeletal and cardiac muscle of inducible *tafazzin* gene knockout mice that also exhibit a loss in cardiolipin (Acehan *et al*., 2010).

A recently conducted complexome study in mitochondria isolated from cultured fibroblasts of Barth syndrome patients revealed a rise in total MICOS and MICOS-MIB complexes, although with an unusually lesser molecular mass compared to the normal MICOS complex (Van Strien *et al*., 2019). However, the cause of this altered migration pattern remains unclear, and cardiolipin is not linked with any direct role in facilitating MICOS assembly.

2.6.4. Cancer

Cancer is a leading cause of death globally, both head and neck cancer squamous cell carcinoma (HNSCC) rank as 6th most common cancer worldwide amounting to over 650 000 cases and causing 350 000 deaths annually (Chadler *et al.,* 2020). Alcohol consumption and tobacco usage are the

major risk factors linked to head and neck cancer. Compared to women, men are most likely to be diagnosed with oral cavity cancer (Bray *et al*., 2018). Mitochondria of cancer cells undergo considerable modification to support their uncontrolled growth, proliferation, and survival (Vyas *et al*., 2016). In addition, mitochondrial structure and function can be altered further by oxygen levels, cellular stress response and nutrient availability in the tumour microenvironment (Brat *et al*., 2018). The expression of Mic60 is prevalent in several mammalian tissues and novel research highlighting the significance of this IMM protein continues to emerge, however, it also generates data that is conflicting about whether Mic60 has negative or positive influences. A prominent example is the study conducted by (Nordgaard *et al*., 2008) and (Pfohler *et al*., 2007), where Mic60 expression increased in cancer patients in later stages of disease.

2.7. Utility of Caenorhabditis elegans (C. elegans) in mitochondrial research

The nematode *C. elegans* has become a major model to unravel mitochondrial dysfunction since its discovery by Sydney Brenner over the past four decades (Brenner. 1974). Compared to other commonly used model organisms like mitomice (Kazuto *et al*., 2001) and *Saccharomyces cerevisiae* (Gaiever *et al*., 2002). *C. elegans* are small and less complex to culture in laboratory settings (Brenner. 1974). Their small size, high reproductive rate as well as low-cost maintenance affords researchers the ability to use more individual worms for testing. Moreover, their transparent body structure is an added advantage to study internal mitochondrial structure (Haroon *et al*., 2018). *C elegans* also share 80% genetic homology with humans in terms of genes that are linked with diseases (Gaiever *et al*., 2002).

Most of the current knowledge involving MICOS complex have been performed on *Saccharomyces cerevisiae* (Weber *et al*., 2013; Anand *et al*., 2016). The use of *C. elegans* in mitochondrial research, particularly MICOS is emerging (Mun *et al*., 2010; Head *et al*., 2011) in which Mic60 homologs were investigated in relation to cristae morphology. The utility of this nematode in mitochondrial research is rooted in the highly conserved nature of mitochondrial structure, composition and function across evolution (Polyak *et al*., 2011; Haroon *et al*., 2018). Recent developments in *C. elegans* shows positive outcomes as a mitochondrial disease model considered *in vivo* (The *C. elegans* Deletion Mutant Consortium 2012; Mun *et al*., 2010; Haroon *et al*., 2018).

Discovery and husbandry of *C. elegans*

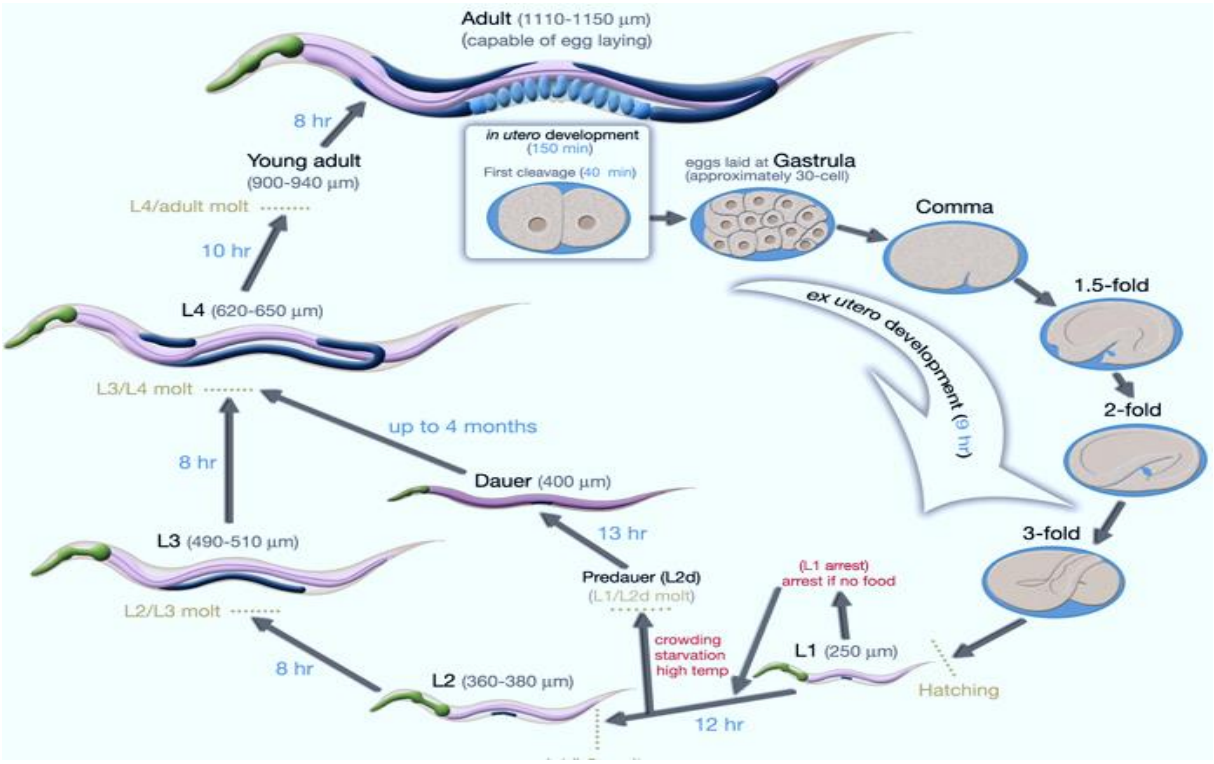

Figure 2-7: *C. elegans* life cycle at 20°C. Approximately 300 eggs are produced by an adult hermaphrodite. There are four larval stages (L1-L4) post embryogenesis. Image adapted from (Altun and Hall 2006).

As illustrated by figure 2-7 above, the nematode *C. elegans* undergoes four stages in its life cycle (Atun and Hall 2006; Muchiol *et al.*,2009). In the case of prolonged exposure to harsh environmental conditions like high temperature or depletion of nutrients in the medium *C. elegans* arrest at the dauer stage (Riddle *et al*., 1997; Muschiol *et al*., 2009). The nematodes completely stop developing and reproducing during the dauer stage, which is L2, once the conditions are improved (e.g transfering into fresh medium containing sufficient nutrients) the L2 staged nematodes in the dauer stage will develop into L4 stage. Recognition of long living mutants and the ability to enter the dauer stage, together with relatively short life cycle and adult lifespan make *C. elegans* a suitable model organism to study aging (Kennyon, 1993). In addition, functional genes in *C. elegans* can be analysed by hindering their expression using generic approaches like RNAi. The RNAi can be introduced by feeding *C. elegans* with bacteria expressing gene-specific dsRNA, the dsRNA are then processed by RNAi machinery into small interferring RNA (siRNA) that mediateds gene silencing once the nematodes ingest the dsRNA (Muschiol *et al.*, 2009).

The N2 Bristol strain is widely used in most research as a WT strain. This strain was collected from mushroom compost in 1951 in Bristol, England (Brenner, 1974; Sterken *et al*., 2015). *C. elegans* can be grown at temperatures between 16 and 25°C in either liquid or solid medium depending on experimental requirements, completing their life cycle two times faster when grown at higher temperature. In both cases they are fed a standardized *Escherichia coli* strain (OP50) used specifically for nematode culture in labs globally (Head *et al*., 2010; Nigon and Felix. 2015). All wild type and over 3000 mutant strains can be acquired at the *Caenorhabditis* genetic centre (CGC) (http://www.wormbook.org/chapters/www_strainmaintain/strainmaintain.html)

Recombinant progeny are generated, and their attributes are measured to elucidate the underlying genetic basis of complex attributes (Gaertner and Phillips.,2010). *Saccharomyces cerevisiae* is widely used as a powerful eukaryotic model in quantitative genetics (Bloom *et al*., 2013). However, utility of the nematode *C. elegans* is unmatched (Gaertner and Phillips., 2010). They are characterized by a rapid lifespan (about 76 hours at 20°C) and produce approximately 300 progeny per individual hermaphrodite. Moreover, its genome is well-annotated, they can be frozen and transgenic strains are obtained via CGC and other academic institutions globally.

General considerations when working with *C. elegans*

Figure 2-8: Fluorescent image of N2 strain. This strain is used globally as a wild type.

Due to their relatively small size (~1 mm long), careful handling is imperative to conserve *C. elegans* samples prior to the experimental procedures (Kovacs., 2015). Moreover, the body of *C. elegans is* covered by a tough cuticle often making it impenetrable to fixate for microscopic

analysis (Krenger *et al*., 2020) and isolation of mitochondria for biochemical analysis (Grad *et al*., 2007). Many researchers often cut the nematodes into pieces to allow fixate to penetrate (Sigmond *et al.*, 2008). To overcome the problem of busting the cell to extract mitochondria, sonication or glass beads method was employed (Yang *et al*., 2017). Synchronization (section 3.3) is an added advantage that affords researchers the possibility of performing high-throughput experiments such as sequencing, microarrays, RNAi screens utilizing nematodes at a specific stage (Porta-de-la-Riva *et al*., 2012).

C. elegans can communicate environmental conditions by producing pheromones, which are small sensory molecules that evoke responses in members of the same species (Schroeder 2006). Modern *C. elegans* research demonstrates the production of putative pheromones in ovulating hermaphrodites (McGrath and Ruvinsky., 2019). Such sensory molecules are ubiquitous in higher order life forms and examples have been shown in fungi (Bolker and Kahmann., 1993), bacteria (Cook and Federle., 2014) as well as in animals (Brennan and Zufall., 2006)

2.7.3. Advancements in *C. elegans* research

Over two decades ago, a group of researchers sequenced the genome of *C. elegans*, and this project led to the discovery of 19,000 genes with over 40% significant matches of the predicted protein products in other organisms (The *C. elegans* sequencing consortium 1998). This nematode was the first higher order organism to be fully sequenced after viruses, yeast and several bacteria. The available protein sets from *C. elegans* were compared with *Saccharomyces cerevisiae, Escherichia coli (E. coli)* and *Homo sapiens* to highlight qualitative variation in the predicted protein set. The *C. elegans* genetic sequencing consortium found significant matches among smaller genomes and a large fraction of their protein while large genomes had a high number of matching proteins. Furthermore, the authors revealed more similarities between the nematodes and humans than any other species.

Fourteen years post sequencing, another group of scientists confirmed the presence of 20,377 protein coding genes in *C. elegans* with 6467 genes linked with molecular lesions characterized as either deletions or null mutations (The *C. elegans* Deletion Mutant Consortium 2012). The deletion mutant consortium has three laboratories that were established with the sole purpose of screening for deletions by exposing nematodes to a mutagen and using polymerase chain reaction (PCR) DNA amplification to identify deletions at target loci. Recently, Haroon *et al*. (2018) used *C. elegans* to develop a model for mtDNA diseases. Their findings confirmed that the nematodes display the

major hallmarks of mtDNA in humans, including loss of respiration, shortened life span, reduced neuromuscular function as well as mtDNA instability.

2.7.3.1. Lipidomics in *C. elegans*

Lipidomics is a metabolomics branch that aims to characterize lipophilic/apolar metabolites in biological systems (Castro *et al*., 2012; Wang *et al*., 2017). Untargeted metabolic profiling can be used as a downstream system to identify perturbations in biochemical networks (Dun *et al*., 2008). Moreover, untargeted metabolomics is vital to produce large amount of data due to its ability to provide unbiased an outlook of detectable metabolites (Yang *et al*., 2017). Metabolic networks can respond rapidly to perturbations compared to protein and gene transcripts (Dun *et al.,* 2008; Holmes *et al*., 2008). Substantial developments in nuclear magnetic resonance (NMR), high-performance liquid chromatography (HPLC) and mass spectrophotometry (MS) make the detection of thousands of compounds possible (Masson *et al.,* 2010; John *et al.,* 2016).

The nematode *C. elegans* offers a unique platform to examine aspects of genetics, aging as well as developmental biology (Watson *et al*., 2013). They possess common standards of biological research as they are simple to maintain in laboratory set up, are sustainable for high quantity screens and have a short lifecycle (see chapter 3 below), moreover, they grow in chemically defined medium (NGM plated with OP50) and can be labelled with stable isotopes thus making them a perfect model organism for metabolomics studies (Szewczyk *et al*., 2006; Yang *et al*., 2017). Genetic effects can be easily analysed in these nematodes due to availability of RNA interference (RNAi) libraries and large mutant repositories (Thompson *et al.,* 2015). In addition, generation of genetic reference populations in *C. elegans* possesses natural genetic variation that is at a similar level to that in human populations. Measurement of metabolites in *C. elegans* tissues are limitted (Witting and Schmitt-Kopplin., 2016). Metabolites analyses in *C. elegans* are mainly based on NMR spectroscopy (Yang *et al*., 2006; Watt and Ristow., 2017) and gas chromatography-mass spectrometry (GC-MS) (Geier *et al*., 2011; Watts and Ristow., 2017). However, these methods are disadvantaged by the need for large sample preparations (~8000-120,000 worms) and limited metabolite number that can be quantified (Buttlet *et al*., 2013; Wang *et al*., 2017). Hastings *et al*. (2017) recently developed a method that permits measurement of hundreds of metabolites including amino acids (AA) and fatty acids (FA) using targeted metabolomics with liquid chromatography (LC) from a sample containing as little as ~2000 nematodes.

2.8. Classification of methods mutagenesis in C. elegans

The nematode *C. elegans* is amenable to genetic manipulations, thus mutations can be easily induced into these organisms for application of forward and reverse genetics (Sin *et al*., 2014). Both forward and reverse genetics are dependent upon mutations to identify and distinguish genes of interest. A temporary association between phenotype and mutation can propose wild-type gene action mechanisms and can be utilized for diagnostic prediction (Fire *et al*., 1998). There are three commonly used mutagenesis strategies; (1) genome wide mutagenesis (forward genetics) which is characterized by determining the genetic basis responsible for a phenotype (Brenner, 1974; Chaudhuri *et al*., 2011), (2) target selected mutagenesis (reverse genetics), which is characterized by a mutagenized genome but mutations in a single known gene are screened (Edgley *et al*., 2002) and (3) gene targeted mutagenesis, in which only a single gene is targeted for mutagenesis (Friedland *et al*., 2013; Dickinson *et al*., 2013). Common effects of mutations can be seen in the phenotypes of the nematodes, examples are defects in egg laying, dauer formation etc.

2.8.1. Genome wide mutagenesis

This strategy of mutagenesis can be grouped into (1) chemical mutagenesis, (2) radiation mutagenesis, and (3) transposon insertional mutagenesis. The text below elucidates the fundamental application most frequently utilised methods.

2.8.1.1. Chemical mutagenesis

Chemical mutagenesis offers and easy technique of introducing germline mutations at high prevalence (Thompson *et al.*, 2013). The prevalence of mutation is high thus, to reach saturation, a relatively low number of haploid genomes are interrogated. Ethyl methane sulfonate (EMS) is the most employed type of chemical mutagenesis in *C. elegans* (Jansen *et al*., 1997; Chaudhuri *et al*., 2011; Sin *et al.,* 2014). Other variety of chemical mutagenic spectra include N-ethyl-N-nitrosourea (ENU) (De Stasio and Dorman., 2001), trimethylpsoralen (TMP) (Barstead and Moerman., 2006) etc. A brief description of EMS as a common method follows below:

Ethyl methane sulfonate (EMS)

As an alkylating agent, EMS adds a -CH3-group to guanine thus resulting in the formation of O^6 - ethyl guanine (Chaudhuri *et al*., 2011). The altered guanine (G) pairs improperly with thymine (T) instead of cytosine (C) resulting in a mismatch mutation that undergoes subsequent replication (Bakhoum *et al*., 2014). In a nutshell, mutagenesis is biased towards complementary base pairing transitions which often results in the formation of stop codons (Flibotte *et al*., 2010). Moreover, EMS reacts with N-3 position adenine and N-7 position guanine, but these variations do not give rise to substantial amounts of mutations (Hartman *et al*., 2014). EMS mutation spectrum has been

studied in variety of disease models and has recently gained popularity in *C. elegans* (Flibotte *et al*., 2010; Hartman *et al.,* 2014). Mutations are induced in a healthy germ line by exposing L4/ adult stage nematodes to a mutagen.

2.8.2. Target selected mutagenesis

Several methods have been developed to induce random mutations and alterations in chromosomal structure. The purpose of target selected mutagenesis is to create a library comprising pools of animals that are mutagenized to ease screening of DNA lesions (Lesa., 2006). Construction of a library usually involves ~600,000 randomly mutagenized hermaphrodites (Chen *et al*., 2016). Gravid mutagenized nematodes are bleached to allow L1s to hatch in M9 medium overnight. L1 are subdivided into 1,152 subcultures of 500 nematodes each. 20% of the nematodes per plate are washed off for isolation of genomic DNA post two generations of self-fertilization (Lesa., 2006; Kutscher and Shaham., 2015). This method of mutagenesis can be utilized in mutation identification in a specific gene from genome that is randomly mutagenized (Edgley *et al*., 2002). It includes standard mutagenesis using ultraviolet (UV)/ trimethylpsoralen (TMP) or EMS, followed by screening using polymerase chain reaction (PCR) or other sophisticated methods to recognize animals carrying lesions in the genes of interest. In the text below, PCR is being discussed as a popular reverse genetics method.

2.8.3. Gene targeted mutagenesis

Gene function has been studied extensively in a variety of model organisms through gene targeting using homologous recombination (Kutscher and Shaham., 2014). Homologous recombination is dependent upon the cell capability to repair dsDNA breaks, which gene targeting utilizes to permit endogenous target replacement with an exogenous construct containing sequences homologous to the target (Rafael *et al.,* 2010). The text below describes CRISPR/Cas9 as a commonly used method for rapid gene recovery.

2.8.3.1. CRISPR/Cas9

The CRISPR (clustered regularly interspaced short palindromic repeats)- Cas (CRISPR-associated) technology is a common method for efficient and targeted genome in several model organisms including *C. elegans* (Ausubel *et al*., 2001; Kutscher and Shaham., 2014). Various CRISPR/Cas9 approaches have been recently developed to improve genome engineering using two dsDNA break repair systems; (1) non-homologous end joining (NHEJ) and (2) homologous recombination (HR) (Lok., 2019). The former is characterized by recruitment of KU proteins heterodimer DNA ends accompanied by DNA-PKcs; the latter utilizes extensive homology. Single guide RNA (sgRNA) and codon-optimized nuclear-localized (NLS) Cas9 proteins may be introduced using a variety of

methods into the germ line i.e DNA plasmid (Dickinson *et al*., 2013). PCR-based methods as well as phenotype screening are employed to isolate mutants (Kutscher and Shaham., 2015).

2.9. Problem statement

Mitochondrial cristae aberrations are linked with impaired mitochondrial dysfunction and toxic accumulation of reactive oxygen species (ROS), which are pathological hallmarks of many human diseases. The mitochondrial contact site and cristae organizing system (MICOS) is at the center of mitochondrial morphology management. Loss of one of the core subunits of MICOS (Mic60) is detrimental to cristae structure and may lead to irregular mitochondrial phenotypes. In addition, proteins in the mitochondrial inner membrane such as optic atrophy (OPA1) and ATP synthase subunits have been implicated in the control of morphology, but the mechanism by which cristae morphology is established remains an open question of research. Therefore, it is imperative to better understand the machineries involved in mitochondrial cristae architecture to unravel mitochondrial dysfunction.

Most research done in mitochondrial dysfunction covers constituents of the oxidative phosphorylation (OXPHOS) system [Complex I-IV of the electron transport chain and (ETC) and ATP synthase (complex V)]. Association of MICOS to mitochondrial dysfunction is poorly investigated which delays the diagnosis and treatment of mitochondrial diseases in general. Understanding the interplay between the ETC and MICOS to maintain and regulate mitochondrial function, and how deleterious changes in MICOS subunits affect these factors, could help to identify the underlying mechanisms of disease aetiology and progression, and offer up new targets for therapy.

Most of the current knowledge involving the MICOS complex has been performed on *Saccharomyces cerevisiae* (Weber *et al*., 2013; Anand *et al*., 2016). This study will investigate the effects of MICOS subunit deficiencies on cristae morphology, mitochondrial respiration and function in *C. elegans*. The utility of this nematode in mitochondrial research is rooted in the highly conserved nature of mitochondrial structure, composition and function across evolution (Polyak *et al*., 2011; Haroon *et al*., 2018).

2.10.1. Aim

The aim of this study was to extensively characterize the phenotypes, mitochondrial morphology, and function of a Mic27 deficient *C. elegans* strain (VC1196) and compare it to the wild type (WT) N2 strain.

The VC1196 was generated as part of the international *C. elegans* Gene Knockout Consortium study (The C. elegans Deletion Mutant Consortium, 2012), and has not been characterised to any extent. The N2 Bristol strain has previously been used as wild type/background strain in many studies previously and is almost fully characterized.

2.10.2. Hypothesis

Existing research suggests that the coordination of MICOS complex with respiratory complexes and lipids establishes mitochondrial inner membrane architecture as assembly of two MICOS subunits (Mic27 and Mic10) is dependent on respiratory complexes and mitochondrial lipid cardiolipin. Thus, we hypothesize the MICOS subunit deficiency present in our KO strain will lead to aberrant cristae morphology, decreased mitochondrial OXPHOS enzyme activity and thus respiration, and a diseased phenotype.

2.10.3. Research objectives

I. Confirm the genotype of VC1196 strain, using PCR with agarose gel electrophoresis and by determining the relative expression of nuclear encoded genes from *C. elegans* strain.
II. Perform transmission electron microscopy (TEM) to visualise mitochondrial cristae morphology from MICOS *C. elegans* VC1196-strain compared to *C. elegans* WT-strain.
III. Analyse the impact of cristae morphology changes on lipid metabolism using untargeted lipid metabolism analyses on MICOS *C. elegans* VC1196-strain compared with *C. elegans* WT-strain.
IV. Perform respiratory analyses as a measure of mitochondrial function in MICOS *C. elegans* VC1196-strain, compared with *C. elegans* WT-strain.
V. Perform OXPHOS enzyme activity assays in MICOS *C. elegans* VC1196-strain compared to *C. elegans* WT-strain.
VI. Perform phenotypic characterisation assay of the MICOS *C. elegans* VC1196-strain compared to *C. elegans* wild type (WT) strain.

2.10.3. Experimental design

The primary step in this project was to acquire an import permit for the strain of interest from the Caenorhabditis genetic center (CGC) (https://cgc.umn.edu/). Upon recept, strains were transferred into nutrient growth medium (NGM) seeded with OP50 *E. coli* strain and incubated at 20°C until required stage (L4). The initial step was to confirm the genotypes of the nematodes as per the first of objective of this study. This was followed by biochemical characterization (objective II, III, IV and V) and lastly phenotypic characterization (objective VI). Live nematodes were used for phenotypic characterization and crude mitochondria was used for the biochemical characterisation assays, while the mitochondrial ultrastructure was determined from L4 staged nematodes dissected as described in section 3.4 of the current study.

The biochemical characterization included determination of (1) oxygen consumption rate in intact nematodes using 02k Oroboros instrument (Oroboros Instruments GmbH, Innsbruck, Austria), (2) OXPHOS enzymatic assay (Complex I, Complex III and Complex IV) using 96 well Synergy ^{HT} multi-detection microplate reader (Biotek ® Instruments), (3) mitochondrial ultrastructure morphology using transmission electron microscopy (Thermofisher) and (4) untargeted lipid metabolism using gas chromatography time of flight mass spectrophotometry (GC-TOF-MS). The generation of nematodes was maintained by continuous transfer (chunking) into new plates containing sufficient nutrients every 10 days. All experiments were performed with live age synchronized (L4) staged nematodes with the exception of the OXPHOS enzyme activity assay and untargeted lipid metabolism which were conducted on isolated mitochondria. The flow diagram below (Figure 2-9) shows the experimental design.

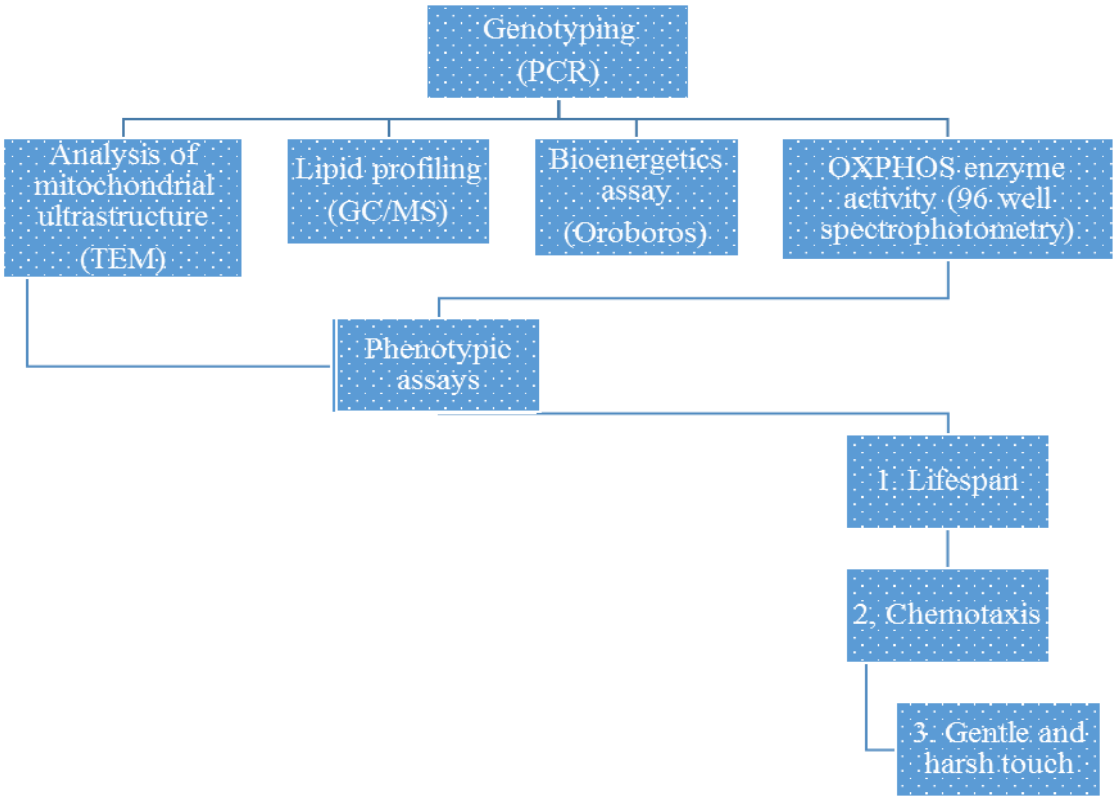

Figure 2-9: Schematic representation of experimental design. Post genotyping, the mitochondrial ultrastructure was determined using transmission electron microscopy. The other biochemical analyses were performed using *C. elegans* enriched mitochondrial fractions with the exception of bioenergetic assay, where basal respiration was measured on 150 L4 staged live nematodes per generic strain. The phenotypic characterization was achieved using of 50 L4 staged live nematodes.

3. CHAPTER THREE: MATERIALS AND METHODS

Chapter summary

This chapter gives a detailed description of methodologies followed to achieve the aims and of objectives of this study. All the materials as well as data tools used are given and explained, the list follows the schematic representation in chapter 2 (Figure 2-9). This study was regarded as a category 0/ no risk study in accordance with the NWU ethics committee (certificate attached in annexure A). Details of ethics follow immediately after this section. All the experiments were performed at the North-West University Potchefstroom campus within the period of September 2021 to February 2022. All the strains were acquired from the Caenorhabditis genetic center (CGC) https://cgc.umn.edu/strains?vt=all at the University of Minnesota in the United States of America (USA). Section 3.3 gives details of all the important tools for *C. elegans* maintenance, the sections thereafter are steps followed to achieve the aims and objectives of this study. Under each method, a summary of the principle as well as the reason for choice off the specific method is given. All the medium and extractions were prepared under strict sterile conditions to prevent bacterial contamination although *C. elegans* can be maintained axenically. The Standard Operating Procedures (SOPs) used are attached in the annexure section. The recipes of maintenance of *C. elegans* are listed in table 3-1.

3.1. *C. elegans* Strains of interest

The strain selected as a disease model (VC1196) in this study and the wild type strain (N2 Bristol) were acquired from the *Caenorhabditis* genetic center (CGC) https://cgc.umn.edu. The VC1196 strain has an apparent homozygous lethal deletion chromosome balanced by *dpy-1*, heterozygotes are wild type. Moreover, VC1196 contains gene *K02F3.11* which is located on chromosome III. The human homologue of this gene is *moma-1* as seen in figure 3-1 below.

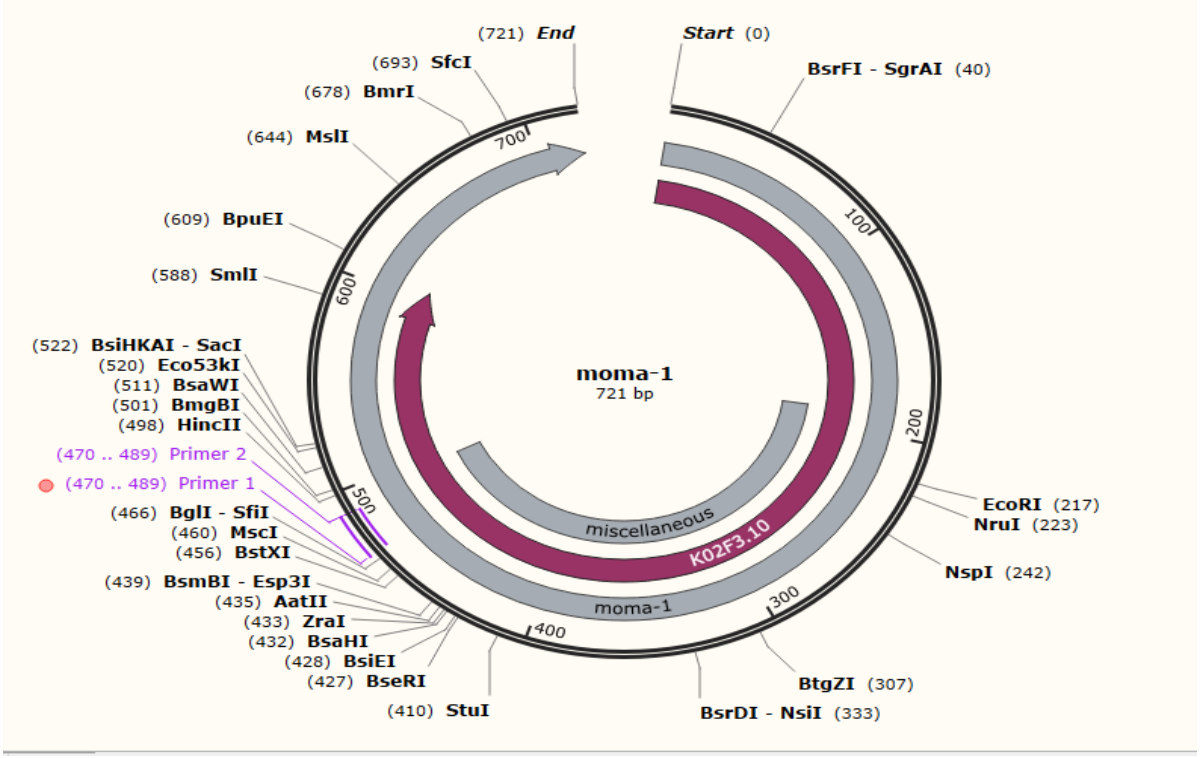

Figure 3-1: *K02F3.11* Snap gene with primes sets and other enzymes. The base pairs of the gene of interest (*moma-1*) as indicated with the cutting sites of specific restiction enzymes**.**

Recent developments in nematode *C. elegans* research shows positive outcomes as a mitochondrial disease model considered *in vivo* (The *C. elegans* Deletion Mutant Consortium 2012; Mun *et al*., 2010; Haroon *et al*., 2018). Thus *C. elegans* strains harbouring mutations related to mitochondrial disease demonstrates all major hallmarks of mitochondrial diseases in humans, including loss of respiration, reduced neuromuscular function, elevated instability and shortened lifespan. To accomplish the objectives of this study, we used the N2 WT-strain with the VC1196 strain which harbours a mutation in the *moma-1* gene (figure 3-1), an ortholog of mammalian *APOOL* which encodes for Mic27. As seen in Table 2-1 in chapter 2 of this study, Mic27 plays a pivotal role in stabilizing Mic10 and consequently cristae morphology (section 2.2.8). According to existing literature, mitochondrial aberrations in *moma-1* mutants resemble those with mitochondrial fission mutants in the muscle cells of *C. elegans* (Mun *et al*., 2010). The mutants are characterized by thin connections and localized swelling in the mitochondria. Moreover, *moma-1* mutants are characterized by a relatively short mitochondrion.

3.2. Ethics

The NWU Animal research ethics committee (AnimCare) provided the ethics clearance prior to the commencement of this study (NWU-00410-21-A5) in March 2021 (Certificate attached in annexure A). The imported nematodes strains (VC1196 and N2 Bristol) were obtained through DAFF

(No:13/11/30/2/0-202007003664) under section 20 Animal Disease Act of 1984. All the nematodes were cultured on the same conditions throughout the completion of this project: Nematodes were incubated at 20°C in a nutrient growth medium (NGM) plate containing OP50 *E. coli* as a food source.

- Nematodes were transferred by 'chunking' to new plates containing fresh nutrients every 10 days to sustain the strains.
- Nematodes were synchronized for most of the experiments performed to minimize biased results.

3.3. Materials and reagents

Acetyl CoA (Sigma, #10101907001), Agarose (Merck, #9012-36-6), Aluminium foil, ATP (Sigma, #A2383), Autoclave machine, 100 mm petri dish (Isotron SA, CAT no: IN-069), Bacteriological agar (Melford laboratories, CAT no: S0520), BCA (Sigma-Aldrich #QPBCA), Benzaldehyde (Sigma-Aldrich, 100-52-7), BSA (Sigma-Aldrich #9048-46-8), Bleach solution (See table 3-1 for recipes), Casein peptone (Biolab #CAP10500), CaCl2. 2H2O (Labchem # 10035-04-8), *C. elegans* strains (CGC https://cgc.umn.edu/strains?vt=all) N2 Bristol & VC1196, Chloroform (Merck, # 1024444000), Cholesterol (Sigma-Aldrich# C3045), CuSO4.5H2O (Sigma-Aldrich # 7758-99-8), Cytochrome C (Sigma, #C7752), 1.5 ml centrifuge tubes (Thermofisher #34484PK), 15 ml centrifuge tubes (Thermofisher # 339650), DMSO (Sigma, #C6164), DTNB (Sigma, #D8130), *E. coli* OP50 (University of Minnesota, CGC), EDTA (Sigma-Aldrich # 03677), Ethanol (Sigma, #E7023), Glass beads (Sigma-Aldrich, # G8772), Glass slides (Thermofisher # C18150), Glycerol (Sigma-Aldrich, # 101094984), Glutaraldehyde solution (Merck, # 111-30-8), Formaldehyde (Sigma-Aldrich, # 50-00-0), FUDR (Thermofisher # 50-91-9), Hexane (Sigma-Aldrich, # 110-54-3), KCl (Sigma-Aldrich #793590), K2HPO4 (Sigma- Aldrich # 7758-11-4), LB broth (Sigma-Aldrich), LB medium (See table 3-1 for recipe), MgCl2 (UnivAR, # A1278), MgSO4.7H2O (Labchem, #10094-99-8), MilliQ water (Thermofisher, # SH30538.01), M9 medium (See table 3-1 for recipe), NaCl (Melford laboratories, # 10035-04-8), NaN3 (Merck, # 26628-22-8), Na2HPO4 (Merck, # 7558-79-4), NGM (see table 3-1 for recipe), Oxaloacetate (Sigma, #O4126), NADH (Sigma, #N4505), S-buffer (See table 3-1 for recipe), Sodium azide (Sigma, #2002), Sodium cacodylate (Sigma-Aldrich, # 6131-99-3) , Sucrose (Sigma, #84100), Triton-X 100 (Sigma-Aldrich #T9284), Tris 1M (Roche # 10099122), Tween 20 (Merck, #822184).

Table 3-1:Common buffers and medium for *C. elegans* maintenance		
Reagents	Quantity	Details
M9 Buffer (1 L)		Autoclave
dH_2O	1 L	
NaCl	5 g	
$KH2PO_4$	3 g	
$NaHPO_4$	6 g	
1 M $MgSO_4$	1000 µl	Add post autoclave
Bleach solution (50 mL)		
dH_2O	35 mL	Gently mix
Bleach	14 mL	
10 M NaOCl	1 Ml	
Nematode growth medium (NGM) 1 L		
NaCl		Autoclave & let it cool at 50 °C
Bacteriological agar		
Peptone		
1 M $CaCl_2$	1000 µl	Add to the cooled medium & swirl to mix
1 M $MgSO_4$	1000 µl	
1 M KPO_4	25 mL	
5 mg/mL Cholesterol	1000 µl absolute ethanol	
Luria Bertani (LB) Medium (50 mL)		
Casein peptone	0.5 g	Autoclave to make agar plates
Yeast extract	0.25 g	
NaCl	0.5 g	
dH_2O	50 mL	

3.3.1. Preparation of bacterial food source (OP50)

The method described below is adapted from (Amrit *et al.*, 2014) and worm book (http://www.wormbook.org/chapters/www_strainmaintain/strainmaintain.html). The nematode *C. elegans* is generally grown monoxenically[5] using a non-pathogenic strain of *E. coli* (OP50) as a source of nutrients (Brenner, 1974). A limited OP50 lawn (~200 µl) is required to allow better mating of nematodes and make observations easy under the microscope. The *E. coli* OP50 starter

[5] Culture free from living organisms other than species required

culture can be obtained from CGC (https://cgc.umn.edu/strain/OP50-1) or can be recovered from nematode plates by a method described below under sterile conditions.

The OP50 strain was streaked on a Luria Bertani (LB) agar plate (See table 3-1 for recipe) grown overnight at 37°C. From the plate a single colony was used to inoculate 10 ml LB medium in a glass bottle, which was incubated at 37°C and shaken at 50 rpm overnight. This starter culture was stored at 4°C.

To prepare an agarose plate (hereafter referred to as NGM plates) containing a lawn of *E. coli* OP50, NGM plates were seeded with 200 µl of *E. coli* OP50 starter culture and incubate at 37°C for 8 hours or 18-24 hours at room temperature. Plates that were incubated at 37°C were left at room temperature for at least half an hour prior to transferring nematodes. Plates sealed with parafilm can be stored in 4°C for several months. Nematodes were transferred using a sterile pick or using a "chunking" method in which a 1 square centimetre piece of agar containing worms was cut from an old plate and transferred onto a new plate containing sufficient nutrients every 10 days.

3.3.2. Preparing of NGM petri dishes and mold decontamination

The nutrient growth medium (NGM) was prepared as described in the recipe table 3-1 according to a protocol adapted from (McLachlan and Flavell., 2019). Larger petri dishes (100 mm diameter) were used as they are suitable for growing large nematode quantities. After autoclaving the mixture (table 3-1), cholesterol and monopotassium phosphate (KH_2PO_4) were added, and the solution was left in a laminar flow cabinet until it reached 50 °C. The agar was poured in the petri dishes and left in the fume hood to solidify and store at 4°C for later use. It is vital to work in a sterile environment to avoid growth of mold on NGM plates which can impact growth of *E. coli* OP50. However, if mold occurred, it was decontaminated in the following ways.

Mold decontamination

If mold contamination was observed on a plate containing nematodes, a chunk of agar was removed from the contaminated plate using a sterile spatula and placed at the edge of a clean seeded plate. The nematodes were allowed to crawl from the chunk across the *E. coli* OP50 seeded plate. Once the nematodes reached the other side of the plate, they were picked with a sterile picker and transferred into a new seeded plate to produce a new generation without any contamination.

3.3.3. *C. elegans* synchronization

Generation of age synchronized nematode population is vital to minimize biased results due to age difference. The method used for *C. elegans* synchronization in this study was adapted from (Porta-

de-la-Riva *et al*., 2012). The method takes advantage of the ability of *C. elegans* eggs resist sodium hypochlorite (NaOCl) destruction compared to adult nematodes.

Gravid adult nematodes were collected in 15 ml tubes by washing in M9 medium (table 3-1) and centrifuged at 400 xg at room temperature for 2 minutes. The pallet was washed 3 times in M9 medium to clean off the bacteria. Bleach solution was added to the pellet and vortexed for 30 seconds. The solution was centrifuged at 400 xg for 60 seconds and supernatant discarded. The pellet was washed three times in 10 ml of M9 medium to remove the excess bleach. The tubes were incubated at 20 °C overnight in an orbital shaker at 100 rpm. Hatched eggs (L1 stage) nematodes were transferred into OP50 seeded plate and allowed to reach a desired stage at 20 °C.

3.3.4. Long term storage of *C. elegans* stocks

The *C. elegans* stocks were stored in -80 °C by adding equal amounts of S buffer (see table 3-1) and 30% glycerol to the nematode solution (3.3) in a 1.5 ml cryovial (Brenner, 1974). The process described in section 3.3 above is paramount to ensure that nematodes survive the freezing because L1 and L2 stage nematodes survive freezing better than adult and dauer stages. The nematodes in the 1.5 ml vial were placed in a Styrofoam container and stored in 80 °C.

As previously discussed, the life cycle of *C. elegans* is rapid and can be divided into 4 larval stages (section 2.7). However, under unfavourable conditions e.g., during starvation, the nematodes can develop into a dauer stage in which development of the nematodes stops until the conditions are improved. When a chunk of the dauer stage nematodes is transferred into a new seeded plate, the nematodes will then develop into L4 stage (White *et al.*, 2019).

3.4. Genotyping

Principle

Sample genotyping is an essential technology that is used worldwide to detect genetic variations that can lead to major phenotypic changes, including both pathological variations underlying a disease and physical variations that make organisms unique (Michno and Stupar., 2018). This technique compares DNA sequence to that of another sample or reference sequence to determine the differences in genetic makeup. Variations in DNA sequences such as small deletions or single nucleotide polymorphism (SNPs) can be tabulated for various types of genotype comparisons (Rasheed *et al.*, 2017). However, analytical approaches as well as experimental designs are replete with ways to overestimate variation levels present within a given sample. Analytical approaches that do not assess reproducibility among samples are susceptible to calling false positive variants.

Upon receiving the nematodes from the CGC, the genotypes were confirmed using a Phire tissue direct PCR protocol from Thermofisher (www.thermoscientific.com/directpcr) together with a protocol adapted from (Chauve *et al.*, 2020). The VC11196 contains gene *K02F3.11*, which is located in chromosome III, the human homologue of this gene is *moma-1*. Thus, the expected genotype for the mutant strain was appearance of two bands with an estimate of 240 and 420 base pairs on the gel as a result of the heterozygosity.

3.4.1. Method

Sample preparation

DNA was extracted from single L4 nematodes randomly picked from seeded plates. The nematodes were washed 3 times in 7 ml of M9 medium to remove excess *E. coli* OP50 and placed in a 1.5 ml tube containing 20 µl of dilution buffer. To this, 0.5 µl of DNA release buffer was added followed by brief vortex and centrifugation at 10 000 xg for a minute. The samples were incubated for 2-5 minutes at room temperature then incubated at 98°C for 2 minutes to denature the proteins and the samples were centrifuged for a minute at 10 000 xg. The supernatant was recovered, and an aliquot was taken for PCR and the remaining supernatant was stored at -20°C for later use.

3.4.2. Setting PCR reaction conditions

Seven 50 µl reactions were made using 2 µl of nematode DNA lysate, 25 µl Phire PCR direct tissue master mix, 1 µl of 100 µM primers (table 3-2) and filling the volume up to 50 µl with milliQ water. A total of 42 cycles were performed with 1 initial denaturation cycle at 98°C for 5 min, followed by 40 cycles of annealing at 55°C for 5 sec and a final extension cycle at 72°C for a minute.

Table 3-2: List of primers

Primers	Sequences	DNA bases	Tm (°C)
VC1196- EX-L	5'- TTA GTC CAA AAA GTG CCT CC- 3'	20	53.7
VC1196- EX-R	5'- AGG CGC TCT TGA TTC ACA TG- 3'	20	56.8
VC1196-IN-L	5'-TAT CGG ATA ACA AAA GGC GG- 3'	20	52.5
VC1196-IN-R	5'- AGC AGC TCG TCC AGT AGC TC- 3'	20	59

3.4.3. Gel electrophoresis and imaging

A 1% w/v agarose gel was made in 1X bionic buffer with of 5 µg/ml of ethidium bromide for each sample, 10 µl of the PCR product was loaded into a well, and the samples subjected to 30 V for 60

minutes. Finally, the gel was visualised using ChemiDoc^{TM} system (Bio-Rad) with image lab software (v 5.2.1).

3.5. Visualizing mitochondrial ultrastructure using transmission electron microscopy (TEM)

Principle

Since the early 1950s, transmission electron microscopy has emerged as a useful tool in mitochondrial research and it contributed significantly to the insight into mitochondrial ultrastructure (Rasmussen., 1995). Although considerable advancements have been made since the discovery of TEM, interpreting the details of the mitochondrial ultrastructure remains a challenging task. Two major contributing factors to this challenge is that (1) it is difficult to view large volumes simultaneously as mitochondria are large and cytosol can cover up to hundreds of microns, (2) it is desirable to acquire high resolution of the details of the structure, but this is costly as such equipment comes with a heavy price tag. Furthermore, sample preparation is of paramount importance to acquire good images.

The use of TEM enables visualization of cellular components by their selective absorption of heavy metals (Palade., 1952). Osmium was among the first heavy metal to be employed in traditional TEM experiments. The success of electron microscopy is highly dependent on sample preparation particularly when working with *C. elegans*. Even though this organism is small (~1 mm), their body is covered by a tough cuticle which is practically impermeable to fixatives thus should first be cut into pieces prior to fixing for visualization. The protocol described below was adapted from (Kovacs., 2015) with some modifications

3.5.1. Method

The L4 nematodes were immersed in 0.8% glutaraldehyde (0.15 mol/L) and 0.1 M sodium cacodylate buffer (pH 7.4) at room temperature in the fume hood. The nematodes were cut into approximately 3-4 pieces with a double edge blade and immersed in 0.1 M sodium cacodylate buffer. The samples were then left at room temperature for 2 hours in a fume hood. The samples were rinsed 3 times the 0.1 M sodium cocodylate buffer and embedded in 1% agarose. Post embedding, samples were treated with 2% osmium for 2 hours in a rotator. The osmium was rinsed with 50%, 70%, 90% ethanol and twice with 100% ethanol for 15 min each. The infiltration schedule was done at room temperature with an embedding machine, wherein samples were incubated in 2 parts of propylene oxide (PO) to 1 part of the resin for 2 hours, followed by 1 part of PO to 1 part of resin for 2 hours with 4 changes in 100% resin over one day. The samples were arranged in flat embedding in mold and polymerized for 65 hours at 60°C. The sections collected were stained in alkaline lead citrate solution and visualized using Leo 912 AB omega TEM (Carl

Zeiss, Oberkochen, Germany). The TEM is made up of three essential systems (1) electron gun which produces the electron beamand the condenser system which focuses the beam onto the object, (2) image producing system consisting of the objective lens which are responsible for prodicing highly magnified images, and (3) image recorder system which converts the electron images into a form perceptible to the human eye.

3.6. Untargeted lipid metabolomics

Principle

Metabolomics is the most downstream of systems biology omic approaches (Geier *et al*., 2011). This untargeted profiling of metabolites method aims to recognize perturbations in biochemical networks (Coen *et al.*, 2008; Swaan *et al*., 2010). Metabolic networks can rapidly respond to perturbations compared to protein and gene transcripts. In addition, metabolomics can give an integrated picture of an organism's interaction with its environment. Recently, metabolite profiling has been used to assign phenotypes to experimentally perturbed *C. elegans* samples like mutants, RNAi etc. (Atherton *et al*., 2008; Yang *et al*., 2017). The complexity of metabolomics networks in the nematode *C. elegans* have been thoroughly investigated in genomic, transcriptomic and proteomic studies conducted by Watson *et al*. (2015). A variety of *C. elegans* studies have been conducted previously using different metabolomics platforms including GC/LC-MS as well as nuclear magnetic resonance (NMR) to dissect whole nematode metabolomics networks (Patti *et al*., 2014; Morgan *et al.*, 2015; Wang *et al*., 2017). An organism's health and survival are influenced by its ability to regulate the production, storage, and release of energy (Evan *et al*., 2011; Henry *et al*., 2016). Lipids play a vital role in the biology of *C. elegans* and are often implicated in energy storage, reproduction, and life span, and may serve as signaling molecules (Hunsen *et al*., 2013). Existing research suggests that the coordination of MICOS complex with respiratory complexes and lipids establishes mitochondrial inner membrane architecture as assembly of two MICOS subcomplexes (Mic27 and Mic10) is dependent on respiratory complexes and mitochondrial lipid cardioplin (Hoppins *et al*., 2011; Friedman *et al.*, 2015). Thus, it is expected that MICOS subunit deficiency present in the VC1196 strains will lead to aberrant cristae morphology, decreased mitochondrial OXPHOS enzyme activity and thus respiration, and a diseased phenotype due to its incapability to store energy.

Identification of lipids is a major limitation in lipid profiling and lipidomics[6] in general, particularly for novel classification of lipids and it requires multidirectional data for better annotation. Current lipidomics methods provide new insight in mechanistic investigations and permits the discovery of

[6] Large-scale study of cellular lipids networks and pathways in biological systems

new biomarkers in variety of fields (Britta *et al*., 2021). In addition, data tools and semi-automatic metabolite annotation have improved the robustness and quality of metabolomic platforms, making it easy to analyse and interpret the data generated.

3.6.1. Methods

Untargeted lipid profiling was achieved using GC-TOF-MS system (see annexure C). The system consisted of an Agilent© gas chromatograph series with Agilent© autosampler attached to a LECO Pegasus HT time of flight mass analyser with an electric impact ionisation source. Data acquisition and extraction was achieved using the LECO corporation ChromaTOF® software (v 4.5x). For this part of the study, mitochondria were isolated as described in section 3.8.1 of this dissertation, the experimental procedure was then conducted according to SOPs standardised by the NWU mitochondrial research laboratory (attached in annexure C) with minor modifications to accommodate the usage of *C. elegans* (Geier *et al*., 2011; Yang *et al.,* 2017). Aproximately 10 thousand nematodes were used to obtain crude mitochondrial samples and two extraction phases were done prior injection into the GC/MS machine. In the initial steps single phase metabolite extraction was used followed by methylation and silylation to extract fatty acids methyl esters (FAMEs). All the extraction and derivatization work were done in the fume hood.

Single phase extraction

The samples (crude mitochondria) were prepared from approximately 5000 L4 staged nematodes for both N2 and VC1196. Methanol was placed in -80°C for an hour, and solvents as well as the nematode suspension were pre-cooled on ice for 15 min prior to the commencement of the experiment. A volume of 1 ml of the cold methanol was added to the samples (four samples for both N2 and VC1196) while on ice, followed by addition of 50 µl internal standard (220 ppm nanodecanoic acid) to attain a final volume of 330 µl. A pellet (tip of a spatula) size of glass beads were added to the solution containing the sample and was shaken for 2 min at 30 Hz on the TissueLyser II (Qiagen). About 100 µl of the homogenate was taken for normalization, after which 330 µl chloroform was added and the sample was vortexed for 30 sec then left for 10 min on ice. Samples were centrifuged at 4°C for 5 min at a speed of 2 000 xg to pellet the glass beads proteins and cell debris. The recovered supernatants were transferred to glass vials and dried under nitrogen at 40°C for 30 min.

Methylation and silylation (extraction of FAMEs)

A 100 µl volume of methanol was added to the dried extracts and vortexed properly to redissolve the samples. 200 µl of freshly prepared methanolic KOH (280 mg KOH in 25 ml methanol) was added to each vial and incubated for an hour at 60°C. The samples were left at room temperature

after removing from the heating block. Then, 400 µl hexane, 200 µl water and 40 µl 1N acetic acid were added to the samples, followed by 4°C centrifugation for 2 min at 2000 xg. The top hexane phase was transferred into a clean vial and dried under nitrogen at 40°C. 50 µl pyridine and BSTFA (containing 1% TMCS) were added to the dried extracts and the samples were incubated at 45°C for 30 min and tranfered into the flat bottom inserts for analysis. The produced data was pretreated in MetaboAnalyst software v 5.0, univariate statistics was done using student t-test.

3.7. Bioenergetic assay: Respirometry measuring using the using O2k Oroboros instrument

Principle

The oxygen consumption rate (OCR), as a measure of mitochondrial bioenergetics, is a vital tool in biology to evaluate cellular function during an organism's lifetime under metabolically challenged or normal conditions (Rya *et al*., 2016). Mitochondrial function (Palikaras *et al*., 2015) as well as factors that mediate the transition from OXPHOS to aerobic glycolysis (Chen *et al.,* 2015) can be studied using tools that measure oxygen consumption rate. *C. elegans* offers an added advantage of studying living mitochondria without the need for extraction and purification of mitochondria (Sarasija and Norman., 2019). The *C. elegans* ATP production process is similar to that of mammals as it occurs through OXPHOS and requires ETC enzymatic complexes activity, which facilitates the production of energy and is driven by the metabolism of several substrates such as fatty acids and intermediates of the TCA cycle (Chen *et al.,* 2015). The high resolution O2k respirometer system incorporates a closed, airtight reaction chamber and utilizes oxygen sensors to measure O_2 concentration and calculate O_2 consumption within the two chambers simultaneously. Each chamber contains a stopper with injection ports, which makes it ideal for optimization of plasma membrane permeability as well as substrate-uncoupler-inhibition titration. Regulated calibration of the sensor response, two-point polarographic O_2 sensor calibration and instrumental background O_2 flux offer the unique experimental basis for high qualitative results accuracy and quality control high resolution respirometry.

The Oroboros instrument allows the measurement of OCR from isolated organelles or intact live nematodes. In this study, live intact nematodes were used to compare the OCR of N2 and VC1196 *C. elegans* strains. As previously mentioned in section 2.3, the assembly and functionality of OXPHOS is regulated mitochondrial cristae structure (Baker *et al*., 2019). Mitochondrial cristae dynamics are regulated by MICOS and OPA1 (Cogliati *et al*., 2016). Since the VC1196 strain is Mic27 deficient, a decrease in OXPHOS and mitochondrial respiration is anticipated.

3.7.1. Methods

The oxygen consumption rate was measured using the Oroboros Oxygraph 2K[7] (Oroboros Instruments GmbH, Innsbruck, Austria) as described in (Macedo *et al*., 2020), with some modifications. Approximately 150 L4 live nematodes per strain were collected and washed 3 times in M9 buffer (Table 3-1) to remove the excess OP50. Before commencement of the experiment, the M9 buffer was placed in a water bath at 20°C and the air conditioner in the room was also set to the same temperature. This is the optimal temperature of normal growth of nematodes. The analyser was calibrated in air saturated solution daily prior experimentation. Oxygen was injected into each chamber to raise the concentration to >400 nmol/ml to initiate the assays using substrate-uncouple-inhibitor-titration (SUIT) protocol. This protocol improves our understanding of pathophysiology of mitochondrial diseases and mitochondrial respiratory control. Respiratory states[8] are defined in efficient terms to account for the metabolic interactions network with stepwise modulation of coupling substrate and control in complex SUIT protocol. Each assay was performed at 20°C with the stirrers set at 750rpm in each chamber. Concentration of oxygen in the chambers was maintained at 200-500 nmol/ml by performing re-oxygenation to prevent limitations because of oxygen diffusion.

The nematodes were transferred to the high-resolution respirometer chamber containing 2.5 ml of pre-warmed M9 buffer. The Oroboros instrument has two chambers. Both chambers were run at the same time, one containing the VC 1196 strain and the other chamber containing the N2 WT strain. Basal oxygen consumption rate was monitored at 20°C for a period of 15 min with constant stirring. Nematodes were recovered post respiration measurements and were counted. The OCR values were normalized to number of nematodes and expressed as nmol O_2/min/ 150 nematodes. The obtained data ware analysed using DatLab 4 software[6], wherein the slope of the straight portion was used to derive the OCR. The results were normalized to the number of nematodes. The above-described experiment was repeated three times, to obtain respiration measurements for each strain in triplicate.

[7] Oroboros Instruments GmbH, Innsbruck, Austria

[8] ADP stimulated respiration of coupled mitochondria isolated in the presence of high ATP and Pi concentrations, supported by a defined substrate combination at saturating O_2 levels (Gnaiger., 2009).

3.8. OXPHOS complex activity: Measuring enzymatic activity using a 96 well spectrophotometer

Principle

The activities of respiratory chain enzymes CI, CIII, CIV as well as citrate synthase (CS) were measured in 96 well plates using enriched mitochondrial fractions from *C. elegans*. Kinetic spectrophotometric assays were used to quantify enzyme activities of the different strains, typically, absorbance of a single-coloured analyte[9] is measured repeatedly over time and used to determine initial rates (V0 mAbs/min). Standard operating procedures (SOPs) standardized by the NWU mitochondrial research laboratory (attached in annexure B) were used to perform the analyses and were adapted from (Shepherd & Garland, 1969; Rahman *et al*., 1996; Janssen *et al.,* 2007; Luo *et al*., 2008; Rodenburg, 2011; Smuts *et al*., 2013) with some modifications. Prior the determining enzymatic activities of the above-mentioned complexes, total protein content of the of the mitochondrial fractions was normalized to citrate synthase activity.

3.8.1. Enrichment of mitochondrial fractions from nematodes

Approximately 5000 L4 nematodes were collected from NGM plates seeded with OP50 and washed 3 times in M9 buffer to remove the excess *E. coli*. The pellet was collected and resuspended in ice-cold isolation buffer (300 mM sucrose, 5 mM TES, 200 µM EGTA, pH 7.2) (Schmit *et al*., 2013). The resuspended pellet in isolation buffer was transferred into a dounce homogenizer to gently push the nematodes through the chamber 5 times with a 1 ml glass syringe fitted with a metal lure lock to obtain mitochondria enriched fractions. A 12 µm ball clearance was used to fracture the tough nematodes cuticle. The homogenate was centrifuged at 4°C for 5 minutes at 800 xg, to pellet large nematode fragments. The supernatant containing mitochondria was collected into a clean 1.5 tube and centrifuged at 4°C for 10 minutes at 9000 xg. The pellet containing the crude mitochondria was resuspended in 70 µl swelling buffer (SWB) (0.2 M sucrose, 10 mM MOPS-Tris, 5 mM succinate, 1 mM H_3PO_4, 10 µM EGTA, 2 µM rotenone).

3.8.2. Methods

The enzyme activity assay was performed according to an in-house SOP (attached in annexure B) version 3 with some modifications to accommodate nematodes. Prior to the assay, the mitochondria were isolated from ~ 5000 nematodes per strain as described by (Dilberger *et al.,* 2019). The activities of respiratory complex I, Complex III and Complex IV as well as citrate synthase (CS) was measured in freeze-thawed enriched mitochondrial fractions from L4 nematodes.

[9] Substrate/product of a two-step coupled reduction-oxidation reaction catalysed by the enzyme

3.8.2.1. BCA method

Principle

The bicinchoninic acid (BCA) method is a total protein quantification method that relies on the formation of copper (II) ion (Cu^{2+}) protein complex in a basic environment followed by the reduction of Cu^{2+} to Cu^{+} (Smith *et al*., 1985). The amount of Cu^{2+} reduced is proportional to the amount of protein present in the solution. A BSA protein standard series ranging from 0 µg to 20 µg was pippeted into the 96 well plate reader (table 3-3). Sampless of the nematode mitochondrial fractions were diluted and 2 µl was pippeted in triplicate into the 96-well plate reader followed by addition of water to make up 20 µl volume in each well. Additionally, 200 µl of a reagent mix, consisting of BCA and $CuSO_4.5H_2O$ in a ratio of 50:1, was added to each well and the plate incubated at 30 ºC for 35 minutes in a Synergy™ HT Multi-detection microplate reader. This was followed by a measurement of the absorption at 562 nm.

Table 3-3:BCA standards series

	S1	S2	S3	S4	S5	S6
BSA (µl)	0	4	8	12	16	20
H_2O (µl)	20	16	12	8	4	0

200 µl BSA reagent was added to standards and test samples and incubated at 25 °C for 30min in synergy 96 well multiplate reader. Absorbance was measured at 562 nm and sample concentration was determined.

3.8.2.2. Citrate synthase activity

Principle

Citrate synthase catalyses the first reaction of the TCA cycle, and this reaction involves the formation of a carbanion at the methyl group of Acetyl-CoA as shown in the reaction equation 3-1. Intrinsic variations are often determined by normalizations of the functional measure of interest to a suitable marker of mitochondrial content. In the present study, mitochondrial content was estimated to the activity of CS because it is an enzyme at the entry of metabolites into the TCA and intersection of fuel catalysis (McLauglin *et al*., 2020).

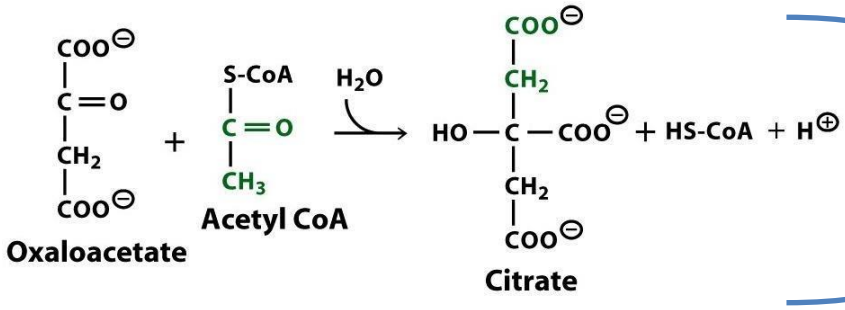

Equation 3-1: Acetyl-CoA condensation

Method

The assay was performed with triplicate reactions for each sample in the 96-well plate in final volume of 200 µl per well. The assay was performed at 25°C with oxaloacetate (OAA) preheated at 30°C. The reaction was made up of 147 µl of the CS master mix consisting of 106.5 µl milliQ water, 1 mM DTNB (0.1 nM), 10% Triton X100 and 3 mM acetyl CoA (0.3 nM) followed by the addition of 3 µl of the supernatant per reaction. The reaction was initiated by adding 50 µl of the preheated OAA post the 10 minutes pre-incubation. The rate of increase was measured at a wavelength of 412 nm for 5 min in 1 min intervals (V_0). Using the linear section of the graph, the initial rate of reaction was determined using equation 3-2 below.

µmol/min/mg (UCS) = (V_1/7465)*0.2/(µl protein x µg/µl/1000)

nmol/min/mg = UCS (unit cytrate synthase) x 1000

Equation 3-2: Protein concentration

3.8.2.3. NADH dehydrogenase (ubiquinone) (Complex I)

Principle

Complex I is the first respiratory ETC enzyme (Sharma *et al*., 2009). This complex oxidizes NADH, which is mainly generated through the TCA cycle and utilizes the two electrons to reduce ubiquinone to ubiquinol. The latter is further re-oxidized by cytochrome bc1 complex and transfer electrons to reduce molecular O_2 to H_2O at complex IV. The CI activity assay is performed in the presence and absence of rotenone to evaluate the nonspecific NADH dehydrogenase activity. Rotenone interferes with the ETC within CI and inhibits the transfer of electrons from iron-sulfur centres in CI to ubiquinone. Activity of CI was determined using the NWU mitochondrial lab SOP as adapted from Rohman *et al*. (1996).

Method

The nematode mitochondrial fractions were thawed one ice and thoroughly mixed, then 6 µl of the sample was loaded in the well in triplicate per genotype in the presence of 50 µl DMSO or

rotenone. A 124 µl volume of the CI master mix (see table 3-4) was added to the assay and incubated for 10 min at 30 °C before adding 20 µl preheated (30 °C) 2 mM NADH. Absorbance was measured at 600 nm for 5 min with 1 min time intervals.

Table 3-4: CI Master mix

Reagents	Amount (µl) & final concentration
KPi (pH 7.6)	10 µl (25 mM)
Coenzyme Q1	1.4 µl (70 µM)
BSA	7 µl (0.35 %)
DCIP	2.4 µl (60 µM)
MilliQ H2O	103.2
Total	124
DMSO and Rotenone	
DMSO / Rotenone	0.2 µl (1 µM)
MilliQ H2O	49.8

The linear rate calculations over the first 3 min were used (R^2 > 0.99 for v1 and v2) see equation 3-3 below:

For 200 µl reactions: ε_{600} = 12712 Abs/mM)

µmol/min/mg = $(v_1 - v_2)$/ (12712) *0.2/ (µl protein*µg/µl/1000)

nmol/min/UCS = µmol/min/mg x 1000/UCS

Equation 3-3: Linear rate calculations CI v_0

3.8.2.4. Ubiquinol-cytochrome c reductase (Complex III)

CIII of the ETC shunts electrons through the IMS to cytochrome c (CytC) (Han *et al*., 2003). The reduction of ferricytochrome c by the reduced coenzyme Q is catalysed by CIII (Luo *et al*., 2008). The activity of CIII was determined using a method adapted from Luo *et al. (*2008), ensuring that the samples and the solutions are always in ice. Prior to the experiment, CIII master mix (table 3-5) was prepared and preheated at 30°C.

Table 3-5: CIII Master mix	
Reagents	Amount (µl) & final concentrations
KPi	20 µl (50 mM)
EDTA	0.8 µl (1 mM)
Tween	4 µl (0.04%)
NaN3	6 µl (3 Mm)
Decylubiquinol	6.5 µl (300 µM)
MilliQ H2O	32.7 µl
Total	70 µl
Diluted CytC	
CytC	2.5 µl (50 µM)
MilliQ H2O	117.5 µl
Total	120 µl

A total concentration of 50 µM CytC was added in reaction wells in triplicate. The sample was diluted 10X in KPi buffer and 10 µl of the dilution was added to the reaction wells in triplicate. Plates were incubated for 10 min in the plate reader at 25°C, after which 70 µl of the preheated CIII master mix was added to the reaction mixture and the linear rate increase was measured at 550 nm for 5 min in 1 min intervals. Linear rate calculations were taken from 0 to 3 minutes with an R^2 > 0.99 for v1 (see equation 3-4). For 200 µl reactions: ε550 = 4180 Abs/mM

µmol/min/mg = $(v_1)/4180)*0.2/(\mu l\ protein*\mu g/\mu l/1000)$

nmol/min/UCS = µmol/min/mg x 1000/UCS

Equation 3-4: Linear rate CIII v_1

3.8.2.5. Cytochrome c oxidase (Complex IV)

ATP production is driven by the complex V (ATP synthase) using proton gradients (Cadenas and Davies, 2000). All four electrons from complex IV must pass onto the more electronegative molecular oxygen in order to maintain the production of ATP. The electron transport chain can result in mono/bivalent oxygen reduction under physiological conditions, thus giving rise to superoxide anions and H_2O_2 respectively (Klotz and Sies, 2009). The master mix was prepared according to table 3-6.

Table 3-6: Complex IV Master mix

Reagent	1x (µl)	Final concentration
KPi buffer (0.5 M) – pH 7.4	8	20 mM
Water	112	
*CytCred (500 µM)	28	70 µM
Total	148	

The assay was performed in duplicates for each sample at 37°C in a 96-well plate, and the final volume of the reaction was 200 µl per well. The reaction mixture contained 8 µl KPi buffer (pH 7.4), 112 µl milliQ water and 28 µl CytCred per reaction. The CIV master mix was then preheated at 40°C. The plate was incubated at 37 ºC after adding 50 µl of diluted Kpi (4 µl KPi and 46 µl MilliQ water), and 2 µl of the of the fina mitochondrial extract. The reaction was initiated by adding 148 µl of the preheated CIV (8 µL of KPi buffer (0.5 M), 28 µl CytCred (500µM) and 112 µl milliQ water per reaction, 148 µl of the master mix) mixture in each well. Linear rate of decrease (v1) was measured at 550 nm for 3 min in 30 sec intervals and enzyme activity was calculated using equation 3-5 below.

$$\mu mol/min/mg = (v_1)/4180)*0.2/(\mu l\ protein*\mu g/\mu l/1000)$$

$$nmol/min/UCS = \mu mol/min/mg \times 1000/UCS$$

Equation 3-5: Linear rate calculation CIV v_1

For 200 µl reactions: ε_{550} = 4180 Abs/mM

3.9. Phenotyping

C. elegans phenotyping is a useful tool to evaluate the health of nematodes using behavioural movement in response to chemical or physical stimuli (Javer *et al.*, 2018). These assays are often done on L4 stage nematodes, however there are other studies that compared behaviour in the different life cycles of the nematodes (Fielenbach *et al*., 2008; Zhang *et al*., 2016). Behavioural assays alone are not a sufficient measure of the defects that may affect the nematodes thus many other sophisticated biochemical analyses are conducted to confirm the presence of a possible disease phenotype caused by a mutation. In this study three assays were used to phenotypically

characterize the mutant strain (VC1196) and compare it to the wild type strain (N2 Bristol) namely life span, chemotaxis and gentle/harsh touch.

3.9.1. Life span assay

Principle

Life span is an important phenotypic assay that has been used frequently to study stress resistance, immunity and aging using *C. elegans* as a disease model (Park *et al*., 2017). The latter is a degenerative process that is characterized by weakening of cellular organelles resulting in mortality (Sutphin *et al*., 2009). Almost every biological system ultimately undergoes a functional deterioration as it grows older. In the nematode *C. elegans* life span is typically the number of days the nematode remains responsive to external stimuli (Amrit *et al.,* 2014). The ability to produce synchronized isogenic populations grant *C. elegans* added advantage to be utilized for such studies. Nematodes can either be propagated in solid (NGM plating) or liquid medium, and methods have been established for measuring lifespan in each condition, in this study all the life span assays were measured using solid medium. The mutant strain (VC1196) life span was compared to the WT strain (N2 Bristol).

To assess the life span of the nematodes in the present study, three different experimental setup, (1) no chemicals added in NGM, (2) FUDR added to NGM for sterilization, and (3) tBPH added to NGM to induce stress to nematodes. The experiments were performed to increase the validity of the assay since manual methods (physical counting of nematodes to distinguish between live and dead) was used to count the number of surviving nematodes. The first experimental setup was done by transferring parents (L4 staged nematodes) onto fresh plates seeded with OP50 *E. coli* every 24 hours using a platinum pick until progeny production ceased. The nematodes were declared dead if they did not respond when gently touched with the platinum pick (Park *et al*., 2017). The second part of the experimental setup was done by treating the nematodes with 150 µM 5-fluoro-2-deoxyuridine (Amrit *et al*., 2014). The utility of FUDR in life the span assay was convenient as it reduced labour of frequently transferring parents onto new seeded plates and it increased reliability as nematodes were no longer exposed to dying due to external stimuli from the platinum pick. Lastly, tert-Butyl hydroperoxide (tBHP) was used to assess life span of the nematodes under physiological stress conditions (Ewald *et al*., 2017). The last two experimental setups were ideal as they did not require frequent transfer of nematodes onto new seeded plates. All the experiments were done in triplicate (three plates per strain) using freshly prepared NGM plates.

Recipe 1 (preparing 150 nM FUDR)

Approximately 33 µl (50 µg/ml) of filtered FUDR (prepared by dissolving ~0.3693 g FUDR in milliQ water) was added to the NGM (table 3-1) when it reached 50°C. The NGM containing plates were seeded with OP50 *E. coli* and incubated at 37°C for 18 hours. Plates were used stored at 4°C and were used withing 10 days of the preparation (Ewald *et al*., 2017).

Recipe 2 tert-Butyl hydroperoxide (tBHP plates)

Approximately 4% agar was dissolved in milliQ water, followed by addition 2.5 ml phosphate buffer (0.1 M pH 7.4), 160 µl cholesterol (50 mg dissolved in 1 ml 99.9% ethanol absolute), 100 µl $MgSO_4$ (120 g MgSO4 in 1 l milliQ water), 100 µl $CaCl_2$ (58 g CaCl2 in 1 L milliQ water) and 214 µl tBHP (0.5 nM).

Methods

3.9.1.1. Lifespan analysis without 5-fluoro-2-deoxyuridine (FUDR)

This protocol was adapted from (Park *et al*., 2017). Age synchronized nematodes were grown at 20°C and 50 L4s were transferred onto freshly seeded plates every 24 hours in triplicate per strain to prevent inclusion of new progeny into the daily count. The nematodes were observed each day to detect live and dead animals. Nematodes that were not moving, were poked gently with a thin platinum wire, to see if they moved or not, and if there was no movement, nematodes were counted as dead and removed from the pate. Nematodes that died because of external pressure (poking) were not included in the final analysis.

3.9.1.2. Lifespan analysis using FUDR

A total of 50 L4 synchronized nematodes were transferred in three freshly seeded plates supplemented with FUDR (See recipe 1 above). The plates were place in 20°C incubator and counted every 48 hours to detect live and dead nematodes until the entire population was dead.

3.9.1.3. Lifespan analysis using tBHP

A total of 50 L4 nematodes were transferred into the centre of a tBHP agar (see recipe 2 above) in triplicate per strain. The plates were incubated at 20°C and survival was scored every 60 minutes until the death of the last member of the population

3.9.2. Chemotaxis assay

Principle

Almost every motile organism can exhibit chemo sensation and respond by moving away or towards it. This is known as chemotaxis [10] (Stock, 2009). Chemotaxis in eukaryotic organisms proceed by mechanisms shared by all cells in the kingdom eukarya which generally involves regulation of microtubule (Lee *et al.*, 2009). This assay was first described almost 5 decades ago and has had far reaching applications since then (Ward., 1973). Chemotaxis is predominantly employed by neurobiologists to test olfactory adaptations[11] using the nematode *C. elegans* as a disease model (Colbert and Bargmann., 1995). Kauffman *et al*. (2011) developed an assay to validate *C. elegans* ability to store-short term and long-term memory by showing that the nematode can make connections between food sources (OP50), temperature and chemo-attractants.

The response of nematodes to the odorant was achieved by placing nematodes in the origin with control and test compounds placed 3 cm from the origin in different quadrants as depicted in figure 3-2 below. The agar only contained nematode growth medium (NGM) that was not seeded with OP50 *E. coli*. According to existing literature, there are two strategies that are used by *C. elegans* to navigate in chemical gradients (Swierczek *et al*., 2011). The nematodes either (1) change direction when a favourable chemical decreases or (2) move their head side to side in the direction of a source of stimulation. Chemosensory mutants have been observed to aggregate on food like the wild type nematodes (Sawin *et al*., 2000). However, the reason behind this remains obscure. The volatile chemical (Benzaldehyde) used to observe how the VC1196 and N2 Bristol behave in the present study has been previously shown to elicit a robust chemotaxis response from *C. elegans* (Bargmann *et al*., 1993). Thus, since we tested it at lower concentration (5%) compared to the higher concentration of the control chemical (99.9%) absolute ethanol, and expected the nematodes to migrate to the benzaldehyde quadrants.

Methods

The application of chemotaxis is evident in the field of neurobiology particularly in olfactory adaptation studies (Hu *et al*., 2015). Certain critical steps must be undertaken to obtain best results in chemotaxis assays (Margie *et al*., 2013). The first step is to ensure that the nematodes contain no excess *E. coli* as it may interfere with the assay. Secondly the nematodes must be age synchronized, as nematodes at different larval stages behave differently. Thirdly, the application of 0.5-1 M NaN_3 is important as it paralyses the nematodes such that they do not climb the walls of the petri dishes,

[10] Migration of organisms toward attractant chemicals or away from repellents.
[11] Simple form of learning and memory.

and hence this chemical is placed at least 2 cm from the origin. A schematic representation of chemotaxis is shown in 3-6 below. The schematic representation of the method employed for chemotaxis is indicated in figure 3-2.

$$\text{Chemotaxis index} = \frac{Sum\ A\&B - Sum\ C\&D}{total\ nematodes\ that\ left\ the\ circle}$$

Equation 3-6: Chemotaxis index

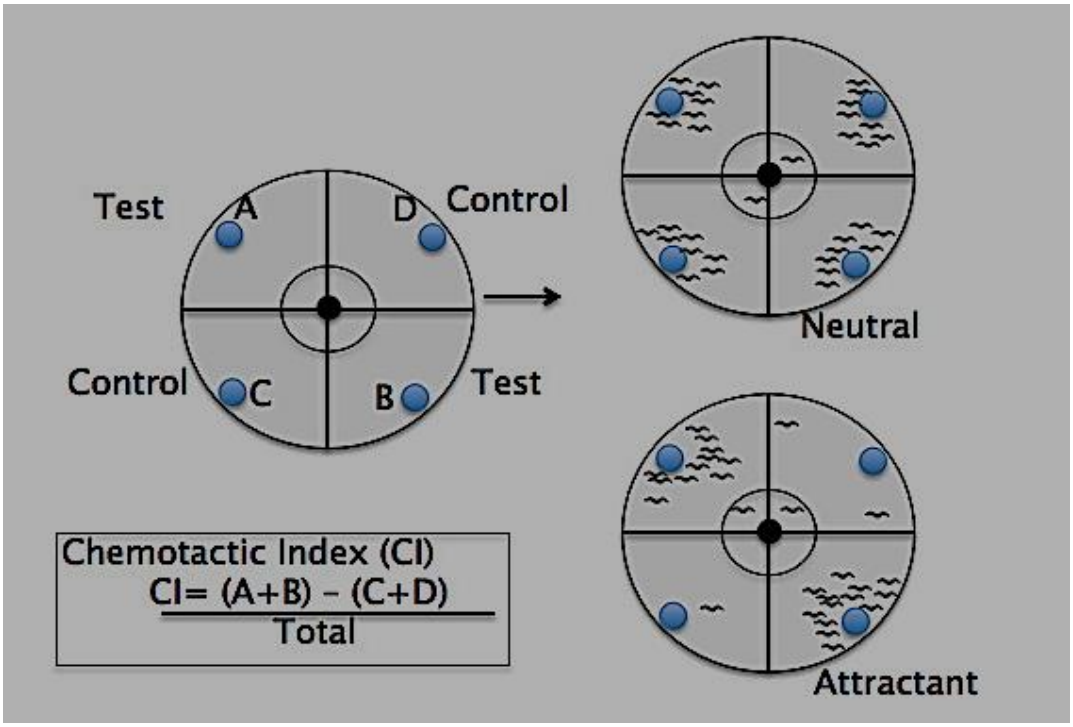

Figure 3-2: Schematic representation of chemotaxis assay. The vertically opposite quadrants contain control (ethanol absolute) or test compounds (varies). Nematodes are placed at the centre and allowed to crawl in search for nutrients. The chemotaxis index is calculated after nematodes were exposed to the chemicals for an hour. Image adapted from (Margie *et al.,* 2013).

The protocol described here was modified from (Lee *et al.,* 2009; Margie *et al.,* 2013). Approximately 100 L4 synchronized nematodes were rinsed 3 times with M9 buffer (See table 3-1) to remove the excess OP50 *E. coli* on the nematodes. NGM plates were demarcated as indicated in figure 3-2 with 1 µl of 5% benzaldehyde added to the test quadrant and 99.9% ethanol in the control quadrant followed by addition of 1 µl 0.5 M NaN_3 to paralyse the nematodes so that they do not pass the test/ control compound and end up climbing the walls of the petri dish. The chemical NaN_3 is important for the chemotaxis assay as it paralyses the nematodes upon reaching the respective quadrants thus making counting easy. After adding all the reagents and nematodes, the plate was inverted and left for an hour after which the location of the nematodes was assessed. The

chemotaxis index (CI) was calculated using equation 3-6. A positive (+1) CI indicates attraction towards the chemoattractant while a negative (-1) CI indicates repulsion.

3.9.3. Gentle touch and harsh assay

Principle

This assay is used to detect how nematodes respond to external stimulus resulting from physical contact with either a platinum wire (harsh touch) or eyelashes (gentle touch). Gentle touch sensation is mediated by five touch receptor neurons[12] (TRNs) (Chalfie and Thomson, 1997). Typically, gentle touch to the posterior of the body results in forward movement while gentle touch to the anterior of the body results in reverse movement.

3.9.3.1. Method

The method described here was adapted from (Chalfie *et al*., 2014), L4 nematodes were transferred into an NGM plate (see table 3-1) and touched 5 times on the head and tail respectively with an eyelash attached to the end of a toothpick[13] and using a platinum pick[14]. Movement in the opposite direction was counted as a response. At least 20 nematodes were tracked over a 10-day lifespan with measurements taken every 2 days.

3.10. Data processing and statistical analysis

The data generated was analysed using Microsoft Excel (2016) and the graphs depicting the data and statistical analyses produced using GraphPad prism (v 9.3.1). The OXPHOS enzyme assay data was produced by Gen5^{TM} (v 1.11.5). The data were analysed using the same methodologies for all the kinetics enzyme assays measured, namely initial reaction velocity (v_1)[15] of the assays was determined over the first 2 minutes (first 3 readings) via linear rate calculation. The linear square regression was used to measure correlation between the results, a coefficient of determination (R^2) greater than 0.99 was considered as sufficient linear relationship. The bioenergetic assays were analysed using DatLab (v.4), the raw data was organised into readable format using Microsoft Excel and analysed using GraphPad prism. Spectral data generated by GC/MS was extracted into matrices, and the data matrices were inspected individually (selection of correct peaks, alignment and data integrity) and pre-processed (data filtering, missing value and normalisation). The P-values (<0.005) were determined using two tailed student's t test.

[12] Neurons that extend long processes that innervate approximately one half of the animal's body length
[13] Gentle touch
[14] Harsh touch
[15] Measured in mAbs/min

4. CHAPTER FOUR: RESULTS AND DISCUSSION

Chapter summary

This chapter gives the outcomes of this research, the findings as per the aims and objectives are discussed thoroughly. Post confirmation of the genotype as the first objective of the study, the mitochondrial ultrastructure was determined using transmission electron microscopy as part of the second objective of this study. Two more biochemical analyses were performed using crude mitochondrial fractions. These biochemical assays were (1) untargeted lipid profilling and (2) OXPHOS enzyme activity assay, which were part of objective 3 and 4 respectively. To achieve the last two objectives of this study. Live L4 nematodes were utilized, and lifespan assays were conducted on three different experimental setups for both strains. The outcomes achieved in this study supports the hypothesis (see section 2.10.3), as the VC1196 strain showed decreased phenotypes and more vividly the aberrant cristae morphology was observed on the VC1196 strain with the aid of transmission electron microscopy. The statistical softwares used as well as meaning of the outputs they generate are defined in detail. All the error bars in the graphs represents the standard deviation (SD).

4.1. Genotyping

The genotype of VC1196 strain was confirmed as described in section 3.3 above to ensure that correct samples were received prior to commencement of experiments. PCR was employed using the combination of internal primers (see table 3-2).

4.1.2. Results

The *moma-1* is characterized by a deletion in Mic27 which a subunit of the MICOS complex that plays a pivotal function in the stabilization of Mic10 subunit and respiratory chain complexes. Heterozygotes are WT and segregate WT. The results of four PCR analyses are indicated in figure 4-1 below. L4 synchronized nematodes were selected randomly from agar plates and washed as described in section 3.2 of this study. The resulting PCR products were separated by agarose gel electrophoresis along with a DNA size marker/ ladder used to estimate size of DNA fragments after they have migrated in the gel as seen in figure 4-1 below.

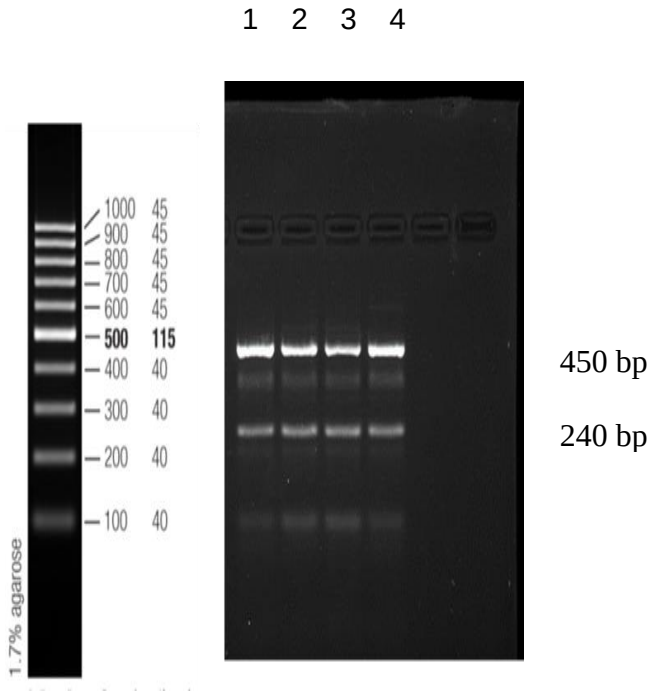

Figure 4-1: Agarose gel electrophoresis data for genotyping. The DNA fragments were resolved on 1% agarose gel. The four lanes (1-4) indicated above are the estimated PCR product sizes of the single L4 VC1196 strains randomly isolated from each plate.

The purity of the isolated DNA was determined using Nanodrop™ [16] , since crude nematode lysate was used as a template DNA. The A260/A280 obtained was ~1.6 thus indicating possible protein contamination. Nonetheless, the PCR products confirmed the genotypes of the *moma-1* mutant as observed in figure 4-1 above, the green and purple arrows indicating heterozygous alleles with estimated 450 and 240 base pairs respectively for all the isolates (lane 1-4). Non-specific bands (lane 3 and 4) were observed despite countless attempts to optimize the temperature via temperature gradient, another contributing factor to the observed non-specific bands, is the method of DNA isolation as crude nematode lysate was used as a template strand. This strain was provided by the *C. elegans* reverse genetics core facility [17] which forms part of the gene knockout consortium (The C. elegans Deletion Mutant Consortium, 2012).

[16] # ND-200
[17] University of British, Columbia

4.2. Detection of alterations in cristae morphology using Transmission electron microscopy (TEM)

Normal mitochondrial functions are intrinsically associated with morphology and ultrastructure (Hoppins *et al*., 2011; Collegari *et al*., 2019). Thus, characterising aberrant mitochondrial morphology features can be a crucial step in providing the insight into the underlying pathogenesis of acquired and inherited mitochondrial diseases. Mitochondrial architecture changes depending on the energy requirements and other signalling events of the cell (Cervantes-Silva *et al*., 2021). It is almost a century since the observations that mitochondria undergo drastic morphological changes during development were made (Smith., 1931).

4.2.1. Results

Mitochondrial cristae are the main OXPHOS and electron transfer sites in mitochondria (Brandt *et al*., 2017). Despite several advancements in mitochondrial research, cristae dynamics and remodeling remain elucive. The traditional method of using electron microscopy cannot reflect the dynamic challenges of mitochondrial cristae in living cells it can only dispay cristae morphology of a certain section in the mitochondrial sample. The images depicted in figure 4-2 shows inner mitochondrial membrane structure of L4 staged nematodes. The images from 1- 4 represent the VC1196 strain which is deficient of the Mic27 subunit of the MICOS and the images from 5- 8 represents the N2 Bristol strain that was used as a WT strain in this study. As observed in figure 4-2 is evident that the internal morphology of the *moma-1* (images 1-4) mitochondria is severely disrupted. The parts demarcated in red in figure 4-2 shows aberrant onion-ring like cristae with no clear cristae junctions. While the images demarcated in green (5-8) shows a mixture of well-defined large tubular and lamellar cristae structures that are characterised by clear cristae junctions. The cristae are connected to the boundary region of the IMM by cristae junctions as indicated by the yellow arrows in images 5 and 7 of figure 4-2 below.

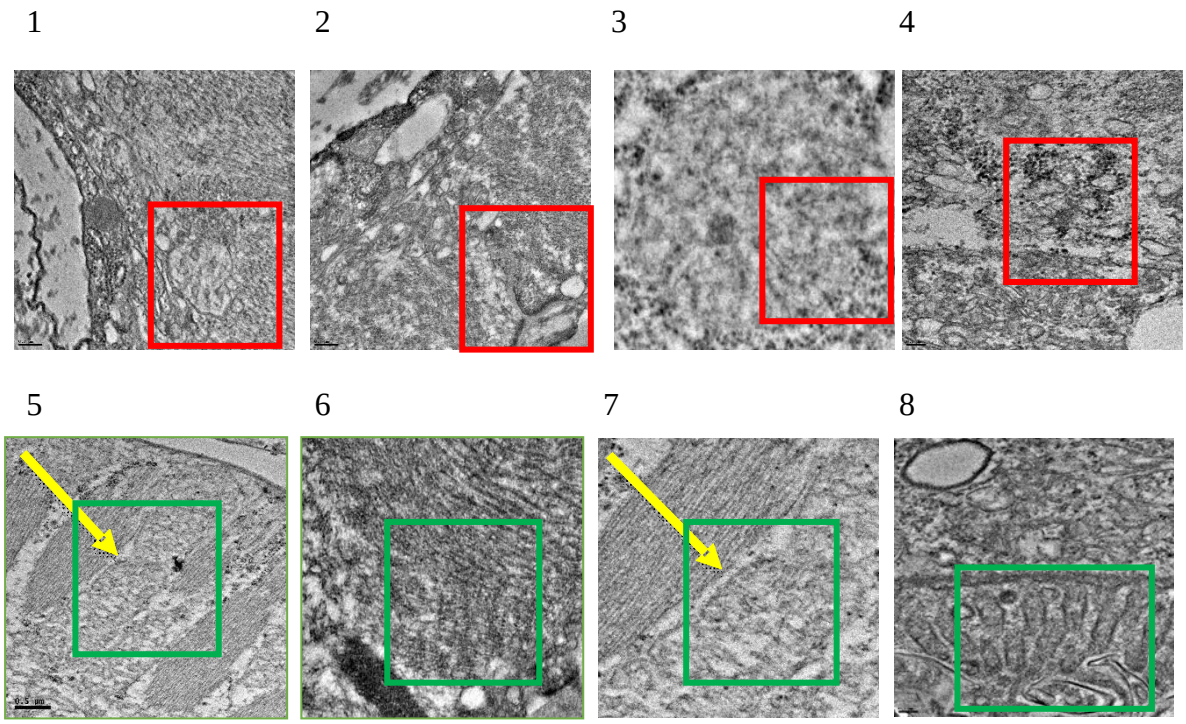

Figure 4-2: Transmission electron microscopy images indicating the mitochondrial ultrastructure of VC1196 (1-4) and N2 (5-8). The images depicted above shows the IMM with cristae and were taken from dissected L4 staged nematodes that were treated with different concentrations of fixatives and washed with different concentrations of ethanol prior image processing. A total of 11 images were taken per strain at 0º angle, non of the images were tilted.

4.2.2. Discussion

Cristae have been proposed to play a pivotal function in the regulation of dynamic distribution of lipids and proteins as well as soluble metabolites between the individual mitochondrial subcompartments (Zick *et al*., 2008; Vincent *et al*., 2016). A typical example is cytochrome c release upon apoptosis induction (Zick *et al*., 2008). These large cristae segments have been shown to account for substantial change in the composition of lipids or large molecular weight proteins (Vincent *et al*., 2016). The aberrations in the first four images (1-4) in figure 4-2 are a result of a mutation in the MICOS which plays a pivotal role in the formation and maintenance of mitochondrial cristae (See section 2.2). The mitochondria observed in images 1 and 4 contain many networks of short pairs of membrane segments which are indicative of onion-ring like cristae. Conversely, mitochondria observed in images 2 and 3 have localised swellings and thin tubular connections. The images demarcated in green (5-8) show a mixture of well-defined large tubular and lamellar cristae structures that are characterised by clear cristae junctions. The cristae are connected to the boundary region of the IMM by cristae junctions as indicated by the yellow arrows in images 5 and 7 of figure 4-2. According to existing literature, severe mitochondrial dysfunction

as anticipated in an organism's disease state has detrimental consequences that may include arrest of development to shortened life span (Rea *et al.,* 2007; Lapierre and Hansen., 2012; Munkacsy and Rea., 2014). These alterations in the inner membrane topology have been demonstrated to have a negative impact on mitochondrial bioenergetic processes (Mannella., 2006).

The observed features of the VC1196 cristae in figure 4-2 (image 1-4) present similar phenotypes to the double knockout Mic27 human cells (Anand *et al.,* 2020). The observed cristae features in the human cells are characterised by more concentric onion-like shape with loss of cristae junctions. It was further revealed that Mic26 and Mic27 complement each other partially, and they fullfil functional roles that cannot be compensated fully by other MICOS subunits. This is indicative that coordinated function of Mic26 and Mic27 is essential for normal formation of cristae junctions and indicates cooperation between Mic26 and Mic27 in the regulation of cristae structure.

4.3. Untargeted lipid metabolism

Despite the great variation in the physiologies of nematodes and mammals, several proteins involved in the synthesis, oxidation and transport of lipids are highly conserved between the two species (Castro *et al*., 2012). For the present study, mitochondria were isolated as described in section 3.6.1, followed by incorporation of two metabolomic extraction procedures as explained in the SOPs standardised by the NWU mitochondrial research laboratory (see annexure C).

4.3.1. Results

The data represented in figure 4-3 below are results of 4 samples of each strain that were prepared using mitochondrial fractions of the nematodes. Several unsuccessful attempts were made to optimize a suitable method that works for nematode lipidomics. These included (1) randomizing samples in the GC-TOF-MS, (2) addition of quality control (QC) samples, (3) large sample preparation, however, there were more free fatty acids in most of the results than methylated fatty acids as anticipated. The results represented below were used as preliminary data as they were better than the previous experiments.

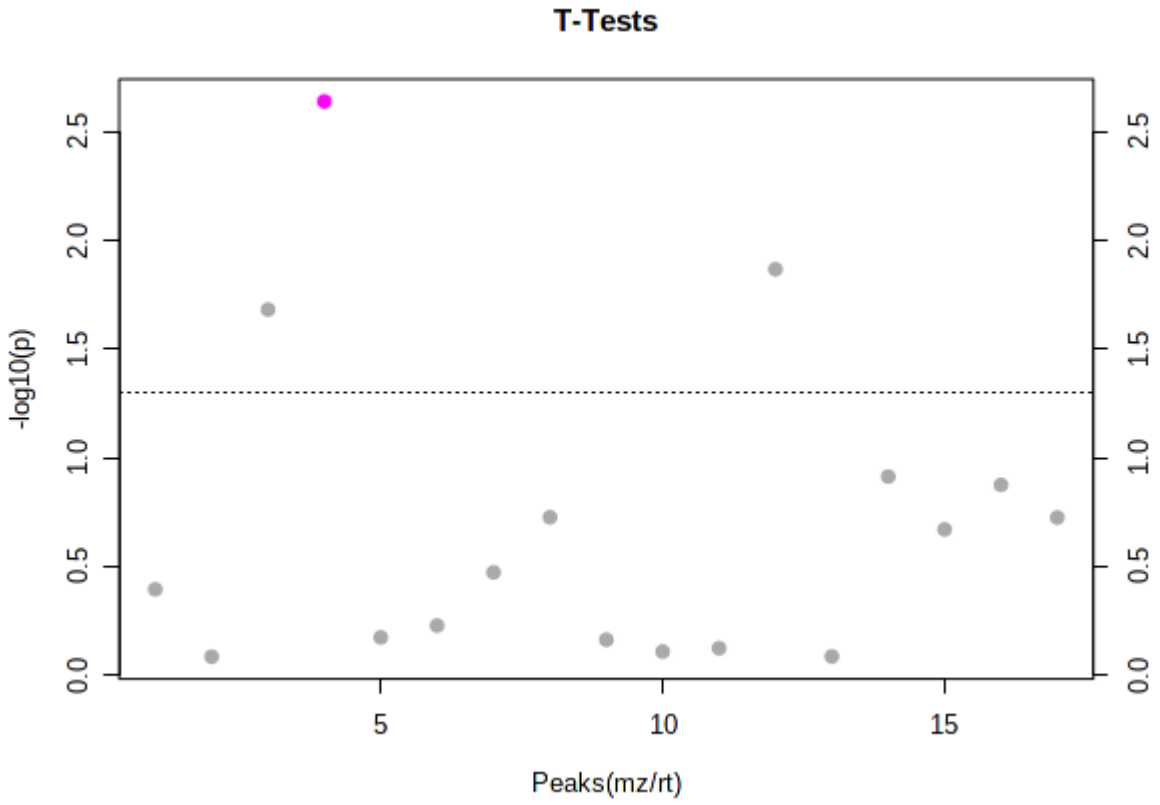

Figure 4-3: **Lipid profilling between N2 and VC1196.** The purple circles represent features above the threshold (0.05).

Univariable statistical methods ware used for exploratory data analyses. For the present study, two tailed student t-tests were used to analyse the statistical significance of fatty acid metabolite levels when comparing the VC1196 to the WT N2 strain. The important features identified by the t-test with a threshold of 0.05 are depicted in figure 4-3 above, the p-values were transformed by -log10 to plot more significant features (with smaller p values) higher on the graph. Table 4-1 below shows a summary of the significant features that are plotted in figure 4-3 above.

Table 4-1: Important features between VC1196 and N2 strain identified by t-test

Peaks(mz/rt)	t.stat	p.value	-log10(p)	FDR
1 Methylmalonic acid 2TMS	5.068	0.0022925	2.6397	0.038973
2. Silanol, trimethyl-, phosphate (3:1)	3.4545	0.013558	1.8678	0.11524
3. N, N-Diethyl(trimethylsilyl)carbamate	3.113	0.02077	1.6826	0.1177

4.3.2. Discussion

Data matrices were individually inspected (correct peak picking and alignment, batch effect and data integrity) as well as pre-processed (data filtering, missing value imputation and normalisation).

Metabolites were normalised to peak area because previous experiments using nonadecanoic acid as an external standard did not yield good results. The compound nonadecanoic acid is classified as a long chain fatty acid (between 13 and 21 C-atoms), and several studies have been published using this aliphatic fatty acid as either an internal or external standard in lipid profiling (Croxton *et al*., 2006; Faizi *et al*., 2014; Williams *et al*., 2021). Important long chain fatty acids such as octadecanoic and hexadecanoic were not significantly different between the two groups. Despite several attempts to optimize a better lipid profiling method, there were still free fatty acids detected by the platform. The possible contributing factors are that (1) the electron ionization mass spectra suffers from frequent weakness of the molecular ions, and (2) only relatively small range of volatile thermally stable compounds are ameable for analysis. Fatty acids can modify lipid membrane structure, altering its physical properties, microdomain organization, and provoking changes in cell signaling (Ibarguren *et al*., 2014). Therefore, it is possible to regulate membrane structure by modulating fatty acids.

As discussed in section 2.5 of the present study, mitochondrial ultrastructure alterations are linked to several diseases. A typical example is Barth syndrome, a mitochondrial disorder caused by mutations in Tafazzin (Acehan *et al*., 2010), which is involved in cardiolipin (a mitochondrial phospholipid) biosynthesis. This is indicative that lipids play a vital role in mitochondrial ultrastructure maintenance. The summarised compounds in table 4-1 above are important features between the two strains. Methylmalonic acid is a relatively neutral and hydrophobic molecule (Zick *et al*., 2008). The ester phospholipids are major structural components of all biological membranes and are vital for indirect and direct regulation of cellular function (Brock *et al*., 2007; Shmookler Reis *et al*., 2011).

4.4. Bioenergetics assays: Measuring oxygen consumption rate

Oxygen consumption rate (OCR) is a crucial marker showing the cellular function during an organism's lifetime under metabolically challenged or normal conditions (Ryu *et al*., 2016). It is utilized to investigate factors mediating the switch from OXPHOS to aerobic glycolysis (Chen *et al*., 2015) or to understand mitochondrial function (Palikaras *et al.*, 2015). The OCR of 150 intact nematodes per genotype was measured at 15 minutes intervals using the Oxygraph 2k high resolution Oroboros respiratory analyser (Oroboros, Instruments, Innsbruk, Austria) containing 2 ml M9 buffer (section 3.6). The high-resolution respirometer traces are shown in figure 4-4 below.

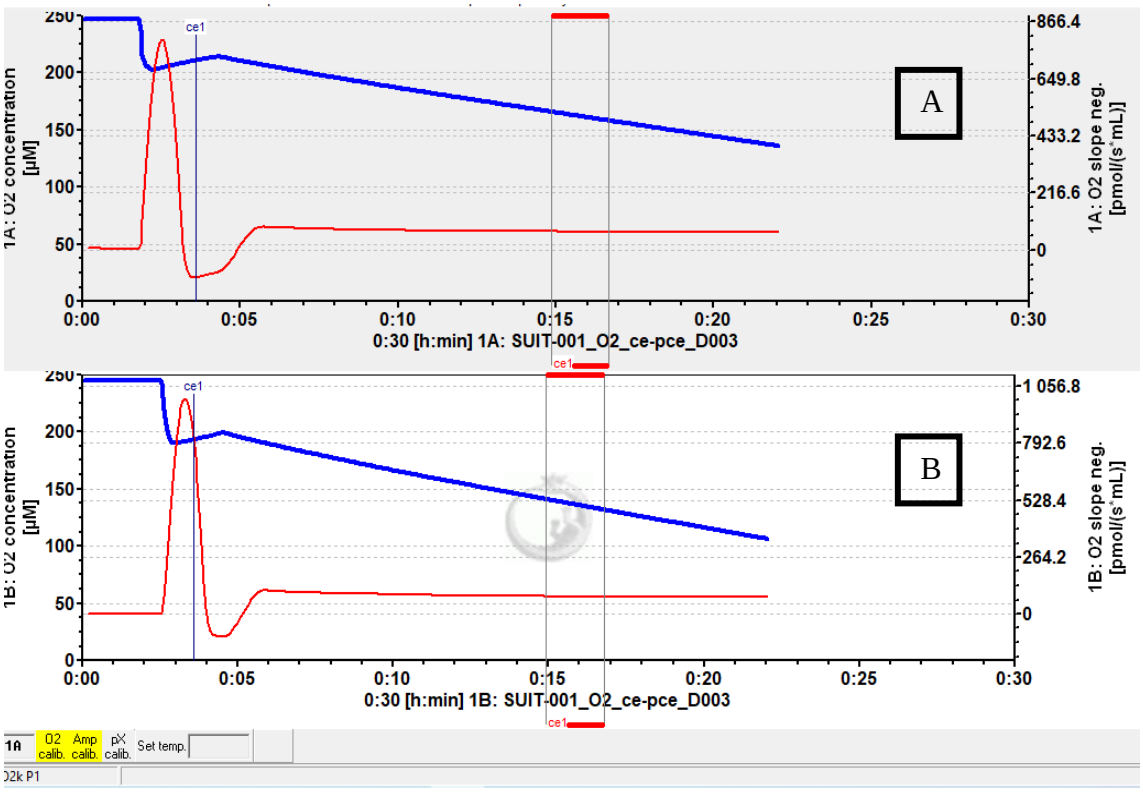

Figure 4-4: **High resolution respirometry traces indicating OCR (red lines**). The blue lines indicate the concentration of oxygen within the chambers (nmol/ml). The N2 strain traces are indicated by (A) and VC1196 traces are indicated by (B), the measurements were taken at 15 minutes for both strains.

There is growing evidence that underlies mitochondrial function as possible contributor in viability and homeostasis in organisms (Vafai and Mootha, 2012). Cellular OCR is recognized highly as an essential indicator of mitochondrial function, reflecting the production of ROS and metabolic activity of the cell. Therefore, several methods have been employed to measure OCR in cells or entire organisms (Dranka *et al.*, 2011; Luz *et al.*, 2015; Perry *et al.*, 2013).

4.4.1. Results

The OCR is a measure of mitochondrial function and energy production rate (Ng and Gruber., 2019). The levels of O_2 were maintained above air saturation to avoid limitation in experimental O_2 of respiration. The analysed data points are indicated in figure 4-5 below.

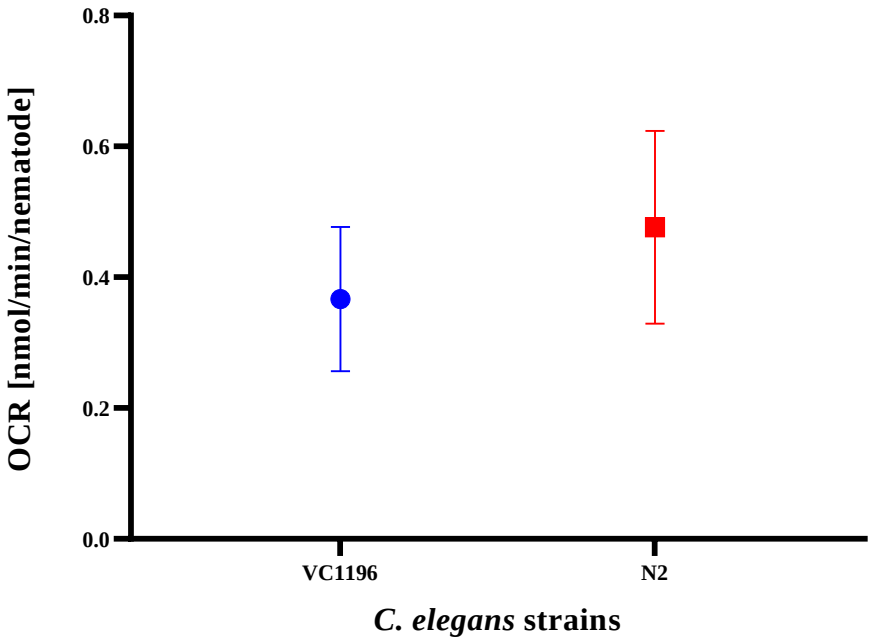

Figure 4-5: Graph depicting the average oxygen consumption rate (OCR) between the WT and mutant C. elegans strain. The Y-axis indicates the ORC per nematode and the X-axis indicates the nematode strains used. The error bars indicate SD with P<0.58 calculated using a two tailed t-test for three repeats.

4.4.2. Discussion

As previously discussed in section 2 of the present study, mitochondrial function is not solely limited to the production of energy, but is also essential for ROS scavenging, apoptosis, and cellular homeostasis (Wallace., 2005; De Marcos-Lousa *et al*., 2006; Reinecke *et al.,* 2009; Eramo *et al.,* 2020). Thus, normal mitochondrial function is critical in organismal health. Previous studies have utilised several assays to assess mitochondrial function, including but not limited to analyses that measure mitochondrial calcium concentration, membrane potential, ROS, and ATP level (Luz *et al*., 2014; Sarasija *et al*., 2018). However, measuring OCR serves as a superior mitochondrial function indicator as it is reliant on sequential events during the production of ATP unlike the other indicators which only provide a single snapshot of mitochondrial function (Perry *et al.,* 2013; Ryu *et al*., 2016). In the present study, the rates of O_2 consumption were calculated using a software (DatLab) and was expressed as nmol/min/nematode.

The average OCR of the N2 and the VC1196 strain are indicated in figure 4-5 above. A total of 150 live L4 age synchronized (see section 3.3) nematodes were used to measure the basal oxygen consumption rate in triplicate as described in section 3.6 of this study. OCR was monitored in real time as a decline in O_2 saturation in both chambers. The outcomes as indicated in figure 4-5 above

indicates the decline in the OCR of the MICOS subunit deficient strain when compared to the WT strain. Since OCR is a decisive indicator of mitochondrial health, these results shows that mitochondrial function of the VC1196 stain is lower (36% decrease compared to the N2 strain) as a result of the mutation that is characterised by aberrations in its inner membrane (See section 4.2 above), although this change was not statistically significant ($P<0.58$). In addition, previous studies show that mild mitochondrial stress that results from either pharmacological or genetic interventions extend *C. elegans* life span, while severe mitochondrial dysfunction, as expected from an organism's disease state can result in shortened life span (Lapierre and Hansen., 2012; Munkacsy and Rea., 2014).

4.5. OXPHOS complex activity assays

Mitochondria harbour pathways involved in the synthesis of ATP through the TCA cycle and OXPHOS. Energy obtained from electron transfer is utilised by respiratory complexes I, III and IV to pump protons from the mitochondrial matrix into the IMS (Dancy *et al*., 2014). A proton motive force is generated in the process and drives ATP synthesis by a flow of protons back into the mitochondrial matrix through ATP synthase. The OXPHOS system is known to have several adaptive responses to counteract dysfunction in a part of the system. Thus, even though the overall respiration was not significantly affected by the *Mic27* deficiency in the VC1196 strain, it is still possible to see differences in individual OXPHOS complex activity.

4.5.1. Results

The three respiratory complexes analysed in the present study (CI, CIII and CIV) have been shown to play a pivotal role in generating the proton gradient across the cristae membranes (reviewed in Kühlbrandt., 2015). Previous studies have shown that the life span of *C. elegans* depends on the normal functioning of the mitochondrial ETC (Ventura *et al.,* 2006; Rea *et al*., 2007; Dancy *et al*., 2014). Respiratory flux measurement in different metabolic states was needed for assessment of the effects on OXPHOS of changes in metabolomic levels, individual enzyme activity or membrane permeability (Dancy *et al*., 2014).

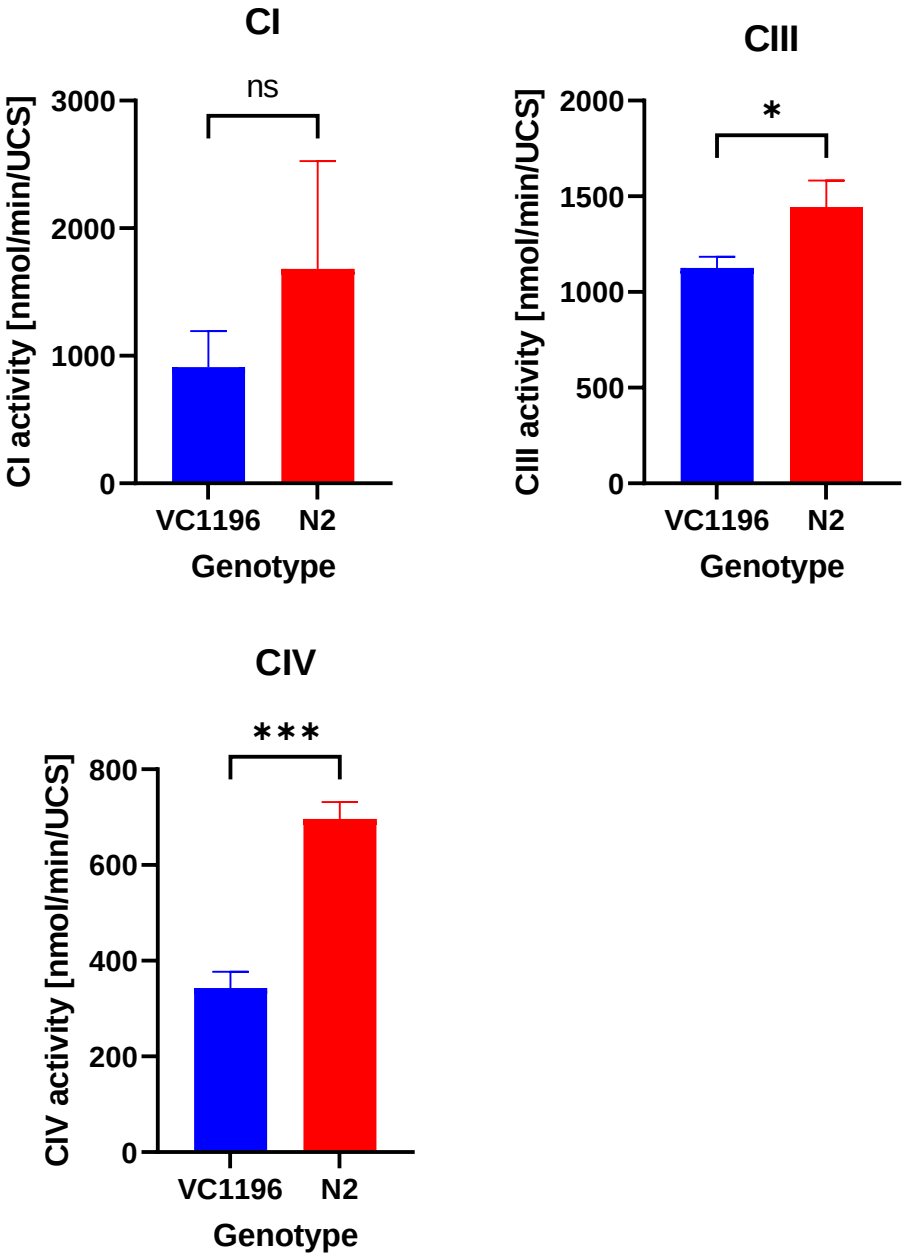

Figure 4-6: Bar charts indicating decrease in VC1196 enzyme activity compared to N2 strain measured for CI, CIII and CIV. The data plotted is the activity of enzyme per unit citrate synthase (UCS) and the error bars represent SD (n=3). The figures representsenzyme activity measures of complex I, complex III and complex IV respectively. The VC1196 strain shows reduced enzyme activity for all the three complexes measured. P-value 0.209, *0.021 and ***0.0002 respectively.

4.5.2. Discussion

Several advancements have been made to better our understanding of mitochondrial bioenergetics using *C. elegans* mutants affecting vital components of the metabolic pathways (Suthammarak *et*

al., 2013; Van der Bliek et al., 2017). In the present study, enzyme activity of three different complexes was spectrophotometrically measured using *C. elegans* mitochondrial fractions (see SOP in annexure B). According to existing literature, mitochondrial supercomplexes containing the above-mentioned respiratory complexes are now regarded as an established entity (Suthammarak *et al*., 2010). These supercomplexes have been theorised to enhance function of the respiratory chain by permitting channelling of quinone between CI and CIII. Analyses were performed in triplicate and were normalised to unit citrate synthase (UCS). Citrate synthase is a common quantitative mitochondrial marker which involves two coupled reactions. The reactions consist of citrate synthase catalysed production of free CoA-SH from oxaloacetate condensation with acetyl-CoA (Jansen *et al*., 2007). Thus, this enzyme is at the intersection of fuel catalysis and entry of metabolites into the TCA cycle making it a superior biomarker of mitochondrial content (McLaughlin *et al*., 2020).

The activity of CI was analysed slightly different to the other two complexes as measurements are obtained in the absence and presence of a classical complex I inhibitor rotenone, thus the initial velocity was calculated as the difference between DMSO (v_1) and rotenone (v_1). Complex I is the largest MRC enzyme and establishes the access point of electrons into the system. As expected, the enzyme activities (nmol/min/UCS) of the mutant strain were lower compared to the WT strain due to defective mitochondrial function (First graph in figure 4-6), although the change was not statistically significant ($P<0.209$).

Complex III forms the central fragment of the ETC, it is responsible for pumping protons to the IMS from the matrix through oxidation of coenzyme Q and cytochrome C reduction (Crofts *et al*., 2008). The enzyme activity of the mutant strain was sustainably reduced for CIII compared to the WT strain. The observed changes between the genotypes were statisrtically significant ($P< 0.021$). The results depicted in figure 4-6 (second graph) above indicates the processed data points (nmol/min/UCS) for the two *C. elegans* strains.

Complex IV/ cytochrome c oxidase (COX) activity was also significantly reduced in VC1196 strain compared to the WT N2 strain ($P<0.0002$). This complex is the last respiratory chain electron acceptor and is involved in the reduction of O_2 to H_2O (Mansilla *et al*., 2018). Evidence from a study conducted by Suthammarak *et al*. (2009) support the interdependence among respiratory chain complexes, however, the mechanism regulating this phenomenon remain elusive. In addition, a year later Suthammarak *et al*. (2010) further revealed that CIII affects supercomplexes I, III & IV formation by acting as a stabilizing factor or an assembly in mutant C. elegans strains they

analysed. The defective mitochondrial function of the VC1196 strain in the present study was suggested by the aberrant cristae morphology as observed in figure 4-2 (images 1-4) due to its deficiency in a MICOS subunit (Mic27) which contains a lipid binding domain (see section 2.2 and 2.5).

4.6. Phenotyping

The second objective of this study was to phenotypically characterise the VC1196 strain compared to the N2 strain which has been used as a background or wild type strain since its discovery over four decades ago (Brenner, 1974). Three assays were tested using live L4 nematodes (Lifespan/survival, chemotaxis, and gentle touch)

4.6.1. Lifespan analysis

Life span assays were performed as described in 3.7.1 of this dissertation with live L4 staged nematodes. The recordings were taken from day one until the last member of the population died. The results presented below are a summary of the outcomes, the p-values in this section were determined using the Mentel-cox test.

4.6.1.1. Results

The results in the subsections below are life span analyses using three different experimental set ups as elucidated in chapter 3 of the present study. All the experiments were performed in triplicate. The error bars represent the standard deviation and, the p-values were calculated using two tailed students' t-test.

4.6.1.2. Lifespan analysis without 5-fluoro-2-deoxyuridine (FUDR)

Biological subsystems are characterized by a functional decline with increasing age, and lifespan is the main endpoint of interest in age related studies. Figure 4-7 below indicates the data recorded from the beginning of the experiment until the last member of the nematode population died.

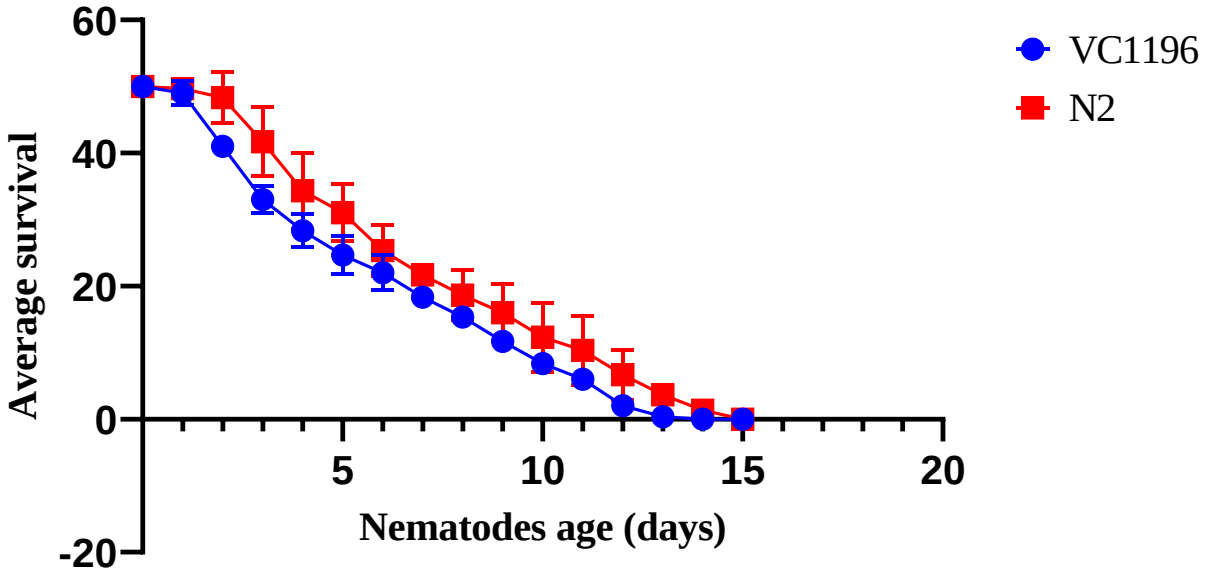

Figure 4-7: **Average lifespan of *C. elegans***. The experiment was conducted in triplicate, datapoints represent the average survival of the nematodes on specific days and the error bars represent the SD (n=3). The P-value calculated using a two tailed student's t-test is 0.159**.**

Lifespan in nematodes typically refers to the number of days the nematodes remain responsive to external stimuli (Angeli *et al.*, 2013; Polisik *et al.*, 2014; Zhang *et al.*, 2021). Lifespan assays involve periodic examination of the nematodes from the beginning of their adulthood until the day the last member of the population dies (Amrit *et al.*, 2014, Haroon *et al.*, 2018). For this part of the project, lifespan was analysed as described in section 3.7.1. The survival curve of two populations was compared to determine the similarities or lack between the two nematode populations. As anticipated, the average lifespan of the mutant strain (VC1196) was shorter but not significantly different compared to the WT strain (N2).

4.6.1.3. Analysing lifespan in nematodes treated with FUDR

The use of 5-fluoro-2-deoxyuridine (FUDR) in *C. elegans* lifespan is a convenient measure that minimizes biased results as it is not necessary to transfer nematodes into new plates every 16 hours to prevent mixture of different larval stages. This method of sterilizing the nematodes is effective and has been proven to extend lifespan of the nematodes (Amrit *et al.*, 2014). The nematodes treated with FUDR (see recipe 1) lived longer compared to the other two lifespan analyses. This is because nutrients in the plate can last longer as the nematodes do not reproduce after treatment with this drug. The statistics were taken on 24 hours intervals, from the results as indicated in figure 4-8, the VC1196 strain was recorded to have a shorter lifespan compared to N2 strain.

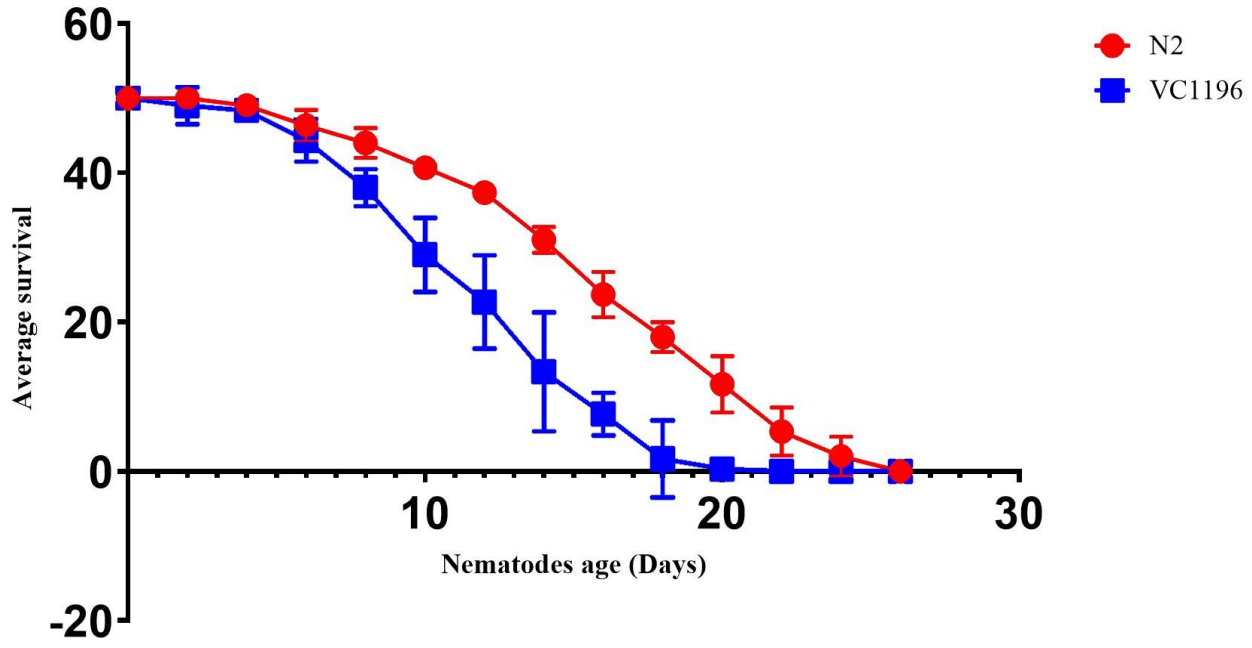

Figure 4-8: Average lifespan of *C. elegans* treated with FUDR. 50 L4 nematodes were sterilized by treating with FUDR, and plated on an NGM plate containing sufficient nutrients (OP50) and incubated at 20°C. The error bars represent SD (n=3) with ***P<0.0001.

4.6.1.4. Lifespan analysis on metabolically stressed nematodes

The results observed in figure 4-9 depicts results of survival of metabolically stressed *C. elegans* strains. The nematodes were grown as described in section 3.3 of this study. A total of 50 L4 staged nematodes were transferred to tBHP agar (Recipe 2) and incubated at 20°C. The measurements were taken every 60 min until the death of the last member of each population group. The chemical tert-Butyl hydroperoxide (tBHP) is an oxidizing agent in a variety of chemical transformations (Wang *et al.*, 2003). Organisms and cells constantly face exposure to ROS either as by-products from internal metabolic processes or the surrounding environment (Ewald *et al.*, 2017). Metabolic stress was induced to the nematodes by exposing them to the chemical tBHP (see section 3.7.5).

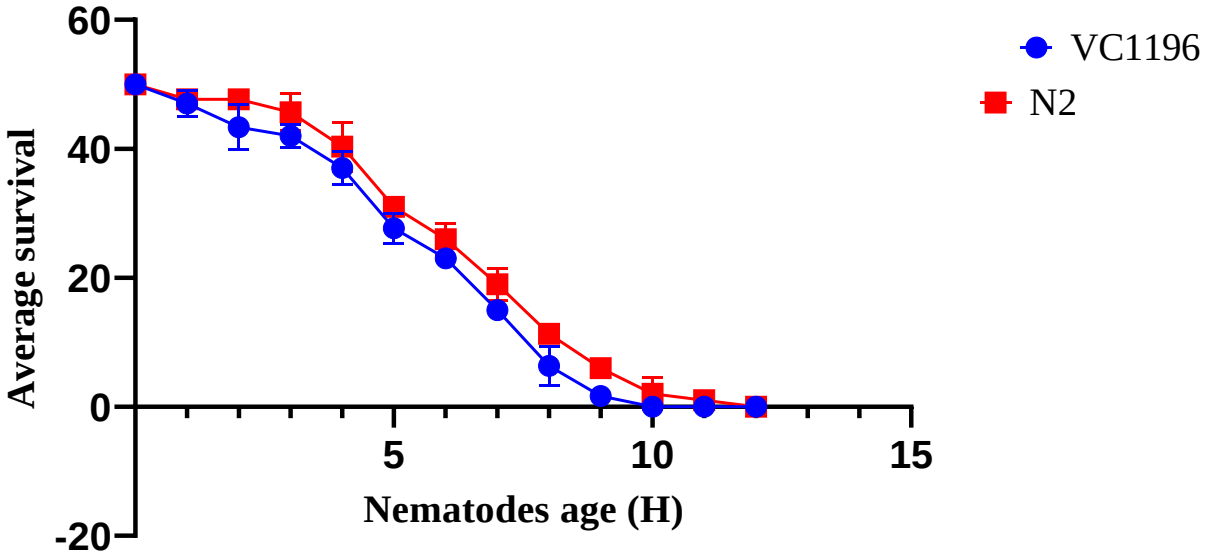

Figure 4-9: Average lifespan of metabolically stressed *C. elegans* strains. 50 nematodes were exposed to harsh conditions to measure the sensitivity to oxidative stress using tert-Butyl hydroperoxide (tBHP) as a source. The data points represent the average survival per hour and the error bars represent SD (n=3) with **P<0.002 calculated using two tailed Student's T test.

Cells have evolved detoxification mechanisms to prevent cellular death from ROS, and the downstream responses and activation of these mechanisms represent an overlapping defence response that can be adapted to distinct ROS sources to protect cells. The results obtained (figure 4-9) is indicative that these protective mechanisms are essential for healthy aging. The mutant strain (VC1196) showed a decreased lifespan in response to the harsh environmental conditions compared to the N2 strain.

4.6.1.5. Discussion

There was statistically significant difference in lifespan between the two genotypes for two of three three experimental setups. The results shown in section 4.6.1 above all indicate that VC1196 had a shorter lifespan compared to the N2 strain although the results were not statistically significant for lifespan analyses done without the use of chemicals like FUDR and tBHP. Survival of N2 strain is used as a benchmark to conclude if treatments or mutations change the lifespan of *C. elegans.* The survival and average lifespan of N2 strain ranges from ~7 to over 35 days in many published peer reviewed articles (Mcroitchel *et al.*, 1979; Lucanic *et al.*, 2017; Haghani *et al.*, 2019). There are several factors that can also influence survival of *C. elegans*, and temperature is the most important contributing factor as nematodes grow much faster at higher temperatures (~22-25°C) compared to lower temperatures (~18-20°C). This rapid increase in nematode progeny results in fast depletion of

nutrients in the plate due to competition among the large population. However, there is inconsistency in the lifespan of N2 strains across published literature. The summarized data in table 4.2 below is randomly collected experimental data from published articles within the last decade including data generated from this study. The changes in lifespan as tabulated below only covers the N2 strain as it has been used as a benchmark in several lifespan studies, there are no studies in literature that have covered lifespan in MICOS nor CI, CIII and CIV defects in *C. elegans*.

Table 4-2: Comparing N2 lifespan under different growth conditions

Initial number of nematodes	Temperature (°C)	Additional supplements/chemicals	Approximate mean lifespan (days)	Reference
100	20°C	Aspartame (ASP)	25	Zhang *et al*., 2021
100	20°C	Cocoa	23	Munasinghe *et al.*, 2021
100	20°C	Ferric acid	22	Li *et al.*, 2021
100	20°C	Carnitine	35	Rasulova *et al*., 2021
100	20°C	Acesulfame potassium	25	Zhang *et al.*, 2019
100	15°C	None	30	Henderson *et al.*, 2018
100	25°C	Fudr	14	Polisik *et al*., 2014
100	25°C	Fudr	18	Angeli *et al*., 2013
50	20°C	Fudr	25	This study
50	20°C	tBHP	12 (Hours)	This study
50	20°C	None	16	This study

There are several physiochemical parameters that have been demonstrated to affect the lifespan of *C. elegans*, such factors include temperature (Amrit *et al*., 2017) and chemical exposure (Polisik *et al*., 2013; Zhang *et al.*, 2021). The usage of the most common supplement in *C. elegans* lifespan assays (Fudr) has been documented to influence survival of nematodes (Amrit *et al*., 2017). However, the utility of FUDR in lifespan experiments has been questioned due to insufficient knowledge on its mechanism of action and potential effects it possesses on the development of the nematode. In a study conducted by Feldman *et al*. (2014), it was revealed that this oncology drug

alters a critical process involved in regulating *C. elegans* lifespan (proteostasis[18]). In addition, Wang *et al*. (2019) further showed that N2 phenotypes are impacted by temporal administration of FUDR and may also increase the lifespan of N2 strains. The inconsistency observed in table 4-2 above is concerning considering that the N2 strain is used commonly as a benchmark in a variety of *C. elegans* studies, thus this inconsistency may lead to false conclusions regarding the role genes in regulating the lifespan of *C. elegans*.

The three lifespan experiments conducted in this study supports the hypothesis (2.10.3) as stated in section 2.10.3 as the Mic27 deficient strain (VC1196) had a shorter lifespan than the N2 stain. The chemical FUDR was used because examining *C. elegans* lifespan without sterilizing the nematodes requires frequent transfer of the nematodes into fresh OP50 seeded plates approximately every 48 hours until end of the analyses. This method is time consuming and is the primary cause of distress to the nematodes. Frequent transfer of nematodes from one plate to another can thus lead to false conclusions as nematodes often die during this process, moreover, this maximizes contamination more especially when not working in the flow cabinet.

4.6.2. Chemotaxis

Many organisms employ chemotaxis to find mates, avoid noxious substances and find food (Ward., 1973). The chemotaxis assay is based on the ability of an organism to respond to an odorant when placed at distance from the source (See figure 3-3). Decreased chemotaxis in adult *C. elegans* can be an indicator of lack of movement caused by dysfunctions of the muscle cells or the motor nearons that innervate the muscle cells, and not an inability to sense the different chemicals (Haroon *et al*., 2018). In addition, chemotaxis assay can be utilised as a screening tool in the identification of genes that can improve the pathology related with mtDNA diseases.

4.6.2.1. Results

C. elegans chemotaxis towards food source (*E. coli* OP50) has been described by sensing both volatile and water-soluble compounds (Zhang *et al.,* 2016). The nematodes are capable of differentiating pathogens from food because they naturally live in soil inhailed by different microorganisms (Beale *et al.*, 2006). In addition, *C. elegans* have been widely used in behavioural studies ranging from simple chemo-sensation to associative learning and memory. In the present study Benzaldehyde (5%) and absolute ethanol (99.9%) were used as test and control compounds respectively. The volatile chemical benzaldehyde evokes a robust *C. elegans* chemotactic response. This chemical has been previously tested as an attractant over a wide range of concentrations

[18] Dynamic regulation of proteins with the cell to ensure a balanced and functional proteome.

(Bargmann *et al*., 1993). The results shown in figure 4-10 below shows the chemotaxis behaviours of the VC1196 and N2 strain in the presence of the test (benzaldehyde) and control (absolute ethanol) compounds.

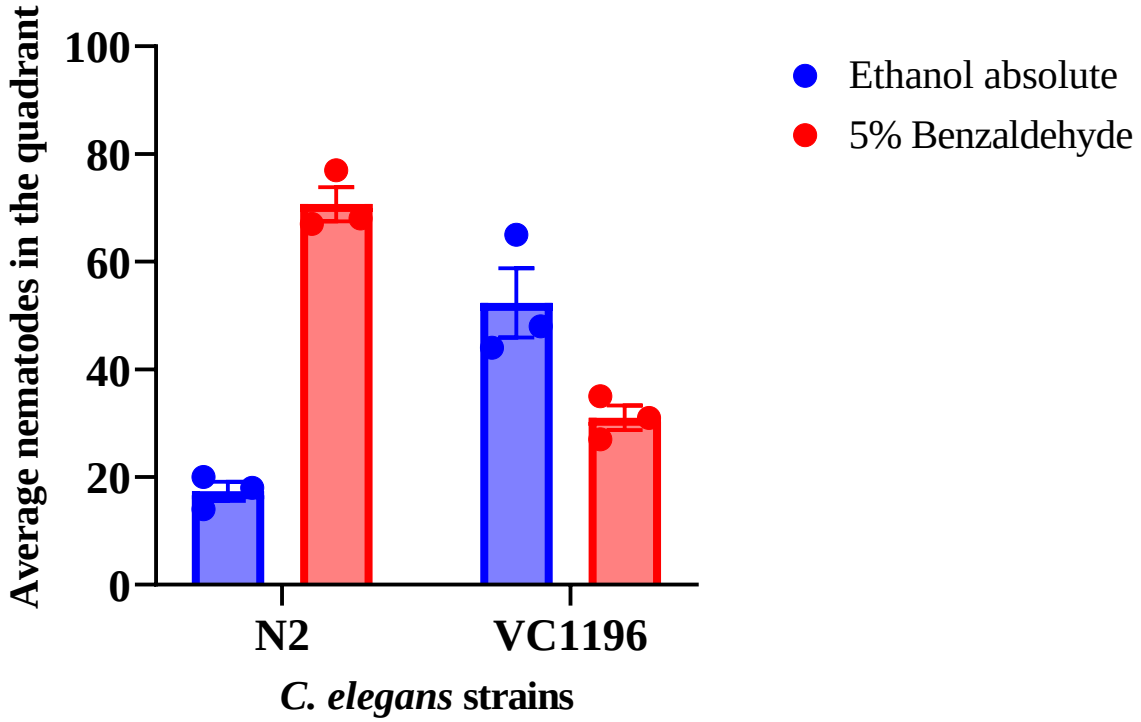

Figure 4-10: Chemotaxis graph depicting the behaviour of starved L4 C. elegans strains under the exposure of different compounds. The control compound was absolute ethanol (99.9%), and the test compound was Benzaldehyde (5%). The chemotaxis index was calculated using equation 3-6. The error bars represent SD (n=3) ***P<0.0001 calculated using two tailed Student's T test.

4.6.2.2. Discussion

As it can be seen in figure 4-10 above, of the 100 L4 staged VC1196 nematodes that were placed in the center of the petri dish as described in section 3.7.2 of this dissertation, 52 nematodes moved to the control compound and 31 moved to the test compound. On contrary, of the 100 L4 staged N2 nematodes placed at the center of the petri dish, 17 nematodes moved to the control compound and 70 nematodes toved to the test compound. The chemotaxis index (equation 3-6) was recorded as -0.25 and +0.61 for the VC1196 and N2 strains respectively. The N2 showed attraction with about 60% of its population arriving at the quadrant containing the test compound (benzaldehyde) while the VC1196 strain showed repulsion with a larger percentage arriving at the quadrants containing the control compound (absolute ethanol).

The rapid response of VC1196 strain to the volatile organic molecule absolute ethanol is indicative that alcohol can spread through the air to be detected by the nematodes due the impaired physiological state supported by most the results presented in the present study. Recent studies have demonstrated that *C. elegans* mutants can often show preference for stimulants (Engleman *et al*., 2018; Iwanir *et al*., 2019). According to existing literature, mitochondrial dysfunctions do not only affect longevity in *C. elegans* but impairs function of neurons and therefore the sensory ability of the nematode to track food (Bargmann., 2006; Magnolia *et al*., 2014). Avoidance behavior in nematodes is triggerred by physiological stress, which often causes the animals to optimize their survival chances by staying away from potential threats (Yueh-Chen *et al.,* 2022). In addition, mitochondrial disruptions induce nematodes to avoid non-pathogenic bacteria through a serotonergic neuronal circuit. This links longevity and chemotaxis through neuronal and cellular impairment that is triggered by oxidative stress.

4.6.3. Gentle and harsh touch sensation

Touch sensitivity allows animals to detect and react to external stimuli resulting from physical contact. Chalfie *et al*. (1997) has contributed significantly to the identification of mechanisms underlying touch responses in the nematode *C. elegans,* the widely used *C. elegans* behavioural assays are gentle touch (stroking nematode with fine hair) or harsh touch (Podding nematodes with platinum pick).

4.6.3.1. Results

The results presented in figure 4-11 below indicates the behaviours of the nematodes to external stimuli. The nematodes were gently touched with an eye lash (gentle touch) and with a platinum wire (harsh touch). The errors bars in the figure below represent the standard deviation, the p-values were determined using two tailed students' t-test.

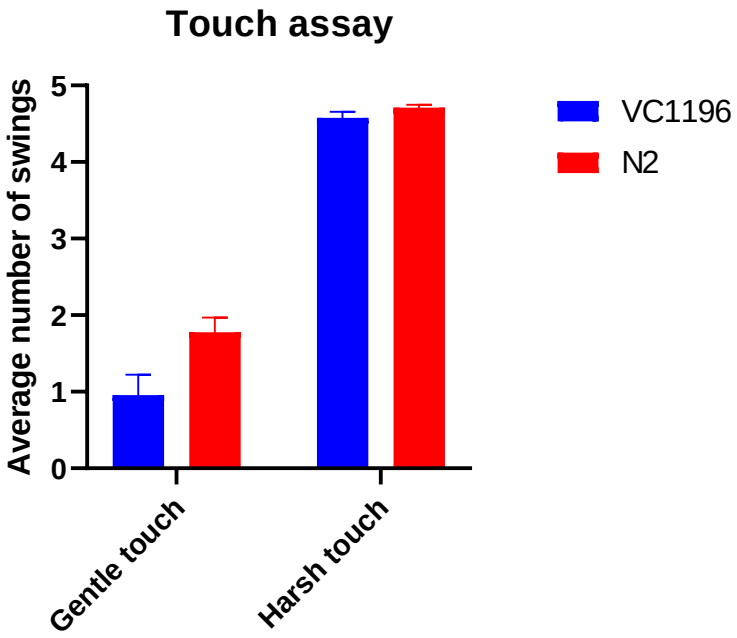

Figure 4-11: Schematic representation of touch responses delivered to different body parts. The Y-axis represents the number of swings (response) per strain and the X-axis represents different strains tested in this assay. The error bar represents SD (n=3) with P***<0.0001 calculated using two tailed stutent's t-test.

4.6.3.2. Discussion

Quantitative understanding of behavioural assays like touch sensitivity is crucial for understanding which genes and cells are essential to distinguish diverse physical properties and administrate diverse features of the response. Gentle touch and harsh touch are traditionally assayed using diverse tools and the nematodes are scored in binary manner as responding or not. Nevertheless, touch responses differ significantly both quantitatively [19] and qualitatively[20]. Figure 4-11 shows the results of the toch response between the VC1196 and the N2 strain. When the nematodes were touched near the center of the body, they induced either forward or reverse movement (results not included) with roughly equivalent odds. The Mic27 deficient strain also showed the same response as the WT strain, however, the average response to gentle touch with eyelash was lower in the mutant strain compared to the WT type strain. Both mutant and WT strain were responsive to harsh touches with a platinum wire.

[19] Distance travelled during response
[20] Movement direction

4.7. Conclusions

From the results presented in this chapter, it can be seen that the Mic27 deficiency of the VC1196 strain results in diseased phenotypes, when compared to the N2 strain. In general, the VC1196 strain performed significantly worse in most biochemical and phenotypic assays compared to the N2 strain. VC1196 nematodes demonstrated statistically significant decreases in CIII and CIV activity, life span, response to gentle touch, and response to a chemical attractant in comparison with N2 nematodes. These decreases also correspond well to the aberrations seen in the mitochondrial morphology, and the decrease respiration rates of VC1196 nematodes compared to N2 nematodes, although respiration rate decreased was not statistically significant. However, there certain factors that are necessary for the betterment of the obtained data, which can be used to unravel mitochondrial dysfunctions.

The TEM part of the study was just to campare the mitochondrial ultrastructure between the VC1196 and N2 strain in order to see the formation of cristae. To improve this, quantifications like multiple measurements of mitochondra or cristae and, measureing mitochondrial mass can be done to support the observations. Although there are several improvements that needs to be applied to fully understand the link between MICOS and mitochondrial dynamics, the results generated in this study can be used as a preliminary data for further investigations.

5. CHARPTER FIVE: FUTURE PROSPECTS, LIMITATIONS AND CONCLUSIONS

Chapter summary

This chapter summarises the data in the context of the aims and objectives of the study, and identifies limitations encountered in the present study as well as some future prospects in the field of nematology and mitochondrial research.

5.1 Aim, hypothesis and objectives

The IMM of the mitochondrion has high protein density and is differentiated into three distinct domains that are interconnected (refer to section 2.2). The cristae membranes house the assembled ETC protein complexes and ATP synthase which function together in the production of ATP through OXPHOS. The MICOS complex is implicated in many disorders including, diabetes, and Parkinson's disease as it is involved in the formation and maintenance of cristae. An organism's survival and health are influenced by its ability to regulate the production, storage as well as the release of energy. Lipids are important molecules that play a pivotal role in an organism's biology and are implicated in storage of energy, reproduction, lifespan, and many other signalling factors. The aim of this study was to extensively characterize the phenotypes, mitochondrial morphology, and function of a MICOS deficient C. elegans strain (VC1196) and compare it to the wild type (WT) N2 strain to better understand the role that the MICOS plays in mitochondrial health and function.

The hypothesis in section 2.10.2 stated that the MICOS subunit deficiency present in the VC1196 strain will lead to aberrant cristae morphology, decreased mitochondrial OXPHOS enzyme activity and thus respiration, and a dicreased phenotypes (lifespan, chemotaxis and touch assay). The results obtained in the present study supports the stated hypothesis. All the biochemical analyses of the MICOS deficient strain indicated decreased measurements compared to the N2 WT strain although some were not statistically significant. In addition, all phenotypic assays strongly suggest a diseased state in the VC1196 mutant strain.

5.1.1. Molecular and biochemical analyses

5.1.1.1. Genotyping

The first objective of the study was to confirm genotype of VC1196-strain, using PCR with agarose gel electrophoresis. The PCR products had several non-specific bands as a result of protein contamination as well as varying annealing temperatures (temperature gradient was used). An alternative method that can produce better results is the use of RT-PCR which is more rapid and

sensitive compared to normal PCR. The method employed in RT-PCR combines reverse transcription of RNA into DNA and amplification of specific DNA targets using PCR.

5.1.1.2 Mitochondrial critae formation

The second and third objectives of this study were to perform transmission electron microscopy (TEM) to visualise mitochondrial cristae morphology and in relation to this to analyse changes in the levels of lipids important for membrane formation, using untargeted lipid metabolite analyses on *C. elegans* VC1196 strain compared with *C. elegans* N2 strain. These findings are thus indicative of mitochondrial dysfunction, which was confirmed by the obtained transmission electron micrographs that showed aberrant cristae morphology in the VC1196 strain as compared to the N2 strain. These objectives were partially achieved as shown by disruptive cristae morphology on the mutant strain.

5.1.2. Biochemical characterization

The fourth and fifth objectives of this study were to perform respiratory analyses and OXPHOS enzyme activity assays as a measure of mitochondrial function in MICOS C. elegans VC1196 strain, compared with C. elegans N2 strain. The result obtained in this section of the study showed decrease in the OXPHOS enzyme activity of two respiratory chain complexes[21] analysed for the mutant strain compared to the WT strain. In addition, OCR of the mutant strain was lower compared to WT N2 strain, although it was not statistically different.

5.1.2.1. Phenotyping characterization

The sixth objective was to perform phenotypic characterisation assay of the MICOS C. elegans KO-strain compared to C. elegans wild type (WT) strain. The phenotypic assays that were used to characterize the Mic27 deficient *C. elegans* strain (VC1196) and compared to the N2 WT strain were (1) life span, (2) chemotaxis and (3) touch. All these assays evaluate the behaviour of *C. elegans* and can be used as a primary determinant to detect mutations in the nematodes. In two of the lifespan assays, the VC1196 strain was recorded to have a shorter life span compared to the WT N2 strain, this supported the hypothesis as stated in chapter 2. The experiments were performed with 50 L4 age synchronized nematodes to minimize biased results from different populations that often leads to false conclusions as the nematodes behave differently at different larval stages. Moreover, different experimental conditions were analysed to increase reliability of the results because a manual method was employed to count the nematodes.

The touch sensitivity results showed the same response between the mutant and WT strain, however, the average response to gentle touch with eyelash was lower in the mutant strain

[21] complex III and complex IV

compared to the WT type strain. In addition, the mutant strain responded to touches in the mid-posterior body thus reflecting the possible absence of TRN function. Both mutant and WT strain were responsive to harsh touches with a platinum wire. These objectives were successfully achieved as indicated by figures in chapter 4 and corresponding statistical discussions.

5.2. Limitations

There were several limitations that were identified during the processes of acquiring data in the present study. Despite the advantages *C. elegans* have over other model animals used to study mitochondrial dysfunction, there are several disadvantages when using *C. elegans* as a disease model. One major limitation is that the nematodes have a transparent body thus they lack several defined organs or tissues. This may narrow our understanding of tissue specific signalling such as where the gene is expressed since all the biochemistry is performed on the whole nematode/ extracts. Due to the small size of *C. elegans,* thousands of nematodes[22] are often required to perform other biochemical tests, this requires more space and preparation of reagents. In addition, it was difficult to optimize suitable methods as there is no sufficient existing literature that covers the use of *C. elegans* as per the objectives of this study. The importance of cristae in mitochondrial function has been elucidated in chapter two of the present study. TEM was only applied for comparing the inner mitochondrial structures of the VC1196 and N2 strain, other experiments that could have added value to the obtained results could not be performed due to limitted access to the laboratory as a result of the covid19 regulations that were imposed.

Sophisticated techniques can be employed particularly for all the phenotypic characterization assayed in the present study as the manual methods are time consuming and requires sharp concentration. For example, one widely used technique to quantitatively analyse chemotactic responses in *C. elegans* is the use of a microfluidic device (Hu *et al*., 2015). The nematodes swim upstream of the flow based microfluidic chip which generates eight flow streams containing stepwise chemical concentrations without the flow velocity difference. The chemotaxis behaviour of nematodes can be quantitatively analysed when they swim into the upstream observes ion channel containing different concentrations. However, these methods are limited by their low throughput and qualitative nature. A recent development is the introduction of a micro fluid device in which nematodes are subject to spatially localised stimuli with variable amplitude (McClanahan *et al*., 2017).

Touch sensitivity is a major technique that is used to detect an organism's behaviour in response to a stimulus. The limitation however, to traditional touch assays particularly in the nematode *C.*

[22] 5000- 20000 nematodes were used in several metabolomics studies

elegans is the degree of difficulty in controlling the stimulus strength that is delivered to the nematode by hand. Thus, although these results support the initially stated hypothesis (2.10.3), more quantitative results can be obtained by using advanced techniques like the microfluidic device. With the aid of this device, relative threshold response of gentle and harsh touch as well as the covered distance can be measured. In addition, the number of stimuli can be kept the same thus providing an even more accurate overview of how the nematodes respond to different touches. The most limitting factor in this study particularly for phenotypic assays was the use of manual methods to track the survival as well as mobility of the nematodes. Transfering nematodes from one agar to another using a platinum wire can induce stress and also result in death of the nematodes.

5.3. Future prospects

Genotyping is an essential technique that determines the differences in the genetic make-up of an individual, DNA sequences of an individual are examined and compared to a reference sequence or sequences of other individuals. For the present study, PCR technique was used to confirm the genotypes of the VC1196. However, more qualitative techniques can be employed, like sequencing the bands to confirm the amplification, or use qPCR to look for expression of Mic27 RNA to confirm if expression of its isoform is lost.

The mitochondrial morphology has been investigated to better understand its impact on the maintenance and function of the organelle. However, the mechanism in which cristae are formed and how their shape is regulated remains elusive to date. The analysis of morphology can be in *C. elegans* can be improved by using immunoflouresense using specific antibodies against mitochondrial components. This can improve desease dignosis and help scientists come with effective theurapetic mechanisms to unravel many mitochondrial disorders. In addition, existing literature associates OPA1 to dual role in cristae biogenesis and mitochondrial fussion. The complex between the long and short OPA1 forms is proposed to maintain the width of cristae junctions, which can restrict movement of metabolites such as cytochrome c. These are the most recent break through that has been made in persuit to understant the mechanism of cristae formation.

Emerging evidence positions the MICOS complex at the center of mitochondrial morphology management. Although it is still unknown how MICOS assembles and regulates cristae junctions, an understanding of this mechanism can be crucial in the development of theurapetics treatments for mitochondrial disorders. The traditional TEM technique applied in this study display the crista morphology of a certain section of a mitochondrial sample and does not reflect the dynamic changes of mitochondrial cristae in living cells. Thus, for better understanding of the mitochondrial

ultrastructure, tilting eyepiece can be mounted in the microscope to provide continuous adjustment of the tilt angle through a range of zero and 45 degrees for viewing at the optimum eyepoint level.

5.4. Conclusion

In short, the aim and objectives of this study were successfully accomplished despite a few challenges encountered. This VC1196 strain was successfully characterised phenotypically, and at biochemical level. This strain has not been characterised to any extent previously thus the data obtained in this study are novel and support the hypothesis stated in Chapter 2, that the Mic27 KO VC1196 strain presents with a mitochondrial diseased phenotype, however, the results can be improved by using other techniques mentioned in literature and the limitation section of this study.

6. LITERATURE CITED

Roger, A. J., Muñoz-Gómez, S. A., & Kamikawa, R. 2017. The Origin and Diversification of Mitochondria. Current Biology, 27(21), R1177–R1192. doi:10.1016/j.cub.2017.09.015.

Khosravi, S., & Harner, M. E. 2020. The MICOS complex, a structural element of mitochondria with versatile functions. Biological Chemistry, 401(6-7), 765–778. doi:10.1515/hsz-2020-0103.

Hamza, I., & Dailey, H. A. 2012. One ring to rule them all: Trafficking of heme and heme synthesis intermediates in the metazoans. Biochimica et Biophysica Acta (BBA) - Molecular Cell Research, 1823(9), 1617–1632. doi:10.1016/j.bbamcr.2012.04.009.

Hajnóczky, G., Davies, E., & Madesh, M. 2003. Calcium signaling and apoptosis. Biochemical and Biophysical Research Communications, 304(3), 445–454. doi:10.1016/s0006-291x(03)00616-8.

Cserép, C., Pósfai, B., Schwarcz, A.D., Dénes, Á 2018.. Mitochondrial Ultrastructure Is Coupled to Synaptic Performance at Axonal Release Sites. eNeuro.ENEURO. 504(2), 687-699. doi: 10.1523/ENEURO.0390-17.2018. PMID: 29383328; PMCID: PMC5788698.

Huynen, M.A., M. Mühlmeister, K. Gotthardt, S. Guerrero-Castillo, and U. Brandt. 2016. Evolution and structural organization of the mitochondrial contact site (MICOS) complex and the mitochondrial intermembrane space bridging (MIB) complex. Biochim. Biophys. Acta. 1863:91–101. https://doi.org/10.1016/j.bbamcr.2015.10.009.

Bornhövd, C., Vogel, F., Neupert, W., & Reichert, A. S. 2006. Mitochondrial Membrane Potential Is Dependent on the Oligomeric State of F_1F_0-ATP Synthase Supercomplexes. Journal of Biological Chemistry, 281(20), 13990–13998. doi:10.1074/jbc.m512334200.

Hoppins, S., Collins, S.R., Cassidy-Stone, A., Hummel, E., Devay, R.M,, Lackner, L.L., Westermann, B., Schuldiner, M., Weissman, J.S., Nunnari, J. 2011. A mitochondrial-focused genetic interaction map reveals a scaffold-like complex required for inner membrane organization in mitochondria. *J Cell Biol*. 211(18), 12990–12998 doi: 10.1083/jcb.201107053. Epub. PMID: 21987634; PMCID: PMC3198156.

Stoldt, S., Stephan, T., Jans, D. C., Brüser, C., Lange, F., Keller-Findeisen, J., … Jakobs, S. 2019. Mic60 exhibits a coordinated clustered distribution along and across yeast and mammalian mitochondria. Proceedings of the National Academy of Sciences, 201820364. doi:10.1073/pnas.1820364116.

Malsburg, von der, K., Müller, J.M., Bohnert, M., Oeljeklaus,S., Kwiatkowska, P., Becker, T., Loniewska-Lwowska, A.,Wiese, S., Rao, S., Milenkovic, D., et al. (2011). Dual role of mitofilin in mitochondrial membrane organization and protein biogenesis. Dev. Cell 21, 694–707.

Callegari, S., Müller, T., Schulz, C., Lenz, C., Jans, D. C., Wissel, M., … Deckers, M. 2019. A MICOS–TIM22 Association Promotes Carrier Import into Human Mitochondria. Journal of Molecular Biology, 431(15), 2835–2851. doi:10.1016/j.jmb.2019.05.015

Davies, K. M., Anselmi, C., Wittig, I., Faraldo-Gomez, J. D., & Kuhlbrandt, W. 2012. Structure of the yeast F1Fo-ATP synthase dimer and its role in shaping the mitochondrial cristae. *Proceedings of the National Academy of Sciences,* 109(34), 13602–13607. doi:10.1073/pnas.1204593109.

Yamaguchi, R., Lartigue, L., Perkins, G., Scott, R. T., Dixit, A., Kushnareva, Y., … Newmeyer, D. D. 2008. Opa1-Mediated Cristae Opening Is Bax/Bak and BH3 Dependent, Required for Apoptosis, and Independent of Bak Oligomerization. Molecular Cell, 31(4), 557–569. doi:10.1016/j.molcel.2008.07.010

Deckers-Hebestreit, G., & Altendorf, K. (1996). THE F0F1-TYPE ATP SYNTHASES OF BACTERIA: Structure and Function of the F0Complex. *Annual Review of Microbiology*, 50(1), 791–824. doi:10.1146/annurev.micro.50.1.7.

Ishihara, N., Fujita, Y., Oka, T., & Mihara, K. 2006. Regulation of mitochondrial morphology through proteolytic cleavage of OPA1. The EMBO Journal, 25(13), 2966–2977. doi:10.1038/sj.emboj.7601184.

Zanna, C., Ghelli, A., Porcelli, A. M., Karbowski, M., Youle, R. J., Schimpf, S., … Carelli, V. 2007. OPA1 mutations associated with dominant optic atrophy impair oxidative phosphorylation and mitochondrial fusion. Brain, 131(2), 352–367. doi:10.1093/brain/awm335

Cartoni, R., Arnaud, E., Médard, J.-J., Poirot, O., Courvoisier, D. S., Chrast, R., & Martinou, J.-C. 2010. Expression of mitofusin 2R94Q in a transgenic mouse leads to Charcot–Marie–Tooth neuropathy type 2A. Brain, 133(5), 1460–1469. doi:10.1093/brain/awq082.

Cho, D.-H., Nakamura, T., Fang, J., Cieplak, P., Godzik, A., Gu, Z., & Lipton, S. A. 2009. S-Nitrosylation of Drp1 Mediates β-Amyloid-Related Mitochondrial Fission and Neuronal Injury. Science, 324(5923), 102–105. doi:10.1126/science.1171091.

Deng, H., Dodson, M. W., Huang, H., & Guo, M. 2008. The Parkinson's disease genes pink1 and parkin promote mitochondrial fission and/or inhibit fusion in Drosophila. Proceedings of the National Academy of Sciences, 105(38), 14503–14508. doi:10.1073/pnas.0803998105.

Youle, R. J., & van der Bliek, A. M. (2012). Mitochondrial Fission, Fusion, and Stress. Science, 337(6098), 1062–1065. doi:10.1126/science.1219855.

Garrett, R.H and Grisham, C.M. (2013). Biochemistry. 4th ed. Mary Finch. Boston, USA.

Garcia, G. C., Bartol, T. M., Phan, S., Bushong, E. A., Perkins, G., Sejnowski, T. J., … Skupin, A. (2019). Mitochondrial morphology provides a mechanism for energy buffering at synapses. Scientific Reports, 9(1). doi:10.1038/s41598-019-54159-1.

Chinnery, P. F., & Hudson, G. (2013). Mitochondrial genetics. British Medical Bulletin, 106(1), 135–159. doi:10.1093/bmb/ldt017.

Sickmann, A., Reinders, J., Wagner, Y., Joppich, C., Zahedi, R., Meyer, H. E., … Meisinger, C. 2003. The proteome of Saccharomyces cerevisiae mitochondria. Proceedings of the National Academy of Sciences, 100(23), 13207–13212. doi:10.1073/pnas.2135385100 .

Reinders, J., Zahedi, R. P., Pfanner, N., Meisinger, C., & Sickmann, A. 2006. Toward the Complete Yeast Mitochondrial Proteome: Multidimensional Separation Techniques for Mitochondrial Proteomics. Journal of Proteome Research, 5(7), 1543–1554. doi:10.1021/pr050477f.

Ramachandran, A., Nandakumar, D., Deshpande, A. P., Lucas, T. P., R-Bhojappa, R., Tang, G.-Q., … Patel, S. S. 2016. The Yeast Mitochondrial RNA Polymerase and Transcription Factor Complex Catalyzes Efficient Priming of DNA Synthesis on Single-stranded DNA. Journal of Biological Chemistry, 291(32), 16828–16839. doi:10.1074/jbc.m116.740282.

Rizzuto, R., Marchi, S., Bonora, M., Aguiari, P., Bononi, A., De Stefani, D., … Pinton, P. 2009. Ca2+ transfer from the ER to mitochondria: When, how and why. Biochimica et Biophysica Acta (BBA) - Bioenergetics, 1787(11), 1342–1351. doi:10.1016/j.bbabio.2009.03.015.

Becker, T., Pfannschmidt, S., Guiard, B., Stojanovski, D., Milenkovic, D., Kutik, S., … Wiedemann, N. 2007. Biogenesis of the Mitochondrial TOM Complex. Journal of Biological Chemistry, 283(1), 120–127. doi:10.1074/jbc.m706997200.

Bohnert, M., Zerbes, R. M., Davies, K. M., Mühleip, A. W., Rampelt, H., Horvath, S. E., … van der Laan, M. 2015. Central Role of Mic10 in the Mitochondrial Contact Site and Cristae Organizing System. Cell Metabolism, 21(5), 747–755.doi:10.1016/j.cmet.2015.04.007.

Perkins, G. A., & Ellisman, M. H. 2011. Mitochondrial configurations in peripheral nerve suggest differential ATP production. Journal of Structural Biology, 173(1), 117–127. doi:10.1016/j.jsb.2010.06.017.

Perkins, E., Sun, D., Nguyen, A., Tulac, S., Francesco, M., Tavana, H., Nguyen, H., Tugendreich, S., Barthmaier, P., Couto, J., Yeh, E., Thode, S., Jarnagin, K., Jain, A., Morgans, D., Melese, T.

2001. Novel inhibitors of poly(ADP-ribose) polymerase/PARP1 and PARP2 identified using a cell-based screen in yeast. Cancer Res (10):4175-83. PMID: 11358842.

Vögtle, F.-N., Wortelkamp, S., Zahedi, R. P., Becker, D., Leidhold, C., Gevaert, K., … Meisinger, C. 2009. Global Analysis of the Mitochondrial N-Proteome Identifies a Processing Peptidase Critical for Protein Stability. Cell, 139(2), 428–439. doi:10.1016/j.cell.2009.07.045.

Wiedemann, N., & Pfanner, N. 2017. Mitochondrial Machineries for Protein Import and Assembly. Annual Review of Biochemistry, 86(1), 685–714. doi:10.1146/annurev-biochem-060815-014352.

Willey, J.M., Sandman, K.M., Wood, D.H. 2014. Prescott's Microbiology. McGraw-Hill. New York.

Reinecke, F., Smeitink, J. A. M., & van der Westhuizen, F. H. 2009. OXPHOS gene expression and control in mitochondrial disorders. Biochimica et Biophysica Acta (BBA) - Molecular Basis of Disease, 1792(12), 1113–1121. doi:10.1016/j.bbadis.2009.04.003.

Wallace, D. C. 2005. A Mitochondrial Paradigm of Metabolic and Degenerative Diseases, Aging, and Cancer: A Dawn for Evolutionary Medicine. Annual Review of Genetics, 39(1), 359–407. doi:10.1146/annurev.genet.39.1103.

Ng, L. F., & Gruber, J. (2019). Measurement of Respiration Rate in Live *Caenorhabditis elegans*. *Bio-protocol*, 9(10), e3243. https://doi.org/10.21769/BioProtoc.3243.

Rea, S. L., Ventura, N., & Johnson, T. E. 2007. Relationship Between Mitochondrial Electron Transport Chain Dysfunction, Development, and Life Extension in Caenorhabditis elegans. PLoS Biology, 5(10), e259. doi:10.1371/journal.pbio.0050259.

Maglioni, S., Mello, D. F., Schiavi, A., Meyer, J. N., & Ventura, N. (2019). Mitochondrial bioenergetic changes during development as an indicator of C. elegans health-span. Aging, 11(16), 6535–6554. https://doi.org/10.18632/aging.102208.

Vincent, Amy E.; Ng, Yi Shiau; White, Kathryn; Davey, Tracey; Mannella, Carmen; Falkous, Gavin; Feeney, Catherine; Schaefer, Andrew M.; McFarland, Robert; Gorman, Grainne S.; Taylor, Robert W.; Turnbull, Doug M.; Picard, Martin (2016). The Spectrum of Mitochondrial Ultrastructural Defects in Mitochondrial Myopathy. Scientific Reports, 6(), 30610–. doi:10.1038/srep30610.

Mannella CA. (2006). The relevance of mitochondrial membrane topology to mitochondrial function. *Biochim Biophys Acta*. 1762:140–7. [PubMed: 16054341].

Kayser, E.-B., Sedensky, M. M., Morgan, P. G., & Hoppel, C. L. 2004. Mitochondrial Oxidative Phosphorylation Is Defective in the Long-lived Mutantclk-1. Journal of Biological Chemistry, 279(52), 54479–54486. doi:10.1074/jbc.m403066200

Byrne, J. J., Soh, M. S., Chandhok, G., Vijayaraghavan, T., Teoh, J.-S., Crawford, S., … Neumann, B. 2019. Disruption of mitochondrial dynamics affects behaviour and lifespan in Caenorhabditis elegans. Cellular and Molecular Life Sciences, 76(10), 1967–1985. doi:10.1007/s00018-019-03024-5.

Twig, G., Elorza, A., Molina, A. J. A., Mohamed, H., Wikstrom, J. D., Walzer, G., … Shirihai, O. S. 2008. Fission and selective fusion govern mitochondrial segregation and elimination by autophagy. The EMBO Journal, 27(2), 433–446. doi:10.1038/sj.emboj.7601963.

Kanazawa, T., Zappaterra, M. D., Hasegawa, A., Wright, A. P., Newman-Smith, E. D., Buttle, K. F., … van der Bliek, A. M. (2008). The C. elegans Opa1 Homologue EAT-3 Is Essential for Resistance to Free Radicals. PLoS Genetics, 4(2), e1000022. doi:10.1371/journal.pgen.1000022.

Danne, L., Aktas, M., Unger, A., Linke, W. A., Erdmann, R., & Narberhaus, F. 2017. Membrane Remodeling by a Bacterial Phospholipid-Methylating Enzyme. mBio, 8(1). doi:10.1128/mbio.02082-16.

Muhleip, A.W., Joos, F., Wigge, C., Frangakis, A.S., Kuhlbrandt, W and Davies KM 2016 Helical arrays of U-shaped ATP synthase dimers form tubular cristae in ciliate mitochondria. Proceedings of the National Academy ofSciences 113, 8442–8447.

Frezza, C., Cipolat, S., Martins de Brito, O., Micaroni, M., Beznoussenko, G. V., Rudka, T., … Scorrano, L. 2006. OPA1 Controls Apoptotic Cristae Remodeling Independently from Mitochondrial Fusion. Cell, 126(1), 177–189. doi:10.1016/j.cell.2006.06.025.

Escobar-Henriques, M., & Anton, F. 2013. Mechanistic perspective of mitochondrial fusion: Tubulation vs. fragmentation. Biochimica et Biophysica Acta (BBA) - Molecular Cell Research, 1833(1), 162–175. doi:10.1016/j.bbamcr.2012.07.016.

Olichon, A., Guillou, E., Delettre, C., Landes, T., Arnauné-Pelloquin, L., Emorine, L. J., … Belenguer, P. 2006. Mitochondrial dynamics and disease, OPA1. Biochimica et Biophysica Acta (BBA) - Molecular Cell Research, 1763(5-6), 500–509. doi:10.1016/j.bbamcr.2006.04.003.

Barrera, M., Koob, S., Dikov, D., Vogel, F., & Reichert, A. S. 2016. OPA1 functionally interacts with MIC60 but is dispensable for crista junction formation. FEBS Letters, 590(19), 3309–3322. doi:10.1002/1873-3468.12384.

Vogel, F., Bornhövd, C., Neupert, W., & Reichert, A. S. 2006. Dynamic subcompartmentalization of the mitochondrial inner membrane. The Journal of Cell Biology, 175(2), 237–247. doi:10.1083/jcb.200605138.

Rizzuto, R., De Stefani, D., Raffaello, A., & Mammucari, C. 2012. Mitochondria as sensors and regulators of calcium signalling. Nature Reviews Molecular Cell Biology, 13(9), 566–578. doi:10.1038/nrm3412.

Kukat, C., Davies, K. M., Wurm, C. A., Spåhr, H., Bonekamp, N. A., Kühl, I., … Larsson, N.-G. 2015. Cross-strand binding of TFAM to a single mtDNA molecule forms the mitochondrial nucleoid. Proceedings of the National Academy of Sciences, 112(36), 11288–11293. doi:10.1073/pnas.1512131112.

Kühlbrandt, W. (2015). Structure and function of mitochondrial membrane protein complexes. BMC Biology, 13(1). doi:10.1186/s12915-015-0201-x.

Perkins, G., Renken, C., Martone, M. E., Young, S. J., Ellisman, M., & Frey, T. 1997. Electron Tomography of Neuronal Mitochondria: Three-Dimensional Structure and Organization of Cristae and Membrane Contacts. Journal of Structural Biology, 119(3), 260–272. doi:10.1006/jsbi.1997.3885.

Brandt, T., Mourier, A., Tain, L.S., Partridge, L., Larsson, N.G., Kuhlbrandt, W .2017. Changes of mitochondrial ultrastructure and function during ageing in mice and Drosophila. Elife 6: e24662.

Palade, G. E. (1953). An electron microscope study of the mitochondrial structure. Journal of Histochemistry & Cytochemistry, 1(4), 188–211. doi:10.1177/1.4.188.

Anand, R., Kondadi, A.K., Meisterknecht, J., Golombek, M., Nortmann O, Riedel J, Peifer-Weiß L, Brocke-Ahmadinejad, N., Schlütermann, D., Stork. B,, Eichmann, T.O., Wittig, I., Reichert, A.S.. 2020. MIC26 and MIC27 cooperate to regulate cardiolipin levels and the landscape of OXPHOS complexes. Life Sci Alliance. 11;3(10):e202000711. doi: 10.26508/lsa.202000711.

Rabl, R., Soubannier, V., Scholz, R., Vogel, F., Mendl, N., Vasiljev-Neumeyer, A., … Reichert, A. S. 2009. Formation of cristae and crista junctions in mitochondria depends on antagonism between Fcj1 and Sue/g. The Journal of Cell Biology, 185(6), 1047–1063. doi:10.1083/jcb.200811099.

Harner, M. E., Unger, A.-K., Geerts, W. J., Mari, M., Izawa, T., Stenger, M., … Neupert, W. 2016. An evidence based hypothesis on the existence of two pathways of mitochondrial crista formation. eLife, 5. doi:10.7554/elife.18853.

Patten, D. A., Wong, J., Khacho, M., Soubannier, V., Mailloux, R. J., Pilon-Larose, K., … Slack, R. S. 2014. OPA1-dependent cristae modulation is essential for cellular adaptation to metabolic demand. The EMBO Journal, 33(22), 2676–2691. doi:10.15252/embj.201488349.

Ott, C., Dorsch, E., Fraunholz, M., Straub, S., Kozjak-Pavlovic, V, Cobine, P. A .2015. Detailed Analysis of the Human Mitochondrial Contact Site Complex Indicate a Hierarchy of Subunits. PLOS ONE, 10(3), e0120213–. doi:10.1371/journal.pone.0120213.

Dolezal, P. 2006. Evolution of the Molecular Machines for Protein Import into Mitochondria. Science, 313(5785), 314–318. doi:10.1126/science.1127895.

Horvath, S. E., Rampelt, H., Oeljeklaus, S., Warscheid, B., van der Laan, M., & Pfanner, N. 2015. Role of membrane contact sites in protein import into mitochondria. Protein Science, 24(3), 277–297. doi:10.1002/pro.2625.

Schmidt, O., Pfanner, N., & Meisinger, C. 2010. Mitochondrial protein import: from proteomics to functional mechanisms. Nature Reviews Molecular Cell Biology, 11(9), 655–667. doi:10.1038/nrm2959.

Neupert, W., & Herrmann, J. M. 2007. Translocation of Proteins into Mitochondria. Annual Review of Biochemistry, 76(1), 723–749. doi:10.1146/annurev.biochem.76.05.

Habib, S.J., T. Waizenegger, A. Niewienda, S.A. Paschen, W. Neupert, and D. Rapaport. 2007. The N-terminal domain of Tob55 has a receptor-like function in the biogenesis of mitochondrial β-barrel proteins. J. Cell Biol. 176:77–88. [PMC free article] [PubMed] [Google Scholar].

Gentle, I., K. Gabriel, P. Beech, R. Waller, and T. Lithgow. 2004. The Omp85 family of proteins is essential for outer membrane biogenesis in mitochondria and bacteria. J. Cell Biol. 164:19–24. [PMC free article] [PubMed] [Google Scholar].

Mossmann, D., Vögtle, F.-N., Taskin, A. A., Teixeira, P. F., Ring, J., Burkhart, J. M., … Meisinger, C. 2014. Amyloid-β Peptide Induces Mitochondrial Dysfunction by Inhibition of Preprotein Maturation. Cell Metabolism, 20(4), 662–669. doi:10.1016/j.cmet.2014.07.024.

De Marcos-Lousa, C., P Sideris, D., & Tokatlidis, K. 2006. Translocation of mitochondrial inner-membrane proteins: conformation matters. Trends in Biochemical Sciences, 31(5), 259–267. doi:10.1016/j.tibs.2006.03.006.

Curran, S. P., Leverich, E. P., Koehler, C. M., & Larsen, P. L. 2004. Defective Mitochondrial Protein Translocation Precludes Normal Caenorhabditis elegans Development. Journal of Biological Chemistry, 279(52), 54655–54662. doi:10.1074/jbc.m409618200.

Fischer, M., Horn, S., Belkacemi, A., Kojer, K., Petrungaro, C., Habich, M., … Riemer, J. 2013. Protein import and oxidative folding in the mitochondrial intermembrane space of intact mammalian cells. Molecular Biology of the Cell, 24(14), 2160–2170. doi:10.1091/mbc.e12-12-0862.

Welker R, Hohenberg H, Tessmer U, Huckhagel C, Krausslich HG, 2000. Biochemical and structural analysis of isolated mature cores of human IMMUNODEFICIENCY virus type 1. J. Virol. 74, 1168–1177. [PMC free article] [PubMed] [Google Scholar].

Hoeks, J., Hesselink, M., & Schrauwen, P. 2012. Mitochondrial Respiration. Encyclopedia of Exercise Medicine in Health and Disease, 587–590. doi:10.1007/978-3-540-29807-6_136

Chacinska, A., Pfannschmidt, S., Wiedemann, N., Kozjak, V., Sanjuán Szklarz, L. K., Schulze-Specking, A., … Pfanner, N. 2004. Essential role of Mia40 in import and assembly of mitochondrial intermembrane space proteins. The EMBO Journal, 23(19), 3735–3746. doi:10.1038/sj.emboj.7600389.

Höhr, A. I. C., Straub, S. P., Warscheid, B., Becker, T., & Wiedemann, N. 2015. Assembly of β-barrel proteins in the mitochondrial outer membrane. Biochimica et Biophysica Acta (BBA) - Molecular Cell Research, 1853(1), 74–88. doi:10.1016/j.bbamcr.2014.10.006.

Kojer, K., Bien, M., Gangel, H., Morgan, B., Dick, T. P., & Riemer, J. 2012. Glutathione redox potential in the mitochondrial intermembrane space is linked to the cytosol and impacts the Mia40 redox state. The EMBO Journal, 31(14), 3169–3182. doi:10.1038/emboj.2012.165.

Imai, K., Fujita, N., Gromiha, M.M., and Horton, P. 2011 Eukaryote-wide sequence analysis of mitochondrial beta-barrel outer membrane proteins. BMC Genomics 12: 79.

Huynen, M.A., M. Mühlmeister, K. Gotthardt, S. Guerrero-Castillo, and U. Brandt. 2016. Evolution and structural organization of the mitochondrial contact site (MICOS) complex and the mitochondrial intermembrane space bridging (MIB) complex. Biochim. Biophys. Acta. 1863:91–101. https://doi.org/10.1016/j.bbamcr.2015.10.009.

Rampelt, H., Zerbes, R. M., van der Laan, M., & Pfanner, N. 2017. Role of the mitochondrial contact site and cristae organizing system in membrane architecture and dynamics. Biochimica et Biophysica Acta (BBA) - Molecular Cell Research, 1864(4), 737–746. doi:10.1016/j.bbamcr.2016.05.020.

Eramo, M.J., Lisnyak, V., Formosa, L.E., Ryan, M.T. 2020. The 'mitochondrial contact site and cristae organising system' (MICOS) in health and human disease. J Biochem.. doi: 10.1093/jb/mvz111. PMID: 31825482.

Li, H., Ruan, Y., Zhang, K., Jian, F., Hu, C., Miao, L., … Song, Z. 2016. Mic60/Mitofilin determines MICOS assembly essential for mitochondrial dynamics and mtDNA nucleoid organization. Cell Death & Differentiation, 23(3), 380–392. doi:10.1038/cdd.2015.102.

Stephan, T., Brüser, C., Deckers, M., Steyer, A. M., Balzarotti, F., Barbot, M., … Jakobs, S. 2020. MICOS assembly controls mitochondrial inner membrane remodelling and crista junction redistribution to mediate cristae formation. The EMBO Journal. doi:10.15252/embj.2019104105.

Osellame, L. D., Blacker, T. S., & Duchen, M. R. 2012. Cellular and molecular mechanisms of mitochondrial function. Best Practice & Research Clinical Endocrinology & Metabolism, 26(6), 711–723. doi:10.1016/j.beem.2012.05.003O.

Boekema, E. J., & Braun, H.-P. 2006. Supramolecular Structure of the Mitochondrial Oxidative Phosphorylation System. Journal of Biological Chemistry, 282(1), 1–4. doi:10.1074/jbc.r600031200.

Osellame, L.D., Blacker, T.S., Duchen, M.R. (2012). Cellular and molecular mechanisms of mitochondrial function. Best Pract Res Clin Endocrinol Metab.. doi: 10.1016/j.beem.2012.05.003. Epub 2012 Jun 23. PMID: 23168274; PMCID: PMC3513836.

Raffaello, A., Mammucari, C., Gherardi, G., Rizzuto, R. (2016). Calcium at the Center of Cell Signaling: Interplay between Endoplasmic Reticulum, Mitochondria, and Lysosomes. Trends Biochem Sci. doi: 10.1016/j.tibs.2016.09.001. PMID: 27692849; PMCID: PMC5123979.

Wiedemann, N., Kozjak, V., Chacinska, A., Schönfisch, B., Rospert, S., Ryan, M. T., … Meisinger, C. 2003. Machinery for protein sorting and assembly in the mitochondrial outer membrane. Nature, 424(6948), 565–571. doi:10.1038/nature01753.

Ott, C., Ross, K., Straub, S., Thiede, B., Gotz, M., Goosmann, C., … Kozjak-Pavlovic, V. 2012. Sam50 Functions in Mitochondrial Intermembrane Space Bridging and Biogenesis of Respiratory Complexes. Molecular and Cellular Biology, 32(6), 1173–1188. doi:10.1128/mcb.06388-11.

Darshi, M., Mendiola, V. L., Mackey, M. R., Murphy, A. N., Koller, A., Perkins, G. A., … Taylor, S. S. 2010. ChChd3, an Inner Mitochondrial Membrane Protein, Is Essential for Maintaining Crista Integrity and Mitochondrial Function. Journal of Biological Chemistry, 286(4), 2918–2932. doi:10.1074/jbc.m110.171975.

Hashimi, H. 2019. A parasite's take on the evolutionary cell biology of MICOS. PLOS Pathogens, 15(12), e1008166. doi:10.1371/journal.ppat.1008166.

Calvo, S., Jain, M., Xie, X., Sheth, S. A., Chang, B., Goldberger, O. A., … Mootha, V. K. 2006. Systematic identification of human mitochondrial disease genes through integrative genomics. Nature Genetics, 38(5), 576–582. doi:10.1038/ng1776.

Altum, Z.F and Hall, D.H. 2008. Introduction to C. elegans Anatomy: life cycle. In WormAtlas of C. elegans anatomy- an illustrated handbook: https://www.wormatlas.org/hermaphrodite/introduction/mainframe.htm Accessed 06- July 2021

Bloom JS, et al. Finding the sources of missing heritability in a yeast cross. Nature. 2013;494:234–237. [PMC free article] [PubMed] [Google Scholar]

Bolker, M and Kahmann, R. 1993. Sexual Pheromones and Mating Responses in Fungi. THE PLANT CELL ONLINE,5(10), 1461–1469. doi:10.1105/tpc.5.10.1461.

Brenner S. 1974. The genetics of Caenorhabditis elegans. Genetics.;77(1):71-94. doi: 10.1093/genetics/77.1.71. PMID: 4366476; PMCID: PMC1213120.

Bohnert M, Zerbes RM, Davies KM, Muhleip AW, Rampelt H, Horvath SE, et al.2015. Central role of Mic10 in the mitochondrial contact site and cristae organizing system. Cell Metab.;21:747–55.

Brennan, P.A and Zufall, F. 2006. Pheromonal communication in vertebrates. Nature , 444:308–315. [PubMed: 17108955]

Cook, Laura C and Federle, Michael J. 2014. Peptide pheromone signaling in Streptococcus and Enterococcus. FEMS Microbiology Reviews, 38(3), 473–492. doi:10.1111/1574-6976.12046

Brandt, Tobias; Mourier, Arnaud; Tain, Luke S; Partridge, Linda; Larsson, Nils-Göran; Kühlbrandt, Werner 2017. Changes of mitochondrial ultrastructure and function during ageing in mice and Drosophila. eLife, 6(), –. doi:10.7554/eLife.24662.

Pfanner, N., Wiedemann, N., Meisinger, C., & Lithgow, T. 2004. Assembling the mitochondrial outer membrane. Nature Structural & Molecular Biology, 11(11), 1044–1048. doi:10.1038/nsmb852 .

Cogliati, S., Enriquez, J. A. & Scorrano, L.2016. Mitochondrial Cristae: Where Beauty Meets Functionality. *Trends Biochem*. Sci. 41, 261–273.

Cogliati, Sara; Frezza, Christian; Soriano, Maria Eugenia; Varanita, Tatiana; Quintana-Cabrera, Ruben; Corrado, Mauro; Cipolat, Sara; Costa, Veronica; Casarin, Alberto; Gomes, Ligia C.; Perales-Clemente, Ester; Salviati, Leonardo; Fernandez-Silva, Patricio; Enriquez, Jose A.; Scorrano, Luca (2013). Mitochondrial Cristae Shape Determines Respiratory Chain Supercomplexes Assembly and Respiratory Efficiency. *Cell*, 155(1), 160–171. doi:10.1016/j.cell.2013.08.032.

Mannella, A.C. (2006). Structure and dynamics of the mitochondrial inner membrane cristae. , 1763(5-6), 542–548. doi:10.1016/j.bbamcr.2006.04.006.

Rea SL, Ventura N, Johnson TE. Relationship between mitochondrial electron transport chain dysfunction, development, and life extension in Caenorhabditis elegans. PLoS Biol. 2007; 5:e259. https://doi.org/10.1371/journal.pbio.0050259 PMID:17914900,

Lapierre, L and Hansen, M. (2012). Lessons from C. elegans: signalling pathways for longevity. , 23(12), –. doi:10.1016/j.tem.2012.07.007.

Munkácsy, E and Rea. S. L. (2014). The paradox of mitochondrial dysfunction and extended longevity. Experimental Gerontology, 56(), 221–233. doi:10.1016/j.exger.2014.03.016.

Gaertner BE, Phillips PC. Caenorhabditis elegans as a platform for molecular quantitative genetics and the systems biology of natural variation. Genetics research. 2010;92:331–348. [PubMed] [Google Scholar].

Harner, Max E; Unger, Ann-Katrin; Geerts, Willie JC; Mari, Muriel; Izawa, Toshiaki; Stenger, Maria; Geimer, Stefan; Reggiori, Fulvio; Westermann, Benedikt; Neupert, Walter (2016). An evidence based hypothesis on the existence of two pathways of mitochondrial crista formation. eLife, 5(), –. doi:10.7554/eLife.18853.

Flibotte, S., Edgley, M. L., Chaudhry, I., Taylor, J., Neil, S. E., Rogula, A., … Moerman, D. G. 2010. Whole-Genome Profiling of Mutagenesis in Caenorhabditis elegans. Genetics, 185(2), 431–441. doi:10.1534/genetics.110.116616 .

Friedland, A. E., Tzur, Y. B., Esvelt, K. M., Colaiácovo, M. P., Church, G. M., & Calarco, J. A. 2013. Heritable genome editing in C. elegans via a CRISPR-Cas9 system. Nature Methods, 10(8), 741–743. doi:10.1038/nmeth.2532 .

Dickinson, D. J., Ward, J. D., Reiner, D. J., & Goldstein, B. 2013. Engineering the Caenorhabditis elegans genome using Cas9-triggered homologous recombination. Nature Methods, 10(10), 1028–1034. doi:10.1038/nmeth.2641.

Edgley, M., D'Souza, A…….Bastead, R. 2002. Improved detection of small deletions in complex pools of DNA. Nucleic Acids Research, 30(12), 52e–52. doi:10.1093/nar/gnf051.

Jansen, G., Hazendonk, E., Thijssen, K. L., & Plasterk, R. H. A. 1997. Reverse genetics by chemical mutagenesis in Caenorhabditis elegans. Nature Genetics, 17(1), 119–121. doi:10.1038/ng0997-119.

Lemarie, A., & Grimm, S. 2011. Mitochondrial respiratory chain complexes: apoptosis sensors mutated in cancer? Oncogene, 30(38), 3985–4003. doi:10.1038/onc.2011.167.

Bartlett K, Eaton S. (2003). Mitochondrial beta-oxidation. Eur J Biochem.. doi: 10.1046/j.1432-1033.2003.03947.x. PMID: 14728673.

Chaudhuri, J., Parihar, M., & Pires-daSilva, A. 2011. An Introduction to Worm Lab: from Culturing Worms to Mutagenesis. Journal of Visualized Experiments, (47). doi:10.3791/2293

Kukat, Christian; Davies, Karen M.; Wurm, Christian A.; Spåhr, Henrik; Bonekamp, Nina A.; Kühl, Inge; Joos, Friederike; Polosa, Paola Loguercio; Park, Chan Bae; Posse, Viktor; Falkenberg, Maria; Jakobs, Stefan; Kühlbrandt, Werner; Larsson, Nils-Göran 2015. Cross-strand binding of TFAM to a single mtDNA molecule forms the mitochondrial nucleoid. Proceedings of the National Academy of Sciences, 112(36), 11288–11293. doi:10.1073/pnas.1512131112

McGrath, P.T and Ruvinsky, I. 2018. A primer on pheromone signaling in C. elegans for systems biologists. Current Opinion in Systems Biology, (), S2452310018300702–. doi:10.1016/j.coisb.2018.08.012

Merkwirth, C.; Dargazanli, S.; Tatsuta, T.; Geimer, S.; Lower, B.; Wunderlich, F. T.; von Kleist-Retzow, J.-C.; Waisman, A.; Westermann, B.; Langer, T. (2008). Prohibitins control cell proliferation and apoptosis by regulating OPA1-dependent cristae morphogenesis in mitochondria. Genes & Development, 22(4), 476–488. doi:10.1101/gad.460708.

De Stasio, E. A., & Dorman, S. 2001. Optimization of ENU mutagenesis of Caenorhabditis elegans. Mutation Research/Genetic Toxicology and Environmental Mutagenesis, 495(1-2), 81–88. doi:10.1016/s1383-5718(01)00198-x.

Sousa, J. S., D'Imprima, E., & Vonck, J. 2018. Mitochondrial Respiratory Chain Complexes. Membrane Protein Complexes: Structure and Function, 167–227. doi:10.1007/978-981-10-7757-9_7.

Maechler, P., Carobbio, S., & Rubi, B. 2006. In beta-cells, mitochondria integrate and generate metabolic signals controlling insulin secretion. The International Journal of Biochemistry & Cell Biology, 38(5-6), 696–709. doi:10.1016/j.biocel.2005.12.006.

Patten, D. A.; Wong, J.; Khacho, M.; Soubannier, V.; Mailloux, R. J.; Pilon-Larose, K.; MacLaurin, J. G.; Park, D. S.; McBride, H. M.; Trinkle-Mulcahy, L.; Harper, M.-E.; Germain, M.; Slack, R. S. (2014). OPA1-dependent cristae modulation is essential for cellular adaptation to metabolic demand. The EMBO Journal, 33(22), 2676–2691. doi:10.15252/embj.201488349

Perkins, G., Renken, C., Martone, M.E,, Young, S.J., Ellisman, M., Frey, T. 1997. Electron tomography of neuronal mitochondria: three-dimensional structure and organization of cristae and membrane contacts. J Struct Biol. 1997;119(3):260–72

Rabl, R.; Soubannier, V.; Scholz, R.; Vogel, F.; Mendl, N.; Vasiljev-Neumeyer, A.; Korner, C.; Jagasia, R.; Keil, T.; Baumeister, W.; Cyrklaff, M.; Neupert, W.; Reichert, A. S. 2009. Formation of cristae and crista junctions in mitochondria depends on antagonism between Fcj1 and Su e/g. The Journal of Cell Biology, 185(6), 1047–1063. doi:10.1083/jcb.200811099.

Sin, O., Michels, H., & Nollen, E. A. A. 2014. Genetic screens in Caenorhabditis elegans models for neurodegenerative diseases. Biochimica et Biophysica Acta (BBA) - Molecular Basis of Disease, 1842(10), 1951–1959. doi:10.1016/j.bbadis.2014.01.015.

Rizzuto, R., De Stefani, D., Raffaello, A., Mammucari, C.2012. Mitochondria as sensors and regulators of calcium signalling. Nat Rev Mol Cell Biol.;13(9):566–78.

Tang, Junhui; Zhang, Kuan; Dong, Jun; Yan, Chaojun; Hu, Chao; Ji, Hongchao; Chen, Liangyi; Chen, Shi; Zhao, Huabin; Song, Zhiyin .2019. Sam50–Mic19–Mic60 axis determines mitochondrial cristae architecture by mediating mitochondrial outer and inner membrane contact. Cell Death & Differentiation, (), –. doi:10.1038/s41418-019-0345-2 .

Wurn, A and Jakobs, S 2006. Differential protein distributions define two sub-compartments of the mitochondrial inner membrane in yeast. , 580(24), 5628–5634. doi:10.1016/j.febslet.2006.09.012.

Barstead, R. J., & Moerman, D. G. 2006. C. elegans Deletion Mutant Screening. C. Elegans, 51–58. doi:10.1385/1-59745-151-7:51.

Bakhoum, S. F., Kabeche, L., Murnane, J. P., Zaki, B. I., & Compton, D. A. 2014. DNA-Damage Response during Mitosis Induces Whole-Chromosome Missegregation. Cancer Discovery, 4(11), 1281–1289. doi:10.1158/2159-8290.cd-14-0403

Hartman, P. S., Barry, J., Finstad, W., Khan, N., Tanaka, M., Yasuda, K., & Ishii, N. 2014. Ethyl methane sulfonate induces mutations in Caenorhabditis elegans embryos at a high frequency. Mutation Research/Fundamental and Molecular Mechanisms of Mutagenesis, 766-767, 44–48. doi:10.1016/j.mrfmmm.2014.05.011.

Chen, X., Feng, X., & Guang, S. 2016. Targeted genome engineering in Caenorhabditis elegans. Cell & Bioscience, 6(1). doi:10.1186/s13578-016-0125-3.

Lesa, G.M. 2006. Isolation of Caenorhabditis elegans gene knockouts by PCR screening of chemically mutagenized libraries. Nat Protoc.):2231-40. doi: 10.1038/nprot.2006.345. PMID: 17406462.

Kutscher, L.M., Shaham, S. 2014. Forward and reverse mutagenesis in C. elegans. WormBook.. doi: 10.1895/wormbook.1.167.1. PMID: 24449699; PMCID: PMC4078664.

Weim, A., Yuan, A., Fawcett, G., Butler, A., Davis, T., Xu, S.Y., Salkoff, L. 2002. Efficient isolation of targeted Caenorhabditis elegans deletion strains using highly thermostable restriction endonucleases and PCR. Nucleic Acids Research, 30(20), 110e–110. doi:10.1093/nar/gnf109.

Rafael P. Vázquez-Manrique; James C. Legg; Birgitta Olofsson; Sung Ly; Howard A. Baylis. 2010. Improved gene targeting in C. elegans using counter-selection and Flp-mediated marker excision. , 95(1), 0–46. doi:10.1016/j.ygeno.2009.09.001.

Ausubel, Frederick M.; Brent, Roger; Kingston, Robert E.; Moore, David D.; Seidman, J.G.; Smith, John A.; Struhl, Kevin. 2001. Current Protocols in Molecular Biology |CRISPR-Cas9-Guided Genome Engineering in C. elegans. 31.7.1–31.7.18. doi:10.1002/cpmb.7.

Lok, James B. 2019. CRISPR/Cas9 Mutagenesis and Expression of Dominant Mutant Transgenes as Functional Genomic Approaches in Parasitic Nematodes. Frontiers in Genetics, 10(), 656–. doi:10.3389/fgene.2019.00656.

Hoppins, S., Collins, S.R., Cassidy-Stone, A., Hummel, E., Devay, R.M,, Lackner, L.L., Westermann, B., Schuldiner, M., Weissman, J.S., Nunnari, J. 2011. A mitochondrial-focused genetic interaction map reveals a scaffold-like complex required for inner membrane organization in mitochondria. J Cell Biol. doi: 10.1083/jcb.201107053. Epub. PMID: 21987634; PMCID: PMC3198156.

Muñoz-Gómez, S. A., Slamovits, C. H., Dacks, J. B., Baier, K. A., Spencer, K. D., & Wideman, J. G. 2015. Ancient Homology of the Mitochondrial Contact Site and Cristae Organizing System Points to an Endosymbiotic Origin of Mitochondrial Cristae. Current Biology, 25(11), 1489–1495. doi:10.1016/j.cub.2015.04.006.

Kozjak-Pavlovic, V. 2016. The MICOS complex of human mitochondria. Cell and Tissue

Pfanner, N., van der Laan, M., Amati, P., Capaldi, R. A., Caudy, A. A., Chacinska, A., … Nunnari, J. 2014. Uniform nomenclature for the mitochondrial contact site and cristae organizing system. The Journal of Cell Biology, 204(7), 1083–1086. doi:10.1083/jcb.201401006.

Tateo, I., Tohoru, I., Yukie, M., Fumio, H., Kazuhiko, K., & Nobuo, T. 1994. A novel human gene that is preferentially transcribed in heart muscle. Gene, 144(2), 301–306. doi:10.1016/0378-1119(94)90394-8 .

Odgren, P.R, Toukatly G, Bangs PL, Gilmore R, Fey EG. Molecular characterization of mitofilin (HMP), a mitochondria-associated protein with predicted coiled coil and intermembrane space targeting domains. J Cell Sci. 1996 Sep;109 (Pt 9):2253-64. PMID: 8886976

Gieffers, C. 1997. Mitofilin Is a Transmembrane Protein of the Inner Mitochondrial Membrane Expressed as Two Isoforms. Experimental Cell Research, 232(2), 395–399. doi:10.1006/excr.1997.3539.

Hessenberger, M., Zerbes, R. M., Rampelt, H., Kunz, S., Xavier, A. H., Purfürst, B., … Daumke, O. 2017. Regulated membrane remodeling by Mic60 controls formation of mitochondrial crista junctions. Nature Communications, 8, 15258. doi:10.1038/ncomms15258

Guarani, V., Jardel, C., Chrétien, D., Lombès, A., Bénit, P., Labasse, C., Lacène, E., Bourillon, A., Imbard, A., Benoist, J.F,, Dorboz, I., Gilleron, M., Goetzman, E.S., Gaignard, P., Slama, A., Elmaleh-Bergès, M., Romero, N.B., Rustin, P., Ogier de Baulny H, Paulo JA, Harper JW, Schiff M. 2016. QIL1 mutation causes MICOS disassembly and early onset fatal mitochondrial encephalopathy with liver disease. Elife. doi: 10.7554/eLife.17163. PMID: 27623147; PMCID: PMC5021520.

Friedman, J.R., Mourier, A., Yamada, J., McCaffery, J.M., and Nunnari, J. 2015. MICOS coordinates with respiratory complexes and lipids to establish mitochondrial inner membrane architecture. Cell biology.

Kondadi, A. K., Anand, R., Hänsch, S., Urbach, J., Zobel, T., Wolf, D. M., … Reichert, A. S. 2020. Cristae undergo continuous cycles of membrane remodelling in a MICOS -dependent manner. EMBO Reports. doi:10.15252/embr.201949776.

Von der Malsburg, K., Müller, J. M., Bohnert, M., Oeljeklaus, S., Kwiatkowska, P., Becker, T., … van der Laan, M. 2011. Dual Role of Mitofilin in Mitochondrial Membrane Organization and Protein Biogenesis. Developmental Cell, 21(4), 694–707. doi:10.1016/j.devcel.2011.08.026.

Russ, W. P., & Engelman, D. M. (2000). The GxxxG motif: A framework for transmembrane helix-helix association. Journal of Molecular Biology, 296(3), 911–919. doi:10.1006/jmbi.1999.3489 .

Schauble, S., King, C. C., Darshi, M., Koller, A., Shah, K., & Taylor, S. S. 2007. Identification of ChChd3 as a Novel Substrate of the cAMP-dependent Protein Kinase (PKA) Using an Analog-sensitive Catalytic Subunit. Journal of Biological Chemistry, 282(20), 14952–14959. doi:10.1074/jbc.m609221200.

Sakowska, Paulina; Jans, Daniel C.; Mohanraj, Karthik; Riedel, Dietmar; Jakobs, Stefan; Chacinska, Agnieszka .2015. The oxidation status of Mic19 regulates MICOS assembly. Molecular and Cellular Biology, (), MCB.00578-15–. doi:10.1128/MCB.00578-15.

Favaro, G., Romanello, V., Varanita, T., Andrea Desbats, M., Morbidoni, V., Tezze, C., … Sandri, M. (2019). DRP1-mediated mitochondrial shape controls calcium homeostasis and muscle mass. Nature Communications, 10(1). doi:10.1038/s41467-019-10226-9.

An J., Shi J., He Q., Lui K., Liu Y., Huang Y., Sheikh M.S. 2012. CHCM1/CHCHD6, novel mitochondrial protein linked to regulation of mitofilin and mitochondrial cristae morphology. J. Biol. Chem. 287:7411–7426 10.1074/jbc.M111.277103 [PMC free article] [PubMed] [CrossRef] [Google Scholar]

Ding C, Wu Z, Huang L, Wang Y, Xue J, Chen S, Deng Z, Wang L, Song Z, Chen S. 2015. Mitofilin and CHCHD6 physically interact with Sam50 to sustain cristae structure. Sci Rep 5:16064.

Bódis, K., Jelenik, T., Lundbom, J., Markgraf, D. F., Strom, A., Zaharia, O.-P., … Roden, M. 2019. Expansion and Impaired Mitochondrial Efficiency of Deep Subcutaneous Adipose Tissue in Recent-Onset Type 2 Diabetes. The Journal of Clinical Endocrinology & Metabolism, 105(4), e1331–e1343. doi:10.1210/clinem/dgz267.

Gödiker, J., Grüneberg, M., DuChesne, I., Reunert, J., Rust, S., Westermann, C., … Marquardt, T. 2018. QIL1-dependent assembly of MICOS complex–lethal mutation in C19ORF70 resulting in liver disease and severe neurological retardation. Journal of Human Genetics, 63(6), 707–716. doi:10.1038/s10038-018-0442-y.

Koob, S., Barrera, M., Anand, R., & Reichert, A. S. (2015). The non-glycosylated isoform of MIC26 is a constituent of the mammalian MICOS complex and promotes formation of crista junctions. Biochimica et Biophysica Acta (BBA) - Molecular Cell Research, 1853(7), 1551–1563. doi:10.1016/j.bbamcr.2015.03.004.

Benincá, C., Zanette, V., Brischigliaro, M., Johnson, M., Reyes, A., Valle, D. A. do, … Zeviani, M. (2020). Mutation in the MICOS subunit gene APOO (MIC26) associated with an X-linked recessive mitochondrial myopathy, lactic acidosis, cognitive impairment and autistic features. Journal of Medical Genetics, 58(3), 155–167. doi:10.1136/jmedgenet-2020-106861.

Weber, T. A., Koob, S., Heide, H., Wittig, I., Head, B., van der Bliek, A., … Reichert, A. S. (2013). APOOL Is a Cardiolipin-Binding Constituent of the Mitofilin/MINOS Protein Complex Determining Cristae Morphology in Mammalian Mitochondria. PLoS ONE, 8(5), e63683. doi:10.1371/journal.pone.0063683.

Eydt, K., Davies, K.M., Behrendt, C., Wittig, I., Reichert, A.S. 2017. Cristae architecture is determined by an interplay of the MICOS complex and the F1FO ATP synthase via Mic27 and

Mic10. Microb Cell;4(8):259-272. doi: 10.15698/mic2017.08.585. PMID: 28845423; PMCID: PMC5568431.

An, J. J.,Shi, Q., He, K., Lui, Y., Liu, Y., Huang, and M.S. Sheikh. 2012. CHCM1/ CHCHD6, novel mitochondrial protein linked to regulation of mitofilin and mitochondrial cristae morphology. J. Biol. Chem. 287:7411–7426. http://dx.doi.org/10.1074/jbc.M111.277103.

Hashimi, H. (2019). A parasite's take on the evolutionary cell biology of MICOS. PLOS Pathogens, 15(12), e1008166. doi:10.1371/journal.ppat.1008166.

Tang, J. X., Thompson, K., Taylor, R. W., & Oláhová, M. (2020). Mitochondrial OXPHOS Biogenesis: Co-Regulation of Protein Synthesis, Import, and Assembly Pathways. International Journal of Molecular Sciences, 21(11), 3820. doi:10.3390/ijms21113820.

Rackham, O., Filipovska, A. 2014 Analysis of the Human Mitochondrial Transcriptome Using Directional Deep Sequencing and Parallel Analysis of RNA Ends. In: Rorbach J., Bobrowicz A. (eds) Polyadenylation. Methods in Molecular Biology (Methods and Protocols), vol 1125. Humana Press, Totowa, NJ. https://doi.org/10.1007/978-1-62703-971-0_21.

Baker, N., Patel, J., & Khacho, M. 2019. Linking mitochondrial dynamics, cristae remodeling and supercomplex formation: How mitochondrial structure can regulate bioenergetics. Mitochondrion. doi:10.1016/j.mito.2019.06.003.

Lauridsen, P. E., Rasmussen, L. J., & Desler, C. 2019. Mitochondrial oxidative phosphorylation capacity of cryopreserved cells. Mitochondrion. doi:10.1016/j.mito.2019.04.011.

Goetzman, E. S., & Prochownik, E. V. 2018. The Role for Myc in Coordinating Glycolysis, Oxidative Phosphorylation, Glutaminolysis, and Fatty Acid Metabolism in Normal and Neoplastic Tissues. Frontiers in Endocrinology, 9. doi:10.3389/fendo.2018.00129 .

Wang, Y., Gross, M. L., & Taylor, J.-S. 2001. Use of a Combined Enzymatic Digestion/ESI Mass Spectrometry Assay To Study the Effect of TATA-Binding Protein on Photoproduct Formation in a TATA Box†. Biochemistry, 40(39), 11785–11793. doi:10.1021/bi0111552.

Beale, E.; Li, G.; Tan, M.-W.; Rumbaugh, K. P. (2006). Caenorhabditis elegans Senses Bacterial Autoinducers. Applied and Environmental Microbiology, 72(7), 5135–5137. doi:10.1128/AEM.00611-06.

Mick, D. U., Dennerlein, S., Wiese, H., Reinhold, R., Pacheu-Grau, D., Lorenzi, I., … Rehling, P. 2012. MITRAC Links Mitochondrial Protein Translocation to Respiratory-Chain Assembly and Translational Regulation. Cell, 151(7), 1528–1541. doi:10.1016/j.cell.2012.11.053.

Chinnery, P. F., & Hudson, G. 2013. Mitochondrial genetics. British Medical Bulletin, 106(1), 135–159. doi:10.1093/bmb/ldt017.

Maynard, S., Hejl, A.M., Dinh, T.S., Keijzers, G., Hansen, Å.M., Desler, C., Moreno-Villanueva, M., Bürkle, A., Rasmussen, L.J., Waldemar, G., Bohr, V.A. 2015.. Defective mitochondrial respiration, altered dNTP pools and reduced AP endonuclease 1 activity in peripheral blood mononuclear cells of Alzheimer's disease patients. Aging (Albany NY). doi: 10.18632/aging.100810. PMID: 26539816; PMCID: PMC4637207.

Desler, C., Frederiksen, J. H., Angleys, M., Maynard, S., Keijzers, G., Fagerlund, B., … Rasmussen, L. J. 2015. Increased deoxythymidine triphosphate levels is a feature of relative cognitive decline. Mitochondrion, 25, 34–37. doi:10.1016/j.mito.2015.09.002.

Bhatti, J. S., Bhatti, G. K., & Reddy, P. H. 2017. Mitochondrial dysfunction and oxidative stress in metabolic disorders — A step towards mitochondria based therapeutic strategies. Biochimica et Biophysica Acta (BBA) - Molecular Basis of Disease, 1863(5), 1066–1077. doi:10.1016/j.bbadis.2016.11.010.

Acehan, D., Vaz, F., Houtkooper, R. H., James, J., Moore, V., Tokunaga, C., … Khuchua, Z. 2010. Cardiac and Skeletal Muscle Defects in a Mouse Model of Human Barth Syndrome. Journal of Biological Chemistry, 286(2), 899–908. doi:10.1074/jbc.m110.171439.

Claypool, S. M., & Koehler, C. M. 2012. The complexity of cardiolipin in health and disease. Trends in Biochemical Sciences, 37(1), 32–41. doi:10.1016/j.tibs.2011.09.003.

Osman, C., Voelker, D. R., & Langer, T. 2011. Making heads or tails of phospholipids in mitochondria. The Journal of Cell Biology, 192(1), 7–16. doi:10.1083/jcb.201006159.

Schlame, M., & Ren, M. 2006. Barth syndrome, a human disorder of cardiolipin metabolism. FEBS Letters, 580(23), 5450–5455. doi:10.1016/j.febslet.2006.07.022.

Saini-Chohan, H. K., Holmes, M. G., Chicco, A. J., Taylor, W. A., Moore, R. L., McCune, S. A., … Sparagna, G. C. 2008. Cardiolipin biosynthesis and remodeling enzymes are altered during development of heart failure. Journal of Lipid Research, 50(8), 1600–1608. doi:10.1194/jlr.m800561-jlr200.

Mao, K., Ji, F., Breen, P., Sewell, A., Han, M., Sadreyev, R., Ruvkun, G. 2019. Mitochondrial Dysfunction in *C. elegans* Activates Mitochondrial Relocalization and Nuclear Hormone Receptor-Dependent Detoxification Genes. *Cell Metab*. 7;29(5):1182-1191.e4. doi: 10.1016/j.cmet.

Maglioni, S., Schiavi, A., Runci, A., Shaik, A., Ventura, N. 2014. Mitochondrial stress extends lifespan in _C. elegans_ through neuronal hormesis. *Experimental Gerontology*. vol. 56, pp. 89–98.

Bargmann, C.I. 2006. Chemosensation in C. elegans, in Worm- Book: *The Online Review of C. elegans Biology*, WormBook.

Yueh-Chen, C., Chien-Po, L., Chun-Liang, P. 2022. A serotonergic regulates adversive associative learning under mitochondrial stress in C. elegans. *Journal of neuroscience*. 199. 11. https://doi.org/10.1073/pnas.2115533119.

Gohil, V. M., & Greenberg, M. L. 2009. Mitochondrial membrane biogenesis: phospholipids and proteins go hand in hand: Figure 1. The Journal of Cell Biology, 184(4), 469–472. doi:10.1083/jcb.200901127.

Vafai, Scott B.; Mootha, Vamsi K. (2012). Mitochondrial disorders as windows into an ancient organelle. Nature, 491(7424), 374–383. doi:10.1038/nature11707 .

Rackham, O and Filipovska A. (2014). Supernumerary proteins of mitochondrial ribosomes. Biochim Biophys Acta. doi: 10.1016/j.bbagen.2013.08.010. Epub 2013 Aug 17. PMID: 23958563.

Longley, M.J., Graziewicz, M.A., Bienstock, R.J., Copeland, WC. (2005). Consequences of mutations in human DNA polymerase γ. , 354(none), 0131. doi:10.1016/j.gene.2005.03.029 .

Haas, R. H.; Parikh, S.; Falk, M. J.; Saneto, R. P.; Wolf, N. I.; Darin, N.; Cohen, B. H. (2007). Mitochondrial Disease: A Practical Approach for Primary Care Physicians. PEDIATRICS, 120(6), 1326–1333. doi:10.1542/peds.2007-0391.

Schaefer, A. M., Taylor, R. W., Turnbull, D. M., and Chinnery, P. F. (2004). The Epidemiology of Mitochondrial Disorders-Past, Present and Future. Biochim. Biophys. Acta (Bba) - Bioenerg. 1659, 115–120. doi:10.1016/j.bbabio.2004.09.005.

Falk, M. J., Rosenjack, J. R., Polyak, E., Suthammarak, W., Chen, Z., Morgan, P. G., & Sedensky, M. M. (2009). Subcomplex Iλ specifically controls integrated mitochondrial functions in Caenorhabditis elegans. PLoS ONE, 4(8), Article e6607. https://doi.org/10.1371/journal.pone.0006607.t003.

Eramo, M., Lisnyak, V., Formosa, L.E., Ryan, M.T. (2019). The “mitochondrial contact site and cristae organising system” (MICOS) in health and human disease. The Journal of Biochemistry, (), mvz111–. doi:10.1093/jb/mvz111.

Li, S.; Xu, S.; Roelofs, B. A.; Boyman, L.; Lederer, W. J.; Sesaki, H.; Karbowski, M. (2015). Transient assembly of F-actin on the outer mitochondrial membrane contributes to mitochondrial fission. The Journal of Cell Biology, 208(1), 109–123. doi:10.1083/jcb.201404050.

Hoppins, S.; Collins, S. R.; Cassidy-Stone, A.; Hummel, E.; DeVay, R. M.; Lackner, L. L.; Westermann, B.; Schuldiner, M.; Weissman, J. S.; Nunnari, J. (2011). A mitochondrial-focused genetic interaction map reveals a scaffold-like complex required for inner membrane organization in mitochondria. The Journal of Cell Biology, 195(2), 323–340. doi:10.1083/jcb.201107053.

Ritz, Beate; Lee, Pei-Chen; Hansen, Johnni; Lassen, Christina Funch; Ketzel, Matthias; Sørensen, Mette; Raaschou-Nielsen, Ole (2016). Traffic-Related Air Pollution and Parkinson's Disease in Denmark: A Case–Control Study. Environmental Health Perspectives, 124(3), 351–356. doi:10.1289/ehp.1409313.

Van Laar, Victor S.; Otero, P. Anthony; Hastings, Teresa G.; Berman, Sarah B. (2019). Potential Role of Mic60/Mitofilin in Parkinson's Disease. Frontiers in Neuroscience, 12(), 898–. doi:10.3389/fnins.2018.00898.

Bose, A., and Beal, M. F. (2016). Mitochondrial dysfunction in Parkinson's disease. J. Neurochem. 139(Suppl. 1), 216–231. doi: 10.1111/jnc.13731.

Darshi, M.; Mendiola, V. L.; Mackey, M. R.; Murphy, A. N.; Koller, A.; Perkins, G. A.; Ellisman, M. H.; Taylor, S. S. (2011). ChChd3, an Inner Mitochondrial Membrane Protein, Is Essential for Maintaining Crista Integrity and Mitochondrial Function. Journal of Biological Chemistry, 286(4), 2918–2932. doi:10.1074/jbc.M110.171975.

Suketu M. Khandhar; William J. Marks (2007). Epidemiology of Parkinson's Disease. , 53(4), 0–205. doi:10.1016/j.disamonth.2007.02.001.

Delamarre, Anna; Meissner, Wassilios G. (2017). Epidemiology, environmental risk factors and genetics of Parkinson's disease. La Presse Médicale, 46(2), 175–181. doi:10.1016/j.lpm.2017.01.001.

Cieri, Domenico; Vicario, Mattia; Giacomello, Marta; Vallese, Francesca; Filadi, Riccardo; Wagner, Tina; Pozzan, Tullio; Pizzo, Paola; Scorrano, Luca; Brini, Marisa; Calì, Tito (2017). SPLICS: a split green fluorescent protein-based contact site sensor for narrow and wide heterotypic organelle juxtaposition. Cell Death & Differentiation, (), –. doi:10.1038/s41418-017-0033-z.

Van Laar, V.S. and Berman, S.B. (2013) The Interplay of Neuronal Mitochondrial Dynamics and Bioenergetics: Implications for Parkinson's Disease. Neurobiology of Disease, 51, 43-55.

https://doi.org/10.1016/j.nbd.2012.05.015.

Sanders, Laurie H.; McCoy, Jennifer; Hu, Xiaoping; Mastroberardino, Pier G.; Dickinson, Bryan C.; Chang, Christopher J.; Chu, Charleen T.; Van Houten, Bennett; Greenamyre, J.T. (2014).

Mitochondrial DNA damage: Molecular marker of vulnerable nigral neurons in Parkinson's disease. Neurobiology of Disease, 70(), 214–223. doi:10.1016/j.nbd.2014.06.014.

Tsai, P.I., Lin, C.H., Hsieh, C.H., Papakyrikos, A.M., Kim, M.J., Napolioni, V., Schoor, C., Couthouis, J., Wu, R.M., Wszolek, Z.K., Winter, D., Greicius, M.D., Ross, O.A., Wang, X. (2018). PINK1 Phosphorylates MIC60/Mitofilin to Control Structural Plasticity of Mitochondrial Crista Junctions. Mol. Cell 69(5): 744--756.e6.

Baker, Laura D.; Cross, Donna J.; Minoshima, Satoshi; Belongia, Dana; Watson, G. Stennis; Craft, Suzanne (2011). Insulin Resistance and Alzheimer-like Reductions in Regional Cerebral Glucose Metabolism for Cognitively Normal Adults With Prediabetes or Early Type 2 Diabetes. Archives of Neurology, 68(1), –. doi:10.1001/archneurol.2010.225.

Borghetti, A; Baldin, G; Lombardi, F; Ciccullo, A; Capetti, A; Rusconi, S; Sterrantino, G; Latini, A; Cossu, MV; Gagliardini, R; De Luca, A; Di Giambenedetto, S (2018). Efficacy and tolerability of lamivudine plus dolutegravir as a switch strategy in a multicentre cohort of patients with suppressed HIV-1 replication. HIV Medicine, (), –. doi:10.1111/hiv.12611.

Rigotto G, Basso E. (2019). Mitochondrial Dysfunctions: A Thread Sewing Together Alzheimer's Disease, Diabetes, and Obesity. Oxid Med Cell Longev.. doi: 10.1155/2019/7210892. PMID: 31316720; PMCID: PMC6604285.

Liesa, Marc; Shirihai, Orian S. (2013). Mitochondrial Dynamics in the Regulation of Nutrient Utilization and Energy Expenditure. Cell Metabolism, 17(4), 491–506. doi:10.1016/j.cmet.2013.03.002.

Wilcox G. (2005). Insulin and insulin resistance. The Clinical biochemist. Reviews, 26(2), 19–39.

Nielsen J, Gejl KD, Hey-Mogensen M, Holmberg HC, Suetta C, Krustrup P, Elemans CPH, Ørtenblad N. (2017). Plasticity in mitochondrial cristae density allows metabolic capacity modulation in human skeletal muscle. J Physiol.. doi: 10.1113/JP273040. Epub 2016 Nov 13. PMID: 27696420; PMCID: PMC5407961.

Kelley, D. E.; He, J.; Menshikova, E. V.; Ritov, V. B. (2002). Dysfunction of Mitochondria in Human Skeletal Muscle in Type 2 Diabetes. Diabetes, 51(10), 2944–2950. doi:10.2337/diabetes.51.10.2944.

Baseler, W. A.; Dabkowski, E. R.; Williamson, C. L.; Croston, T. L.; Thapa, D.; Powell, M. J.; Razunguzwa, T. T.; Hollander, J. M. (2011). Proteomic alterations of distinct mitochondrial subpopulations in the type 1 diabetic heart: contribution of protein import dysfunction. AJP:

Regulatory, Integrative and Comparative Physiology, 300(2), R186–R200. doi:10.1152/ajpregu.00423.2010.

Schlame, M and Ren, M. (2006). Barth syndrome, a human disorder of cardiolipin metabolism. , 580(23), 0–5455. doi:10.1016/j.febslet.2006.07.022.

Ikon, Nikita; Ryan, Robert O. (2017). Cardiolipin and mitochondrial cristae organization. Biochimica et Biophysica Acta (BBA) - Biomembranes, 1859(6), 1156–1163. doi:10.1016/j.bbamem.2017.03.013.

Van Strien, J., Guerrero-Castillo, S., Chatzispyrou, I. A., Houtkooper, R. H., Brandt, U., and Huynen, M. A. (2019). COmplexome Profiling ALignment (COPAL) Reveals Remodeling of Mitochondrial Protein Complexes in Barth Syndrome. Bioinformatics 35, 3083–3091. doi:10.1093/bioinformatics/btz025.

Chandler PD, Chen WY, Ajala ON, Hazra A, Cook N, Bubes V, Lee IM, Giovannucci EL, Willett W, Buring JE, Manson JE. (2020). Effect of Vitamin D3 Supplements on Development of Advanced Cancer: A Secondary Analysis of the VITAL Randomized Clinical Trial. JAMA Netw Open. 2020 Nov 2;3(11):e2025850. doi: 10.1001/jamanetworkopen.2020.25850. Erratum in: JAMA Netw. PMID: 33206192; PMCID: PMC7675103.

Bray, Freddie; Ferlay, Jacques; Soerjomataram, Isabelle; Siegel, Rebecca L.; Torre, Lindsey A.; Jemal, Ahmedin (2018). Global Cancer Statistics 2018: GLOBOCAN Estimates of Incidence and Mortality Worldwide for 36 Cancers in 185 Countries. CA: A Cancer Journal for Clinicians, (), –. doi:10.3322/caac.21492.

Vyas, Sejal; Zaganjor, Elma; Haigis, Marcia C. (2016). Mitochondria and Cancer. Cell, 166(3), 555–566. doi:10.1016/j.cell.2016.07.002.

Nordgaard CL, Karunadharma PP, Feng X, Olsen TW, & Ferrington DA (2008). Mitochondrial proteomics of the retinal pigment epithelium at progressive stages of age-related macular degeneration. Invest Ophthalmol Vis Sci, 49(7), 2848–2855. [PMC free article] [PubMed] [Google Scholar].

Kazuto Nakada; Kimiko Inoue; Jun-Ichi Hayashi (2001). Mito-mice: animal models for mitochondrial DNA-based diseases. , 12(6), 0–465. doi:10.1006/scdb.2001.0283.

Giaever, Guri; Chu, Angela M.; Ni, Li; Connelly, Carla; Riles, Linda; Véronneau, Steeve; Dow, Sally; Lucau-Danila, Ankuta; Anderson, Keith; André, Bruno (2002). Functional profiling of the Saccharomyces cerevisiae genome. , 418(6896), 387–391. doi:10.1038/nature00935.

Haroon, Suraiya; Li, Annie; Weinert, Jaye L.; Fritsch, Clark; Ericson, Nolan G.; Alexander-Floyd, Jasmine; Braeckman, Bart P.; Haynes, Cole M.; Bielas, Jason H.; Gidalevitz, Tali; Vermulst, Marc (2018). Multiple Molecular Mechanisms Rescue mtDNA Disease in C. elegans. Cell Reports, 22(12), 3115–3125. doi:10.1016/j.celrep.2018.02.099.

Weber, Nora; Gorwa-Grauslund, Marie; Carlquist, Magnus (2014). Exploiting cell metabolism for biocatalytic whole-cell transamination by recombinantSaccharomyces cerevisiae. Applied Microbiology and Biotechnology, 98(10), 4615–4624. doi:10.1007/s00253-014-5576-z.

Polyak, E., Zhang, Z., & Falk, M. J. (2011). Molecular Profiling of Mitochondrial Dysfunction in Caenorhabditis elegans. Mitochondrial Disorders, 241–255. doi:10.1007/978-1-61779-504-6_17.

Amrit, Francis Raj Gandhi; Ratnappan, Ramesh; Keith, Scott Alexander; Ghazi, Arjumand. 2014. The C. elegans lifespan assay toolkit. *Methods*, 68(3), 465–475. doi:10.1016/j.ymeth.2014.04.002.

Sanders, Erin R. 2012. Aseptic Laboratory Techniques: Plating Methods. *Journal of Visualized Experiments*, (63), –. doi:10.3791/3064.

McLachlan, I.G, Flavell, S.W. (2019). Cell Type-specific mRNA Purification in Caenorhabditis elegans via Translating Ribosome Affinity Purification. *Bio Protoc*. doi: 10.21769/BioProtoc.3328. PMID: 33654835; PMCID: PMC7854165.

Porta-de-la-Riva, Montserrat; Fontrodona, Laura; Villanueva, Alberto; Cerón, Julián. 2012. Basic Caenorhabditis elegans Methods: Synchronization and Observation. *Journal of Visualized Experiments*, (64), –. doi:10.3791/4019.

White, P. S., Penley, M. J., Tierney, A. R. P., Soper, D. M., & Morran, L. T. 2019. Dauer life stage of Caenorhabditis elegans induces elevated levels of defense against the parasite Serratia marcescens. *Scientific Reports*, 9(1). doi:10.1038/s41598-019-47969-w.

Chauve, L., Le, Pen, J., Hodge, F., Todtenhaupt, P., Biggins, L., Miska, E.A., Andrews, S., Casanueva, O. 2020. High-Throughput Quantitative RT-PCR in Single and Bulk C. elegans Samples Using Nanofluidic Technology. *J Vis Exp*. doi: 10.3791/61132. PMID: 32538915.

Michno, J.M &Stupar, R.M. (2018). The importance of genotype identity, genetic heterogeneity, and bioinformatic handling for properly assessing genomic variation in transgenic plants. *BMC Biotechnol*. https://doi.org/10.1186/s12896-018-0447-9.

Rasheed, Awais; Hao, Yuanfeng; Xia, Xianchun; Khan, Awais; Xu, Yunbi; Varshney, Rajeev K.; He, Zhonghu (2017). Crop breeding chips and genotyping platforms: progress, challenges, and perspectives. *Molecular Plant* S1674205217301740–. doi:10.1016/j.molp.2017.06.008.

Stock, J.B. (2009). Encyclopedia of Microbiology || Chemotaxis. , (), 71–78. doi:10.1016/B978-012373944-5.00068-7.

Chalfie, M., and Thomson, J.N. (1997). Organization of neuronal microtubules in the nematode Caenorhabditis elegans. Journal of cell biology. 82, 278-289.

Engleman, Eric A.; Steagall, Kevin B.; Bredhold, Kristin E.; Breach, Michaela; Kline, Hannah L.; Bell, Richard L.; Katner, Simon N.; Neal-Beliveau, Bethany S. (2018). Caenorhabditis elegans Show Preference for Stimulants and Potential as a Model Organism for Medications Screening. Frontiers in Physiology, 9(), 1200–. doi:10.3389/fphys.2018.01200.

Iwanir S, Ruach R, Itskovits E, Pritz CO, Bokman E, Zaslaver A. (2019). Irrational behavior in C. elegans arises from asymmetric modulatory effects within single sensory neurons. Nat Commun.. doi: 10.1038/s41467-019-11163-3.

Colbert, H.A & Bargmann, C.I. (1995). Odorant-specific adaptation pathways generate olfactory plasticity in C. elegans. Neuron.. doi: 10.1016/0896-6273(95)90224-4. PMID: 7718242.

Lee J, Jee, C/, McIntire, S.L. (2009). Ethanol preference in C. elegans. Genes Brain Behav.. doi: 10.1111/j.1601-183X.2009.00513.x. Epub 2009 Jun 22. PMID: 19614755; PMCID: PMC2880621.

Swierczek, Nicholas A; Giles, Andrew C; Rankin, Catharine H; Kerr, Rex A (2011). High-throughput behavioral analysis in *C. elegans*. *Nature Methods*, 8(7), 592–598. doi:10.1038/nmeth.1625.

Sawin, E.R., Ranganathan, R. & Horvitz, H.R. (2000). *C. elegans* locomotory rate is modulated by the environment through a dopaminergic pathway and by experience through a serotonergic pathway. *Neuron* 26, 619–631.

Iino, Y. & Yoshida, K. (2009). Parallel use of two behavioral mechanisms for chemotaxis in Caenorhabditis elegans. J. Neurosci. 29, 5370–5380 .

Kauffman, A., Parsons, L., Stein, G., Wills, A., Kaletsky, R., Murphy, C. 2011. C. elegans positive butanone learning, short-term, and long-term associative memory assays. J Vis Exp. doi: 10.3791/2490. PMID: 21445035; PMCID: PMC3197297.

Javer, A., Ripoll-Sánchez, L., & Brown, A. E. X. 2018. Powerful and interpretable behavioural features for quantitative phenotyping of Caenorhabditis elegans. Philosophical Transactions of the Royal Society B: *Biological Sciences*, 373(1758), 20170375. doi:10.1098/rstb.2017.0375.

Park, H.-E. H., Jung, Y., & Lee, S.-J. V. 2017. Survival assays using Caenorhabditis elegans. Molecules and Cells, 40(2), 90–99. doi:10.14348/molcells.2017.0017.

Amrit, F. R. G., Ratnappan, R., Keith, S. A., & Ghazi, A. 2014. The C. elegans lifespan assay toolkit. Methods, 68(3), 465–475. doi:10.1016/j.ymeth.2014.04.002.

Lee, J., Jee, C., & McIntire, S. L. 2009. Ethanol preference in C. elegans. *Genes, Brain and Behavior*, 8(6), 578–585. doi:10.1111/j.1601-183x.2009.00513.x.

Margie, O., Palmer, C., & Chin-Sang, I. 2013. *C. elegans* Chemotaxis Assay. *Journal of Visualized Experiments*, (74). doi:10.3791/50069.

Sutphin, George L.; Kaeberlein, Matt (2009). Measuring Caenorhabditis elegans Life Span on Solid Media. Journal of Visualized Experiments, (27), –. doi:10.3791/1152.

Sarasija, S., Norman, K.R. (2019). Measurement of Oxygen Consumption Rates in Intact Caenorhabditis elegans. *J Vis Exp*. doi: 10.3791/59277. PMID: 30855563; PMCID: PMC6538037.

Nawa, M., Kage-Nakadai, E., Aiso, S., Okamoto, K., Mitani, S., Matsuoka, M.J.C.D. & Differentiation. 2012. Reduced expression of BTBD10, an Akt activator, leads to motor neuron death. 19(8):1398-1407.

McClanahan, P. D., Xu, J. H., & Fang-Yen, C. 2017. Comparing Caenorhabditis elegans gentle and harsh touch response behavior using a multiplexed hydraulic microfluidic *device. Integrative Biology*, 9(10), 800–809. doi:10.1039/c7ib00120g.

Chalfie, M., Hart, A.C., Rankin, C.H. & Goodman, M.B.J.W.t.o.r.o.C.e.b. 2014. Assaying mechanosensation.

Palade, G. E. 1952. A STUDY OF FIXATION FOR ELECTRON MICROSCOPY. *Journal of Experimental Medicine*, 95(3), 285–298. doi:10.1084/jem.95.3.285.

Kovács, A. L. (2015). The application of traditional transmission electron microscopy for autophagy research in Caenorhabditis elegans. *Biophysics Reports*, 1(2), 99–105. doi:10.1007/s41048-015-0014-z.

Ryu, D., Mouchiroud, L., Andreux, P. A., Katsyuba, E., Moullan, N., Nicolet-dit-Félix, A. A., … Auwerx, J. 2016. Urolithin A induces mitophagy and prolongs lifespan in C. elegans and increases muscle function in rodents. *Nature Medicine*, 22(8), 879–888. doi:10.1038/nm.4132.

Chen, Z., Wang, Z., Guo, W., Zhang, Z., Zhao, F., Zhao, Y., … He, X. 2014. TRIM35 Interacts with pyruvate kinase isoform M2 to suppress the Warburg effect and tumorigenicity in hepatocellular carcinoma. *Oncogene*, 34(30), 3946–3956. doi:10.1038/onc.2014.325.

Luz AL, Rooney JP, Kubik LL, Gonzalez CP, Song DH, Meyer JN (2015) Mitochondrial Morphology and Fundamental Parameters of the Mitochondrial Respiratory Chain Are Altered in

Caenorhabditis elegans Strains Deficient in Mitochondrial Dynamics and Homeostasis Processes. *PLoS ONE* 10(6): e0130940. https://doi.org/10.1371/journal.pone.0130940.

Sarasija, Shaarika; Laboy, Jocelyn T; Ashkavand, Zahra; Bonner, Jennifer; Tang, Yi; Norman, Kenneth R (2018). Presenilin mutations deregulate mitochondrial Ca2+ homeostasis and metabolic activity causing neurodegeneration in *Caenorhabditis elegans*. eLife, 7(), e33052–. doi:10.7554/eLife.33052.

Macedo, F., Romanatto, T., Gomes de Assis, C., Buis, A., Kowaltowski, A. J., Aguilaniu, H., & Marques da Cunha, F. 2020. Lifespan-extending interventions enhance lipid-supported mitochondrial respiration in Caenorhabditis elegans. *The FASEB Journal*. doi:10.1096/fj.201901880r.

Dilberger, B., Baumanns, S., Schmitt, F., Schmiedl, T., Hardt, M., Wenzel, U., & Eckert, G. P. 2019. Mitochondrial Oxidative Stress Impairs Energy Metabolism and Reduces Stress Resistance and Longevity of C. elegans. Oxidative Medicine and Cellular Longevity, 2019, 1–14. doi:10.1155/2019/6840540.

Schmitt, S., Saathoff, F., Meissner, L., Schropp, E.-M., Lichtmannegger, J., Schulz, S., … Zischka, H. 2013. A semi-automated method for isolating functionally intact mitochondria from cultured cells and tissue biopsies. *Analytical Biochemistry*, 443(1), 66–74. doi:10.1016/j.ab.2013.08.007.

Van der Westhuizen, F.H., Louw, R., Miller, H.C. 2018. *Laboratory protocols for mitochondrial respiratory chain enzyme analyses (plate reader).* Version 3. North West University Mitochondrial research laboratory. Potchefstroom.

Smith PK, Krohn RI, Hermanson GT, Mallia AK, Gartner FH, Provenzano MD, Fujimoto EK, Goeke NM, Olson BJ, Klenk DC. (1985). Measurement of protein using bicinchoninic acid. *Analytical Biochemistry*. 150, 76-85.

McLaughlin, Kelsey L.; Hagen, James T.; Coalson, Hannah S.; Nelson, Margaret A. M.; Kew, Kimberly A.; Wooten, Ashley R.; Fisher-Wellman, Kelsey H. (2020). *Novel approach to quantify mitochondrial content and intrinsic bioenergetic efficiency across organs. Scientific Reports, 10(1), 17599–*. doi:10.1038/s41598-020-74718-1 .

Sharma, L., Lu, J., & Bai, Y. (2009). Mitochondrial Respiratory Complex I: Structure, Function and Implication in Human Diseases. *Current Medicinal Chemistry*, 16(10), 1266–1277. doi:10.2174/092986709787846578.

Rahman S, Blok RB, Dahl HH, Danks DM, Kirby DM, Chow CW, Christodoulou J, Thorburn DR (1996) Leigh syndrome: clinical features and biochemical and DNA abnormalities. Ann Neurol 39: 343-351.

Han, D., Antunes, F., Canali, R., Rettori, D., & Cadenas, E. (2002). Voltage-dependent Anion Channels Control the Release of the Superoxide Anion from Mitochondria to Cytosol. *Journal of Biological Chemistry*, 278(8), 5557–5563. doi:10.1074/jbc.m210269200.

Chance, B., & Williams, G. R. (2006). The Respiratory Chain and Oxidative Phosphorylation. *Advances in Enzymology and Related Areas of Molecular Biology*, 65–134. doi:10.1002/9780470122624.ch2.

Luo, C., Long, J., & Liu, J. (2008). An improved spectrophotometric method for a more specific and accurate assay of mitochondrial complex III activity. Clinica Chimica Acta, 395(1-2), 38–41. doi:10.1016/j.cca.2008.04.025.

Ibarguren, M., Lopez, D.J., and Escriba, P.V. 2014. The effect of natural and synthetic fatty acids on membrane structure, microdomain organization, cellular functions and human health. *Biochim Biophys Acta*. 1838(6), 1518-1528. https//doi.org/10.1016/jbbamem.2023.12.

Cadenas, E. and Davies, K.J.A. (2000). Mitochondrial free radical generation, oxidative stress, and aging. *Free Radical Biology and Medicine*, 29(3-4):222–230.

Klotz, L.-O., & Sies, H. (2009). Cellular Generation of Oxidants: Relation to Oxidative Stress. Redox Signaling and Regulation in Biology and Medicine, 45–61. doi:10.1002/9783527627585.ch3.

Kumar, S., Egan, B. M., Kocsisova, Z., Schneider, D. L., Murphy, J. T., Diwan, A., & Kornfeld, K. (2019). Lifespan Extension in C. elegans Caused by Bacterial Colonization of the Intestine and Subsequent Activation of an Innate Immune Response. *Developmental Cell*, 49(1), 100–117.e6. doi:10.1016/j.devcel.2019.03.010.

Ewald, C., Hourihan, J., & Blackwell, T. (2017). Oxidative Stress Assays (arsenite and tBHP) in Caenorhabditis elegans. *BIO-PROTOCOL*, 7(13). doi:10.21769/bioprotoc.2365.

Wang, D., Qian, E. W., Amano, H., Okata, K., Ishihara, A., & Kabe, T. (2003). Oxidative desulfurization of fuel oil. Applied Catalysis A: General, 253(1), 91–99. doi:10.1016/s0926-860x(03)00528-3.

Mitchell, D. H., Stiles, J. W., Santelli, J., & Sanadi, D. R. (1979). Synchronous Growth and Aging of Caenorhabditis elegans in the Presence of Fluorodeoxyuridine. *Journal of Gerontology*, 34(1), 28–36. doi:10.1093/geronj/34.1.28.

Haghani, A., Dalton, H. M., Safi, N., Shirmohammadi, F., Sioutas, C., Morgan, T. E., … Curran, S. P. (2019). Air pollution alters Caenorhabditis elegans development and lifespan: responses to traffic-related nanoparticulate matter (nPM). *The Journals of Gerontology:* Series A. doi:10.1093/gerona/glz063

Lucanic, M., Plummer, W. T., Chen, E., Harke, J., Foulger, A. C., Onken, B., … Phillips, P. C. (2017). Impact of genetic background and experimental reproducibility on identifying chemical compounds with robust longevity effects. *Nature Communications*, 8, 14256. doi:10.1038/ncomms14256.

Feldman, N., Kosolapov, L., & Ben-Zvi, A. (2014). Fluorodeoxyuridine Improves Caenorhabditis elegans Proteostasis Independent of Reproduction Onset. *PLoS ONE*, 9(1), e85964. doi:10.1371/journal.pone.0085964.

Wang, H., Zhao, Y., & Zhang, Z. (2019). Age-dependent effects of floxuridine (FUdR) on senescent pathology and mortality in the nematode Caenorhabditis elegans. *Biochemical and Biophysical Research Communications*. doi:10.1016/j.bbrc.2018.12.161.

Evan T. Judd; Frank J. Wessels; Michelle D. Drewry; Matthew Grove; Katharine Wright; Daniel A. Hahn; John D. Hatle (2011). Ovariectomy in grasshoppers increases somatic storage, but proportional allocation of ingested nutrients to somatic tissues is unchanged. , 10(6), 972–979. doi:10.1111/j.1474-9726.2011.00737.x.

Henry, P., Owopetu, O., Adisa, D., Nguyen, T., Anthony, K., Ijoni-Animadu, D., Jamadar, S., Abdel-Rahman, F., & Saleh, M. A. (2016). Fatty acids composition of Caenorhabditis elegans using accurate mass GCMS-QTOF. *Journal of environmental science and health. Part. B, Pesticides, food contaminants, and agricultural wastes*, *51*(8), 546–552. https://doi.org/10.1080/03601234.2016.1170555.

Hansen, Malene; Flatt, Thomas; Aguilaniu, Hugo (2013). Reproduction, Fat Metabolism, and Life Span: What Is the Connection?. Cell Metabolism, 17(1), 10–19. doi:10.1016/j.cmet.2012.12.003.

Zhang, M., Chen, S., Dai, Y., *et al*. 2021. Aspartame and sucralose extend the lifespan and improve the health status of C. elegans. *Food & function*. doi:10.1039/d1fo01579f.

Channel. Cell reports, 11(9), 1414–1424. https://doi.org/10.1016/j.celrep.2015.04.066.

Fielenbach, N., & Antebi, A. (2008). C. elegans dauer formation and the molecular basis of plasticity. Genes & development, 22(16), 2149–2165. https://doi.org/10.1101/gad.1701508.

Munasinghe, M., Almotayri, A., Thomas, J., Heydarian, D., & Jois, M. (2021). Early Exposure is Necessary for the Lifespan Extension Effects of Cocoa in C. elegans. *Nutrition and Metabolic Insights*, 14, 117863882110294. doi:10.1177/11786388211029443.

Li, H., Yu, X., Meng, F., Zhao, Z., Guan, S., & Wang, L. (2021). Ferulic Acid Supplementation Increases Lifespan and Stress Resistance via Insulin/IGF-1 Signaling Pathway in C. elegans. International Journal of Molecular Sciences, 22(8), 4279. doi:10.3390/ijms22084279.

Rasulova, M., Zeˇci´c, A., Monje Moreno, J.M., Vandemeulebroucke, L., Dhondt, I., Braeckman, B.P. 2021. Elevated Trehalose Levels in C. elegans daf-2 Mutants Increase Stress Resistance, Not Lifespan. *Metabolites* 105.https://doi.org/10.3390/metabo 11020105.

Zhang, M., Yang, X., Xu, W., Cai, X., Wang, M., Xu, Y., … Zhu, X. (2019). Evaluation of the effects of three sulfa sweeteners on the lifespan and intestinal fat deposition in C. elegans. *Food Research International*, 122, 66–76. doi:10.1016/j.foodres.2019.03.028.

Henderson, D., Huebner, C., Markowitz, M., Taube, N., Harvanek, Z. M., Jakob, U., & Knoefler, D. (2018). Do developmental temperatures affect redox level and lifespan in C. elegans through upregulation of peroxiredoxin? *Redox Biology*, 14, 386–390. doi:10.1016/j.redox.2017.10.003.

Angeli, S., Klang, I., Sivapatham, R., Mark, K., Zucker, D., Bhaumik, D., Lithgow, G.J., Andersen, J.K. 2013. A DNA synthesis inhibitor is protective against proteotoxic stressors via modulation of fertility pathways in Caenorhabditis elegans. *Aging*. doi: 10.18632/aging.100605. PMID: 24123581; PMCID: PMC3838778.

Possik, E., Jalali, Z., Nouët, Y., Yan, M., Gingras, M.-C., Schmeisser, K., … Pause, A. (2014). Folliculin Regulates Ampk-Dependent Autophagy and Metabolic Stress Survival. *PLoS Genetics*, 10(4), e1004273. doi:10.1371/journal.pgen.1004273.

Ward, S. (1973) Chemotaxis by the nematode Caenorhabditis elegans: identification of attractants and analysis of the response by use of mutants. *Proc. Natl. Acad*. Sci. U.S.A. 70, 817-821.

Bargmann, C. I., Hartwieg, E., & Horvitz, H. R. (1993). Odorant-selective genes and neurons mediate olfaction in C. elegans. *Cell*, 74(3), 515–527. doi:10.1016/0092-8674(93)80053-h.

Hu, L., Ye, J., Tan, H., Ge, A., Tang, L., Feng, X., … Liu, B.-F. (2015). Quantitative analysis of Caenorhabditis elegans chemotaxis using a microfluidic device. *Analytica Chimica Acta*, 887, 155–162. doi: 10.1016/j.aca.2015.07.036.

Palikaras, K., Lionaki, E., & Tavernarakis, N. (2015). Coordination of mitophagy and mitochondrial biogenesis during ageing in C. elegans. *Nature*, 521(7553), 525–528. doi:10.1038/nature14300.

Cervantes-Silva, M. P., Cox, S. L., & Curtis, A. M. (2021). Alterations in mitochondrial morphology as a key driver of immunity and host defence. EMBO reports, 22(9), e53086. https://doi.org/10.15252/embr.202153086.

Smith, D.M. (1931). The ontogenetic history of the mitochondria of the hepatic cell of the white rat. , 52(2), 485–511. doi:10.1002/jmor.1050520206.

Lax, N. Z.; Turnbull, D. M.; Reeve, A. K. (2011). Mitochondrial Mutations: Newly Discovered Players in Neuronal Degeneration. *The Neuroscientist*, 17(6), 645–658. doi:10.1177/1073858411385469.

Wallace, D. C. (1999). Mitochondrial Diseases in Man and Mouse. *Science*, 283(5407), 1482–1488. doi:10.1126/science.283.5407.1482.

Suthammarak, W.; Yang, Y.-Y.; Morgan, P. G.; Sedensky, M. M. (2009). Complex I Function Is Defective in Complex IV-deficient Caenorhabditis elegans. *Journal of Biological Chemistry*, 284(10), 6425–6435. doi:10.1074/jbc.M805733200.

Mito, Takayuki; Kikkawa, Yoshiaki; Shimizu, Akinori; Hashizume, Osamu; Katada, Shun; Imanishi, Hirotake; Ota, Azusa; Kato, Yukina; Nakada, Kazuto; Hayashi, Jun-Ichi; Bai, Yidong (2013). Mitochondrial DNA Mutations in Mutator Mice Confer Respiration Defects and B-Cell Lymphoma Development. PLoS ONE, 8(2), e55789–. doi:10.1371/journal.pone.0055789.

Malina, Carl; Larsson, Christer; Nielsen, Jens (2018). Yeast mitochondria: an overview of mitochondrial biology and the potential of mitochondrial systems biology. *FEMS Yeast Research*, 18(5), –. doi:10.1093/femsyr/foy040.

Kovács, Attila L. (2015). The application of traditional transmission electron microscopy for autophagy research in Caenorhabditis elegans. *Biophysics Reports*, 1(2), 99–105. doi:10.1007/s41048-015-0014-z.

Byrne, Joseph J.; Soh, Ming S.; Chandhok, Gursimran; Vijayaraghavan, Tarika; Teoh, Jean-Sébastien; Crawford, Simon; Cobham, Ansa E.; Yapa, Nethmi M. B.; Mirth, Christen K.; Neumann, Brent (2019). Disruption of mitochondrial dynamics affects behaviour and lifespan in Caenorhabditis elegans. *Cellular and Molecular Life Sciences*, doi:10.1007/s00018-019-03024-5.

Rasmussen, N. (1995). Mitochondrial structure and the practice of cell biology in the 1950s, *J. Hist. Biol*. 381–429.

Crofts, A. R., Holland, J. T., Victoria, D., Kolling, D. R., Dikanov, S. A., Gilbreth, R., et al. (2008). The Q-cycle reviewed: how well does a monomeric mechanism of the bc(1) complex account for

the function of a dimeric complex? *Biochim. Biophys.* Acta 1777, 1001–1019. doi: 10.1016/j.bbabio.2008.04.037.

Benard, G.; Faustin, B.; Passerieux, E.; Galinier, A.; Rocher, C.; Bellance, N.; Delage, J.-P.; Casteilla, L.; Letellier, T.; Rossignol, R. (2006). Physiological diversity of mitochondrial oxidative phosphorylation. AJP: *Cell Physiology*, 291(6), C1172–C1182. doi:10.1152/ajpcell.00195.2006.

Mansilla, N., Racca, S., Gras, D. E., Gonzalez, D. H., & Welchen, E. (2018). The Complexity of Mitochondrial Complex IV: An Update of Cytochrome c Oxidase Biogenesis in Plants. International journal of molecular sciences, 19(3), 662. https://doi.org/10.3390/ijms19030662.

Ono, T., Isobe, K., Nakada, K,. Hayashi, J.I. (2001) Human cells are protected from mitochondrial dysfunction by complementation of DNA products in fused mitochondria. *Nat Genet* 28(3):272–275.

G. Palade. (1953). An electron microscope study of the mitochondrial structure. *J. Histochem. Cytochem.* 1:188–211.

Perry, C. G. R.; Kane, D. A.; Lanza, I. R.; Neufer, P. D. (2013). Methods for Assessing Mitochondrial Function in Diabetes. *Diabetes*, 62(4), 1041–1053. doi:10.2337/db12-1219.

Brand, Martin D.; Nicholls, David G. (2011). Assessing mitochondrial dysfunction in cells. *Biochemical Journal*, 435(2), 297–312. doi:10.1042/bj20110162.

Gnaiger E (2009) Capacity of oxidative phosphorylation in human skeletal muscle. New perspectives of mitochondrial physiology. *Int J Biochem Cell Biol* 41:1837-45.

van der Bliek, Alexander M.; Sedensky, Margaret M.; Morgan, Phil G. (2017). Cell Biology of the Mitochondrion. *Genetics*, 207(3), 843–871. doi:10.1534/genetics.117.300262.

Dancy, Beverley M.; Sedensky, Margaret M.; Morgan, Philip G. (2014). Effects of the mitochondrial respiratory chain on longevity in *C. elegans*. *Experimental Gerontology*, 56(), 245–255. doi:10.1016/j.exger.2014.03.028.

Ventura N, Rea SL, Testi R (2006) Long-lived *C. elegans* mitochondrial mutants as a model for human mitochondrial-associated diseases. *Exp Gerontol* 41: 974–991.

Suthammarak, W., Somerlot, B.H., Opheim, E., Sedensky, M., Philip G. (2013). Novel interactions between mitochondrial superoxide dismutase and the electron transport chain. *Aging Cell*, 12(6), 1132–1140. doi:10.1111/acel.12144.

Mello, D.F., Bergemann, C.M., Fisher, K, Chitrakar, R., Bijwadia, S.R., Wang, Y., Caldwell, A., Baugh, L.R., Meyer, J.N. (2022). Rotenone Modulates Caenorhabditis elegans Immunometabolism

and Pathogen Susceptibility. *Front Immuno*l.doi10.3389/fimmu.2022.840272. PMID: 35273616; PMCID: PMC8902048.

Britta Spanier;Anne Laurençon;Anna Weiser;Nathalie Pujol;Shizue Omi;Aiko Barsch;Ansgar Korf;Sven W. Meyer;Jonathan J. Ewbank;Francesca Paladino;Steve Garvis;Hugo Aguilaniu;Michael Witting; (2021). Comparison of lipidome profiles of Caenorhabditis elegans—results from an inter-laboratory ring trial. Metabolomics, (), –. doi:10.1007/s11306-021-01775-6.

Cecilia Castro, C., Sar, F., Shaw, W.R. Mishima, M,. Miska, E.A., Griffin, J.L. (2012). A metabolomic strategy defines the regulation of lipid content and global metabolism by Δ9 desaturases in Caenorhabditis elegans. , 13(1), 36–. doi:10.1186/1471-2164-13-36.

Croxton, R., Mark G. Baron; David Butler; Terry Kent; Vaughn G. Sears (2006). Development of a GC-MS Method for the Simultaneous Analysis of Latent Fingerprint Components. , 51(6), 1329–1333. doi:10.1111/j.1556-4029.2006.00203.x.

Faizi, Shaheen; Sumbul, Saima; Versiani, Muhammed Ali; Saleem, Rubeena; Sana, Aisha; Siddiqui, Hira (2014). GC/GCMS analysis of the petroleum ether and dichloromethane extracts of M oringa oleifera roots. *Asian Pacific Journal of Tropical Biomedicine*, 4(8), 650–654. doi:10.12980/APJTB.4.201414B141.

Williams, C., Mbuyane, l.L., Bauer, F., Mokwena, L., Divol, B., Buica, A. (2021). A Gas Chromatography-Mass Spectrometry Method for the Determination of Fatty Acids and Sterols in Y Brock, T. J.; Browse, J.; Watts, J. L. (2006). Fatty Acid Desaturation and the Regulation of Adiposity in Caenorhabditis elegans. Genetics, 176(2), 865–875. doi:10.1534/genetics.107.071860.

Shmookler Reis, R.J., Xu, L., Lee H, Chae M, Thaden JJ, Bharill P, Tazearslan C, Siegel E, Alla R, Zimniak P, Ayyadevara S. (2011). Modulation of lipid biosynthesis contributes to stress resistance and longevity of C. elegans mutants. Aging (Albany NY). doi: 10.18632/aging.100275. PMID: 21386131; PMCID: PMC3082008.east and Grape Juice . *Applied Sciences*. doi:10.3390/app11115152.

Brock, T. J.; Browse, J.; Watts, J. L. (2006). Fatty Acid Desaturation and the Regulation of Adiposity in Caenorhabditis elegans. Genetics, 176(2), 865–875. doi:10.1534/*genetics*.107.071860.

Salzer, L and Witting, M. (2021). Quo Vadis Caenorhabditis elegans Metabolomics—A Review of Current Methods and Applications to Explore Metabolism in the Nematode. *Metabolites*.doi:10.3390/metabo11050284.

7. ANNEXURE A: ETHICS CERTIFICATE

Private Bag X1290, Potchefstroom
South Africa 2520

Tel: 086 016 9698
Web: http://www.nwu.ac.za/

North-West University Animal Care, Health and Safety Research Ethics Committee (NWU-AnimCareREC)

Tel: 018 299-1208
Email: Ethics-AnimCare@nwu.ac.za (for animal studies)

21 March 2021

RESEARCH ETHICS COMMITTEE LETTER OF DECISION: NO RISK

Based on the review by the North-West University Animal Care, Health and Safety Research Ethics Committee (NWU-AnimCareREC) on 21/03/2021, the NWU-AnimCareREC hereby clears your study as a no risk study. This implies that the NWU-AnimCareREC grants its permission that, provided the general conditions specified below are met, the study may be initiated, using the ethics number below.

Study title: Functional analysis of the mitochondrial contact site and cristae organizing system (MICOS) subunits in cristae morphology and its association to mitochondrial mutations
Principal Investigator/Study Supervisor/Researcher: Dr M Pretorius
Student: DK Sejo - 24251984

Ethics number: N W U - 0 0 4 1 0 - 2 1 - A 5
(Institution – Study Number – Year – Status)

Status: S = Submission; R = Re-Submission; P = Provisional Authorisation; A = Authorisation

Application Type: Lower invertebrate study
Commencement date: 21/03/2021

Risk: No Risk

General conditions:

The following general terms and conditions will apply:

- *The commencement date indicates the first date that the study may be started.*
- *In the interest of ethical responsibility, the NWU-AnimCareREC reserves the right to:*
  - *request access to any information or data at any time during the course or after completion of the study;*
  - *to ask further questions, seek additional information, require further modification or monitor the conduct of your research;*
  - *withdraw or postpone clearance if:*
    - *any unethical principles or practices of the study are revealed or suspected;*
    - *it becomes apparent that any relevant information was withheld from the NWU-AnimCareREC or that information has been false or misrepresented;*
    - *submission of the required amendments, or reporting of adverse events or incidents was not done in a timely manner and accurately; and/or*
    - *new institutional rules, national legislation or international conventions deem it necessary.*
- *NWU-AnimCareREC can be contacted for further information via Ethics-AnimCare@nwu.ac.za or 018 299 1208*

8. ANNEXURE B: OXPHOS ENZYME ACTIVITY SOP

LABORATORY PROTOCOLS FOR MITOCHONDRIAL RESPIRATORY CHAIN ENZYME ANALYSES

(Plate Reader)

Mitochondria Research Laboratory

Focus Area for Human Metabolomics

North-West University

Version 3

(September 2018)

FH van der Westhuizen

R Louw

HC Miller

Literature References

Total Protein:

- Smith PK, Krohn RI, Hermanson GT, Mallia AK, Gartner FH, Provenzano MD, Fujimoto EK, Goeke NM, Olson BJ, Klenk DC. (1985). Measurement of protein using bicinchoninic acid. Analytical Biochemistry. 150, 76-85

Citrate synthase:

- Sheperd D and Garland PB (1969). The kinetic properties of citrate synthase from rat liver mitochondria. Biochemical journal 114, 597-610, *as described in*
- Robinson JB, Brent LG, Sumegi B, Srere PA (1987) An enzymatic approach to the study of the Krebs tricarboxylic acid cycle. In *Mitochondria: a Practical Approach*. IRL Press, Oxford, UK, 153-170.

Complex I-IV assays are a combination of information obtained from the following publications and communications:

- Rahman S, Blok RB, Dahl HH, Danks DM, Kirby DM, Chow CW, Christodoulou J, Thorburn DR (1996) Leigh syndrome: clinical features and biochemical and DNA abnormalities. *Ann Neurol* 39: 343-351. (complex I-IV)
- Janssen AJ, Trijbels FJ, Sengers RC, Smeitink JA, van den Heuvel LP, Wintjes LT, Stoltenborg-Hogenkamp BJ, Rodenburg RJ (2007) Spectrophotometric assay for complex I of the respiratory chain in tissue samples and cultured fibroblasts. *Clin Chem* 53: 729-734. (complex I, II).
- Luo C, Long J, Liu J. 2008. An improved spectrophotometric method for a more specific and accurate assay of mitochondrial complex III activity. *Clinica Chimica Acta* 395: 38-41. (complex III)
- Dr DR Thorburn, Murdoch Children's Hospital, Melbourne, Australia, personal communication.
- Rodenburg, R.J., 2011. Biochemical diagnosis of mitochondrial disorders. *Journal of inherited metabolic disease*, *34*(2), pp.283-292.

- Gellerich, F.N., Mayr, J.A., Reuter, S., Sperl, W. and Zierz, S., 2004. The problem of interlab variation in methods for mitochondrial disease diagnosis: enzymatic measurement of respiratory chain complexes. *Mitochondrion*, *4*(5), pp.427-439.
- Spinazzi, M., Casarin, A., Pertegato, V., Salviati, L. and Angelini, C., 2012. Assessment of mitochondrial respiratory chain enzymatic activities on tissues and cultured cells. *Nature protocols*, *7*(6), p.1235.
- Errede, B. et al., Preparation and properties of complex IV (ferrocytochrome c:Oxygen Oxidoreductase EC 1.9.3.1). Methods in Enzymology, 53, 40-47 (1978).

1. REAGENTS AND STORAGE

1.1. Reagents

- Acetyl-CoA (trilithium salt, Sigma-Roche 10101907001, Mr 827.4) *(4°C)*
- ATP (Adenosine 5′-triphosphate disodium salt trihydrate) (Sigma-Roche A2383, Mr 605.2) *(4°C)*
- Bovine serum albumin (BSA) (Sigma-Roche 10775835001, Mr 68 kDa) *(4°C - cell culture lab)*
- Coenzyme Q1 (Sigma C7956, Mr 250.3 g/mol) *(-20°C)*
- Cyclohexane (Merck 4135126) *(safety cabinet)*
- Cytochrome C (CytCox) (Sigma C7752, Mr 12 384) *(4°C)*
- DCIP (2,6-Dichloroindophenol sodium salt hydrate) (Sigma D1878, Mr 290.1) *(OXPHOS cupboard)*
- Decylubiquinone (Sigma D7911, Mr 322.4) *(-20°C)*
- Dialysis (Pierce Slide-A-Lyzer Mini Dialysis unit, Cat # 69570)
- DMSO (Sigma C6164) *(safety cabinet)*
- DTNB (5,5'-Dithio-bis[-2-nitrobenzoic acid]) (Sigma D8130, Mr 396.4) *(4°C)*
- EDTA (ethylenediaminetetraacetic acid disodium salt dihydrate) (Sigma E1644, Mr 372.2) *(OXPHOS cupboard)*
- EGTA (Ethylene glycol-bis(β-aminoethylether) N,N,N',N'-tetraacetic acid) (Sigma E4378, Mr 380.4) *(OXPHOS cupboard)*
- Ethanol (Sigma E7023) *(safety cabinet)*
- HEPES, free acid (Sigma H3375, Mr 238.3) *(OXPHOS cupboard)*
- Hydrochloric acid (cHCl) (Sigma 43,557-0, 37%) *(acids cabinet)*
- Malonic acid (Sigma M1296, Mr 104.1) *(OXPHOS cupboard)*
- Mannitol (Sigma M9546, Mr 182.2) *(OXPHOS cupboard)*
- NADH (β-Nicotinamide adenine dinucleotide, reduced dipotassium salt, Sigma N4505, Mr 741.6 g/mol) *(-20°C)*
- Oxaloacetate (OAA) (Sigma O4126, Mr 132.1) *(4°C)*
- Potassium hydroxide (KOH) (Sigma P5958, Mr 56.1) *(OXPHOS cupboard)*
- Potassium phosphate dibasic (K_2HPO_4) (Sigma P2222, Mr 174.2 g/mol) *(OXPHOS cupboard)*

- Potassium phosphate monobasic (KH_2PO_4) (Sigma P5655, Mr 136.1 g/mol) *(OXPHOS cupboard)*
- Rotenone (Sigma R8875, Mr 394.4) *(poisons cupboard)*
- Sodium ascorbate (Sigma A4034, Mr 198) *(reagents cupboard)*
- Sodium azide (NaN_3) (Sigma S2002, Mr 65.01) *(poisons cupboard)*
- Solid sodium dithionite (Merck 9000954) *(OXPHOS cupboard)*
- Succinate, 1 M (Sigma S7501, Mr 118.1) *(OXPHOS cupboard)*
- Sucrose (Sigma 84100, Mr 342.3) *(OXPHOS cupboard)*
- Triton X-100 (Sigma T9284) *(OXPHOS cupboard)*
- Trizma base (Sigma T1503, Mr 121.14) *(OXPHOS cupboard)*
- Tween 20 (Merck 822184) *(OXPHOS cupboard)*

1.2. Kits

- BCA protein assay kit (Sigma BCA-1) containing BCA (Sigma B9643), $CuSO_4$ (Sigma 2284) and protein standard (bovine serum albumin; BSA) 1 µg/µl (Sigma P0914) (4°C)

1.3. Water

(MilliQ system): Tap water initially passes through a Progard pre-treatment pack. It is designed to remove particles and free chlorine from the water and prevents mineral scaling in hard water areas. The water is pressurized with a pump and then is purified by reverse osmosis (RO). The RO product water then passes through an electrode-ionisation (E.D.I) module. This is the final purification stage used to reduce levels of organic and mineral contaminants. The water is then exposed to UV light at both 185 and 254 nm wavelengths. This oxidises organic compounds and kills bacteria. The function of the Quantum cartridge is to remove trace ions and oxidation by-products produced by the action of the UV light. Purified water then passes through an Ultra filtration (UF) module. The UF module acts as a barrier to colloids, particles and organic molecules with a molecular weight greater than 5000 Daltons. The contaminants retained by the UF are periodically flushed out of the system via tubing to a drain. A manual 3 way valve located in the point of use allows you to direct ultra-pure water through a final filter made up of a 0.22 um membrane. The final filter removes particles and bacteria greater than 0.22 um in size and prevents recontamination of the system from the point of use. The A10 TOC monitor takes samples of ultra-pure water to determine trace organic levels. Samples are taken periodically in product mode

2. PREPARATION OF HOMOGENATES AND SUPERNATANTS FROM MUSCLE TISSUE

2.1. Reagents and equipment

2.1.1 **Zheng buffer** (for homogenate preparation):
2.1.1.1 Mannitol, 210 mM (Sigma M9546, Mr 182.2); *3.83 g/100 ml*
2.1.1.2 Sucrose, 70 mM (Sigma 84100, Mr 342.3); *2.40 g/100 ml*
2.1.1.3 HEPES, free acid, 5 mM (Sigma H3375, Mr 238.3); *0.119 g/100 ml*
2.1.1.4 EGTA, 0.1 mM (Sigma E4378, Mr 380.4);

- Make up a 100 mM EGTA stock solution – pH must be set to 7.2 using 1 M KOH (~23% of the final volume) in order for EGTA to dissolve. *0.038 g/1 mL*
- Add 0.1 ml of 100 mM EGTA solution (pH 7.2) per 100 ml Zheng buffer

2.1.1.5 Set pH to 7.2 using 1 M KOH (Sigma P5958, Mr 56.1) *5.61 g/100 ml*
2.1.1.6 Aliquot and store at -80 °C in marked and dated bottle. Prepare fresh once a year.

2.1.2 Cold metal plate on ice - Since each sample is handled on a different area of the plate (to prevent cross-contamination), the plate is only washed (with Jik-solution) after all the samples have been prepared.

2.1.3 Potter-Elvehjam homogenizer (stored in OXPHOS cupboard at RT) – Wash with 70% EtOH between samples.

2.1.4 Tweezers – Wash with 70% EtOH after handling each sample.

2.1.5 Blades – use new blade for each sample

2.2. Procedure (600g supernatant preparations)

2.2.1. Muscle tissue (± 300 mg) is collected in an ice cooled sterile container and, without any other preparation, preferably immediately wrapped in tin foil, placed in a micro-centrifuge or other type tube and frozen at -80°C. The sample name or reference number and date of biopsy have to be written on the tube. The sample has to be processed in this way within 3 hrs after collection. Transport has to be done on dry ice.
2.2.2. For sample preparation, thaw sample on ice and remove foil.
2.2.3. Remove fat tissue and cut a clean piece of the sample (± 100 mg) with a sterile blade on a cold metal plate. Weigh this sample.
2.2.4. Using the blade pressed on the cold plate cut the sample as fine as possible.
2.2.5. Suspend in Zheng Buffer to 10% (w/v), e.g. 1000 µl for 100 mg sample.
2.2.6. Homogenise in a Potter-Elvehjam homogenizer placed in ice water using 15 strokes (appearance of homogenate should show even dispersion and no solid parts).
- Old homogenizer – Setting "II" pointing North and set to 500
- Heidolph homogenizer – Set to 6.5

2.2.7. Clean homogenizer using water, 70% ethanol and water again. Spin at high speed to remove excess water – do not towel dry.
2.2.8. *Transfer at least 100 µl of the homogenate to a marked clean micro centrifuge tube (500 µl type marked with sample number and "H") (Use for DNA analysis).
2.2.9. Centrifuge remaining homogenate at 600 x g for 10 min at 4 °C.
2.2.10. Transfer supernatant (at least 500 µl above pellet) to a marked clean micro centrifuge tube (1.5 ml type marked with sample number and "600g S").
2.2.11. Aliquot 200 µl thereof into a PCR 8-tube strip. Do not vortex.

** For Prof. Izelle Smuts samples only.*

2.3. Storage of samples

2.3.1. Newly received muscle biopsies:
Store in Thermo Scientific -80°C freezer; Box no. ____ (New muscle biopsies).

Any remaining muscle samples are also stored in this tower in box no. _____ (Mito samples).

2.3.2. Homogenates (marked with sample number and "H"):
Store in Box F15

2.3.3. 600 g supernatants (1.5 ml tube and PCR strips marked "600g S"):
Store in Box _____

2.3.4. Reference sample (600g S):
Stored in Box G10

2.4. Freeze-thaw cycles

2.4.1. Defrost the aliquoted 600g supernatant in cold water (sample must remain ice cold at all times) and immediately snap freeze again in liquid nitrogen.
2.4.2. Repeat step 2.4.1.

2.4.3. Finally, store the sample on ice (with water to ensure sample remains ice cold at all times) throughout analyses.

2.5. Reference sample (inter batch comparison)

2.5.1 Prepare a 600g (10% w/v) supernatant from a Bl6 mouse heart/s by homogenizing as described before.

2.5.2 Dilute this homogenate 20x further in Zheng buffer, freeze-thaw 3 times and store in 200 µl aliquots at -80 °C. Use an aliquot as inter batch reference (<10 CV) with each batch of samples.

2.5.3 Prepare this reference sample once a year.

3. PROTEIN ASSAY (BCA METHOD)

3.1. Reagents

3.1.1. BCA protein assay kit (Sigma BCA-1) containing BCA (Sigma B9643), $CuSO_4$ (Sigma 2284) and protein standard, bovine serum albumin (BSA) (Sigma P0914).

3.1.2. *BCA reagent:*
Freshly prepare BCA:$CuSO_4$ solution at a ratio of 50:1.

Volume BCA = Desired total volume x 49/50

Volume $CuSO_4$ = Desired total volume x 1/50

3.1.3. *BSA standard:* Open ampule and transfer the BSA standard solution to a 1.5 ml microcentrifuge tube. 1 mg/ml = 1 µg/µl

3.1.4. Test sample as prepared in Section 2.2 (use undiluted).

3.2. Procedure

3.2.1. Switch on plate reader and allow temperature to reach 37°C.

3.2.2. Prepare BSA standard (S) series as follows, in duplicate:

	S1	S2	S3	S4	S5	S6
BSA (µl)	0	4	8	12	16	20
H_20 (µl)	20	16	12	8	4	0

3.2.3. Add (in duplicate) samples and H_2O to microtiter plate up to a volume of 20 µl (Zheng buffer has no effect on assay compared to H_2O).
600g supernatant: 2 µl sample + 18 µl H_2O

3.2.4. Add 200 µl BCA reagent to standards and test samples *at the same time* and incubate at 37°C for 30 min or longer (samples must become clearly purple).

3.2.5. Use the programme "Protein concentration" on the BioTek Synergy HT microplate reader (Gen5 software) to read absorbance at 562 nm and determine protein concentration in the samples:

- Confirm that the protein standard concentration range is linear ($R^2 > 0.99$). Mask any outlier points on the standard curve.
- From the software, obtain the protein content (µg).
- Divide the protein content with volume used in the analysis (i.e. 2 µl) to obtain the protein concentration value expressed as µg/µl.

4. ASSAYS FOR RESPIRATORY CHAIN ENZYMES AND CITRATE SYNTHASE

4.1. Instrument, consumables and reagents

4.1.1. Synergy HT microplate reader (BioTek Instruments, Inc., P.O. Box 998, Highland Park, Winooski, Vermont 05404-0998 USA) and Gen5™ Data Analysis software (BioTek Instruments, Inc., P.O. Box 998, Highland Park, Winooski, Vermont 05404-0998 USA)

- Standard temperature setting for all enzyme analyses = **37°C**

4.1.2. *Microtiter plates:* 96-well, clear, F-bottom (Greiner Bio-One International, 655101, Lasec SA)

4.1.3. *Pipettes:* Eppendorf Research Plus micro pipettes (marked "OXPHOS").

4.1.4. *Tips:* Eppendorf standard epT.I.P.S. (Sigma Z640093 for 2-200 µl and Z640115 for 100-1000 µl).

4.1.5. *Micro-centrifuge tubes:* Biosmart Scientific 1.5 mL tubes (PBIOTM1.5ML).

4.1.6. Reagents are listed at separate enzymes

4.2. Preparation of reduced cytochrome C

Preparation:

- Dissolve 125 mg cytochrome C (CytC) in 600 ul 10 mM potassium phosphate buffer (pH 7.0) in 5 mL eppendorf tube. Cover with tinfoil. Vortex to dissolve the CytC.
- Dissolve 110 mg sodium ascorbate (Mr 198, 11) in 1 ml of 10 mM potassium phosphate buffer (pH 7.0), thus [ascorbic acid] = 0.555 M. According to Spinazzi et al., 2012, one should adjust the pH to 6.5 – 6.8 with a few grains of Tris powder. NB: This is not necessary when using sodium ascorbate. When dissolved, the pH is between 6 and 7. No need to adjust pH.
- Add 150 ul of the ascorbic acid solution to the 5 mL tube containing the CytC
- Mix for 60 minutes at 4 °C on a rotor (Heidolph Rotamax 120, max speed)

Purification:

Use a Zeba Desalt spin column (Zeba^{TM} desalt spin column, 10 ml, 89893, Thermo Scientific) to remove any access ascorbic acid.

Preparation of column

- Remove the plastic tip at the bottom of a spin column
- Remove the cap of the spin column
- Place the spin column in a clean 50 ml falcon tube
- Weigh tube with the filter in. Make a water balance in another 50 ml tube
- Centrifuge the tubes for 2 minutes at 1000 x g at 4 °C
- Discard the flow through

- Wash the column 3x with 5 mL 50 mM KPi buffer (pH 7.4).
- Load the KPi buffer with a plastic Pasteur pipette. Take care not to disturb the packing material in the spin column

- Place the spin column in a clean 50 mL falcon tube
- Add the reduced CytC solution very carefully on the spin column, without disturbing the packing material of the spin column. The CytC should be loaded one drop at a time in the centre of the tube, not on the side.

- Centrifuge the tubes for 2 minutes at 1000 x g at 4 °C
- Transfer the reduced CytC to an Eppendorf tube.
- Cover with tinfoil and store at -80°C.

Calculate the reduction and concentration:

- Add 5 µl of the CytCred to 995 µl KPi buffer (50 mM, pH 7.4) in a 1 mL cuvette.
- Add 1000 µl KPi buffer (50 mM, pH 7.4) in a 1 mL cuvette and use to blank the spectrophotometer.
- Scan 500-600 nm. (Read Ared 550 and 565 from graph)
- Add a few (3-5) grains of potassium ferricyanide $K_3Fe(CN)_6$ to re-oxidize the CytC. (NB: Using 5, 10 or 15 grains do not make any difference in the absorbance values obtained).
- Mix thoroughly with a 1 mL pipette
- Scan 500-600 nm
- (Read Aox 550 and 565 from graph)

Figure A: Left is the reduced CytC, right is after it has been re-oxidized with $K_3Fe(CN)_6$. Note the change in colour. Reduced is clearly pink, oxidized is red/orange

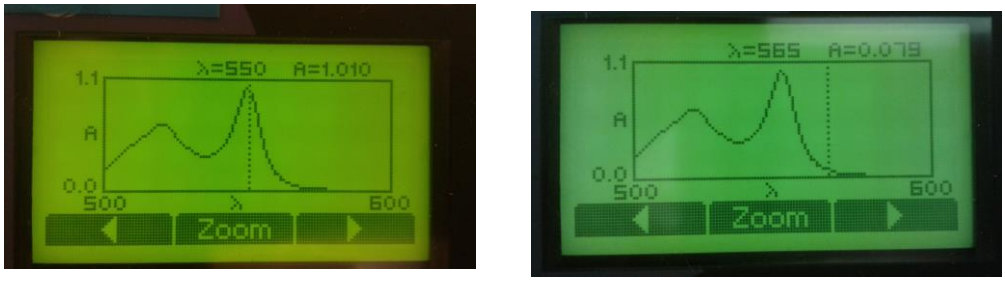

Figure B: Wavescan of reduced CytC from 500-600 nm with the absorbance at 550 indicated (left) and that at 565 (right).

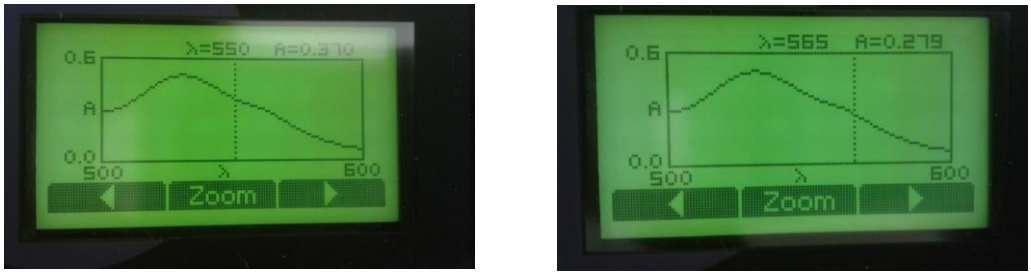

Figure C: Wavescan of oxidized [with $K_3Fe(CN)_6$] CytC from 500-600 nm with the absorbance at 550 indicated (left) and that at 565 (right).

- Reduction: A550red / Ared565
- 1.010 / 0.079
- = 12.78
- If A550/A565 > 8 it is sufficiently reduced.

- Calculate CytCred using the following equation:
- CytCred (mM) = $\frac{(Ared\ 550 - Aox\ 550)}{18.7\ mM^{-1}.cm^{-1}} \times 200$ (dilution)

- (1.010 – 0.279) / 18.7 x 200
- = 7.81 mM

- Dilute the CytCred to 500 µM with 50 mM KPi (pH 7.4).
- Aliquot in 200 µl volumes in microcentrifuge tubes and wrap with parafilm. Store at -80

Extinction coefficient of 18.7 (for reduced minus oxidized CytC <u>in 1 cm cuvette</u>) from Methods in Enzymology, Vol LIII, Part D, p10.

Extinction coefficient for 200 µl under assay conditions was calculate (9-2018) as 4180 Abs/mM**.**

4.3. Citrate (Si)-synthase

acetyl-CoA:oxaloacetate C-acetyltransferase [thioester-hydrolysing, (pro-S)-carboxymethyl forming], E.C. 2.3.3.1

4.3.1. Reagents

4.3.1.1. * Tris.HCl, 1M;
- Trizma base (Sigma T1503, Mr 121.14); *12.1 g/100 ml.*
- Set pH to 8.1 with cHCl (~30% of the final volume)

4.3.1.2. ** 5,5'-Dithio-bis[-2-nitrobenzoic acid] (DTNB), 1 mM (Sigma D8130, Mr 396.4); *0.4 mg/ml in 1M Tris.HCl, pH 8.1.*

4.3.1.3. ** Triton X-100, 10% (v/v) (Sigma T9284);
Add 1 ml Triton X-100 (using a 1000 µl tip cut shorter with a clean blade) to 9 ml milliQ H_2O and vortex well.

4.3.1.4. ** Acetyl-CoA, 3 mM (trilithium salt, Sigma-Roche 10101907001, Mr 827.4); *2.48 mg/ml.*

4.3.1.5. ** Oxaloacetate (OAA), 2 mM, (Sigma O4126, Mr 132.1);
*0.264 mg/ml in **0.1M** Tris.HCl, pH 8.1*.

* Store in aliquots at -80°C (prepare fresh every six months)

** Prepare fresh

4.3.2. Procedure

4.3.2.1. Switch on Synergy multiplate reader, switch on computer, and activate Gen5™ software.

4.3.2.2. Open "Protocols" and in the folder "OXPHOS" select protocol for citrate synthase (CS).

4.3.2.3. At the top of the window click on the temperature display and activate the temperature to preheat to 37°C.

4.3.2.4. Thaw mitochondrial samples on ice water and mix well.

4.3.2.5. Pre-heat the 2 mM OAA at 40°C in a water bath.

4.3.2.6. Prepare the following:

Table 4.3.1. CS Master mix

Reagent	**1x (µl)**	**[end]**
MilliQ water	106.5	
DTNB (1 mM)	20	0.1 mM
Triton X100 (10%)	0.5	0.025%
Acetyl-CoA (3 mM)	20	0.3 mM
Total	147	

4.3.2.7. Place 147 µl of CS master mix into each well (*multichannel pipette*).
4.3.2.8. Place 3 µl **600g supernatant** in triplicate for each sample into each well (*multichannel pipette*).
4.3.2.9. Place plate into plate reader and initiate reading. A 10 minute pre-incubation will be initiated, after which the tray will open.
4.3.2.10. Add 50 µl (preheated to 40°C) OAA ([end] 0.5 mM) to each reaction (*multichannel pipette*) and press enter to continue reading. Record linear rate increase at 412 nm for 5 min in 1 min intervals (ν_1).

4.3.3. Calculation

Use linear rate calculations over the first 2 minutes (first 3 readings) – check R^2 values to be more than 0.99 for ν_1.

For 200 µl reactions: ε_{412} = 7465 Abs/mM)

µmol/min/mg (UCS) = (ν_1/7465)*0.2/(µl protein x µg/µl/1000)

nmol/min/mg = UCS x 1000

4.4. NADH dehydrogenase (ubiquinone) (complex I)

NADH:ubiquinone oxidoreductase, E.C. 1.6.5.3

4.4.1. Reagents

4.4.1.1. * Phosphate buffer (KPi buffer), 0.5 M, pH 7.6.
- Potassium phosphate monobasic (KH_2PO_4), 0.5 M (Sigma P5655, Mr 136.1 g/mol);
  6.81 g/100 ml
- Potassium phosphate dibasic (K_2HPO_4), 0.5 M (Sigma P2222, Mr 174.2 g/mol);
  8.71 g/100 ml
- Add 0.5 M KH_2PO_4 (~13%) to 0.5 M K_2HPO_4 (~87%) until a pH of 7.6 is reached.

4.4.1.2. ** NADH, 2 mM (dipotassium salt, Sigma N4505, Mr 741.6 g/mol); *1.48 mg/ml*.

4.4.1.3. * Bovine serum albumin (BSA), 10% (w/v, Sigma-Roche 10775835001, Mr 68 kDa);
0.1 g/ml in water (store in 1 mL aliquots).

4.4.1.4. * Coenzyme Q1, 10 mM (Sigma C7956, Mr 250.3 g/mol);
2.5 mg/ml in absolute ethanol (store stocks in 100 µL aliquots).

4.4.1.5. ** DCIP (2,6-Dichloroindophenol sodium salt hydrate), 5 mM (Sigma D1878, Mr 290.1);
1.45 mg/ml in water - Since DCIP does not easily dissolve in water, heat for 20 minutes at 30°C and use a spatula to crush any remaining DCIP crystals.

4.4.1.6. * Rotenone, 1 mM (Sigma R8875, Mr 394.4);
- *0.394 mg/ml in DMSO* (store in 1 ml aliquots protected from light).

* Store in aliquots at -80°C (prepare fresh every six months)

** Prepare fresh

4.4.2. Procedure

Activity of complex I in each sample is measured in the presence <u>and</u> absence of rotenone (rotenone-sensitive complex I activity).

4.4.2.1. Switch on Synergy multiplate reader, switch on computer, and activate Gen5™ software.

4.4.2.2. Open “Protocols” and in the folder “OXPHOS diagnostiek” select protocol for complex I.

4.4.2.3. At the top of the window click on the temperature display and activate the temperature to preheat to 37°C.

4.4.2.4. Thaw mitochondrial samples on ice water and mix well.

4.4.2.5. Prepare and mix well a CI master mix and rotenone master mix as follows:

Table 4.4.1. CI Master mix

Reagent	1x (µl)	[end]
KPi buffer (0.5 M) – pH 7.6	10	25 mM
Coenzyme Q1 (10 mM)	1.4	70 µM
BSA (10%)	7	0.35 %
DCIP (5 mM)	2.4	60 µM
MilliQ H_2O	103.2	
Total	124	

Table 4.4.2. Rotenone or DMSO mix

Reagent	1x (µl)	[end]
Rotenone (1 MM) or DMSO	0.2	1 µM
Milli-Q water	49.8	
Total	50	

4.4.2.6. Add, before the assay, into two separate wells for each sample in triplicate (*multichannel pipette*):
- 50 µl DMSO/water (ν_1)
- 50 µl Rotenone/water (ν_2)

4.4.2.7. Add 6 µl 600g supernatant into each well (*multichannel pipette*).
4.4.2.8. Add 124 µl complex I master mix to each well (*multichannel pipette*).
4.4.2.9. Place plate into plate reader tray and initiate reading to pre-incubate for 10 min, after which tray will open.
4.4.2.10. Add 20 µl preheated 2 mM NADH ([end] 0.2 mM) to start reaction (*multichannel pipette*).
4.4.2.11. Press enter to continue reading to record linear rate decrease (ν1) of absorbance at 600 nm for 5 min in 1 min intervals.

4.4.3. Calculation

Use linear rate calculations over first 3 minutes (first 4 readings) – check R^2 values to be more than 0.99 for ν_1 and ν_2.

For 200 µl reactions: ε_{600} = 12712 Abs/mM)

µmol/min/mg = $(\nu_1 - \nu_2)/12712)*0.2/(\mu l\ protein*\mu g/\mu l/1000)$

nmol/min/UCS = µmol/min/mg x 1000/UCS

4.5. Succinate dehydrogenase (ubiquinone) (complex II)

succinate:ubiquinone oxidoreductase, E.C. 1.3.5.1

4.5.1. Reagents

4.5.1.1. * Phosphate buffer (KPi buffer), 0.5 M, pH 7.8.
- See 4.3.1.1
- Add 0.5 M KH_2PO_4 (~9%) to 0.5 M K_2HPO_4 (~91%) until a pH of 7.8 is reached.

4.5.1.2. * Bovine serum albumin (BSA), 10% (See 4.3.1.3)

4.5.1.3. ** ATP (Adenosine 5′-triphosphate disodium salt), 0.1 M, pH 7.2 (Sigma-Roche A2383, Mr 551.15);
- *55.1 mg/ml in water*
- Adjust pH to 7.8 with 2 M KOH (100 µl/ml) using pH indicator paper and set the final volume.
- Dissolve 60.5 mg ATP in 900 µl H_2O and add 100 µl 2M KOH. The pH should be ~ 7.8.

4.5.1.4. * EDTA (ethylenediaminetetraacetic acid disodium salt dihydrate), 250 mM, pH 7.0 (Sigma E1644, Mr 372.2);
- *93.05 mg/ml in water*
- Add 4.65 g to ~40 ml MilliQ water, adjust pH to 7.0 with 2 M KOH and set volume to 50 ml.

4.5.1.5. ** NaN_3 (sodium azide), 100 mM (Sigma S2002, Mr 65.01); *6.501 mg/ml*

4.5.1.6. * Succinate, 1 M (Sigma S7501, Mr 118.1); *0.118 g/ml.*
- When preparing, start with minimum volume and first set pH to 7.8 using KOH pellets.

4.5.1.7. ** DCIP (2,6-dichloroindophenol sodium salt hydrate), 5 mM (See 4.3.1.5).

4.5.1.8. * Decylubiquinone, 10 mM ***in DMSO*** (Sigma D7911, Mr 322.4); *3.224 mg/ml* in DMSO (Sigma C6164).

* Store in aliquots at -80°C (prepare fresh every six months)

** Prepare fresh

4.5.2. Procedure

Activity of complex II in each sample is measured in presence <u>and</u> absence of malonate (malonate-sensitive complex II activity).

4.5.2.1. Switch on Synergy multiplate reader, switch on computer, and activate Gen5™ software.

4.5.2.2. Open “Protocols” and in the folder “OXPHOS diagnostiek” select the protocol for complex II.

4.5.2.3. At the top of the window click on the temperature display and activate the temperature to preheat to 37°C.
4.5.2.4. Thaw mitochondrial samples on ice water and mix well.
4.5.2.5. Prepare CII Master mix as indicated in Table 4.4.1.

Table 4.4.1. CII Master mix

Reagent	1x (µl)	[end]
KPi buffer (0.5 M) – pH 7.8	32	80 mM
BSA (10%)	4	0.2 %
EDTA (250 mM)	1.6	2 mM
ATP (0.1 M)	4	0.2 mM
DCIP (5 mM)	3.2	80 µM
Decylubiquinone (10 mM ***in DMSO***)	1.6	80 µM
Sodium azide (100 mM)	0.6	0.3 mM
MilliQ water	113	
Total	160	

4.5.2.6. Add 160 µl complex II master mix to each well (*multichannel pipette*).
4.5.2.7. Add 10 µl 600g supernatant into each well (*multichannel pipette*).
4.5.2.8. Place plate into plate reader and initiate reading to pre-incubate for 10 minutes after which the tray will open.
4.5.2.9. Prepare a succinate solution: 2 µL 1 M succinate + 28 µL water per well.
Using a multichannel, add to each well 30 µl of the **preheated (40 °C)** succinate solution ([end] = 10 mM).
4.5.2.10. Press enter to continue reading to record linear rate decrease (ν1) at 600 nm for 5 min in 1 min intervals.

4.5.3. Calculation

Use linear rate calculations from 1 to 5 minutes (readings 2 -6) – check R^2 values to be more than 0.99 for ν_1 and ν_2.

For 200 µl reactions: ε_{600} = 12712 Abs/mM

µmol/min/mg = (ν_1)/12712)*0.2/(µl protein*µg/µl/1000)

nmol/min/UCS = µmol/min/mg x 1000/UCS

4.6. Succinate-cytochrome c reductase (complex II+III)

4.6.1. Reagents

4.6.1.1. * Phosphate buffer (KPi buffer), 0.5 M, pH 7.4.
- See 4.3.1.1
- Add 0.5 M KH_2PO_4 (~20%) to 0.5 M K_2HPO_4 (~80%) until a pH of 7.4 is reached.

4.6.1.2. * Succinate, 1 M (See 4.4.1.6)
4.6.1.3. ** NaN_3, 100 mM (See 4.4.1.5)
4.6.1.4. * BSA 10% (w/v) (See 4.3.1.3)
4.6.1.5. * Rotenone, 1 mM (Sigma R8875, Mr 394.4); *0.394 mg/ml in DMSO*
4.6.1.6. * Cytochrome C (CytCox), 4 mM (Sigma C7752, Mr 12 384); *49.5 mg/ml in 10 mM KPi (pH 7.4).*

* Store in aliquots at -80 °C (prepare fresh every six months)

** Prepare fresh

4.6.2. Procedure

4.6.2.1. Switch on the Synergy multiplate reader, switch on the computer, and activate Gen5™ software.
4.6.2.2. Open "Protocols" and in the folder "OXPHOS diagnostiek" select the protocol for complex II+III.
4.6.2.3. At the top of the window click on the temperature display and activate the temperature to preheat to 37 °C.
4.6.2.4. Thaw mitochondrial samples on ice water and mix well.
4.6.2.5. Prepare CII+III Master mix as indicated in Table 4.5.1.

Table 4.5.1. Complex II+III Master mix

Reagent	1x (µl)	[end]
KPi buffer (0.5 M) – pH 7.4	25	62.5 mM
Succinate (1 M)	7.1	35.35 mM
NaN_3 (100 mM)	5	2.5 mM
BSA (10%)	2.5	0.125%
Rotenone (1 mM)	0.2	1 µM
MilliQ water	104.2	
Total	144	

4.6.2.6. Add 144 µl complex II+III master mix per well.
4.6.2.7. Add 6 µl 600g supernatant to the well.

4.6.2.8. Place the plate into the plate reader and initiate reading to pre-incubate for 10 minutes (in order to activate CII), after which the tray will open.

4.6.2.9. Prepare the CytC mix as indicated in Table 4.5.2.

Table 4.5.2. Cyt C mix

Reagent	1x (µl)	[end]
Cytochrome C (4 mM)	5	0.1 mM
Water	45	
Total	50	

4.6.2.10. Add 50 µl CytC mix (multichannel) and press enter to continue reading to record linear rate increase (v1) at 550 nm for 5 min in 1 min intervals.

4.6.3. Calculation

Use linear rate calculations from 0 to 4 minutes (readings 1-5) – check R^2 values to be more than 0.99 for v_1. For 200 µl reactions: ε_{550} = 4180 A/mM

µmol/min/mg = $(v_1)/4180)*0.2/(\mu l\ protein*\mu g/\mu l/1000)$

nmol/min/UCS = µmol/min/mg x 1000/UCS

4.7. Ubiquinol-cytochrome c reductase (complex III)

ubiquinol:ferricytochrome-c oxidoreductase, E.C. 1.10.2.2

4.7.1. Reagents

4.7.1.1. * KPi buffer, 0.5 M, pH 7.8. (See 4.4.1.1)
4.7.1.2. * EDTA, 250 mM, (See 4.5.1.4)
4.7.1.3. ** Tween 20, 2% (v/v, Merck 822184);
Add 0.2 ml Tween 20 (using a 1000 µl tip cut shorter with a clean blade) to 10 ml water.
4.7.1.4. ** NaN_3, 100 mM (See 4.5.1.5)
4.7.1.5. * Cytochrome C (CytCox), 4 mM (Sigma C7752, Mr 12 384);
49.5 mg/ml in 10 mM KPi (pH 7.8)
4.7.1.6. * Decylubiquinol (reduced decyubiquinone/DB.H_2), 9.26 mM;
Prepare the following reagents and store*:

- 10 mM decylubiquinone (DB, Sigma D7911, Mr 322.4); *3.224 mg/ml in ethanol.*
- 0.1 N HCl in ethanol.
- 3.0 N HCl in ethanol.
- Potasium borohydride (BDH)

Procedure (30 reactions):

1. To 250 µl DB, add a few grains of potassium borohydride
2. Acidify mixture by 10 µl 0.1 N HCl/ethanol and mix in vortex until mixture changes from yellow and becomes clear (1 minute)
3. Add 10 µl 3 N HCl/ethanol to stabilize DB.H_2
4. Centrifuge 1 min at 10 000 g and transfer 200 µl of the supernatant to a fresh tube for further use.

* Store in aliquots at -80°C (prepare fresh every six months)

** Prepare fresh

4.7.2. Procedure

4.7.2.1. Switch on the Synergy multiplate reader, switch on the computer, and activate Gen5™ software.
4.7.2.2. Open “Protocols” and in the folder “OXPHOS diagnostiek” select the protocol for complex III.
4.7.2.3. At the top of the window click on the temperature display and activate the temperature to preheat to 37°C.
4.7.2.4. Thaw mitochondrial samples on ice water and mix well.
4.7.2.5. Prepare the Cyt C dilution as indicated in Table 4.6.1.

Table 4.6.1. Cytochrome C dilution

Reagent	1x (µl)	[end]
Cyt C (4 mM)	2.5	50 µM
Water	117.5	
Total	120	

4.7.2.6. In each well, add 120 µl of the CytC dilution ([end] = 50 µM).

4.7.2.7. In unused wells at the bottom of the multi well plate, dilute the 600g samples 10x by adding 10 µl sample to 90 ul water. Add 10 µl of this 10x dilution for each reaction in triplicate.

4.7.2.8. Place plate into plate reader tray and initiate reading to incubate for 10 min, after which tray will open.

4.7.2.9. Prepare in advance the CIII Master mix and preheat it to 40°C as indicated in Table 4.6.2.

Table 4.7.2. CIII Master mix.

Reagent	1x (µl)	[end]
KPi buffer (0.5 M) – pH 7.8	20	50 mM
EDTA (250 mM)	0.8	1 mM
Tween 20 (2%)	4	0.04%
NaN_3 (100 mM)	6	3 mM
Decylubiquinol (9.26 mM)	6.5	300 µM
Water	32.7	
Total	70	

4.7.2.10. To start the reaction, add 70 µl of the preheated CIII master mix to each well and press enter to continue reading to record the linear rate increase (ν1) at 550 nm for 5 min in 1 min intervals.

4.7.3. Calculation

Use linear rate calculations from 0 to 3 minutes (readings 1 - 4) – check R^2 values to be more than 0.99 for ν_1 .

For 200 µl reactions: ε_{550} = 4180 Abs/mM

µmol/min/mg = $(\nu_1)/4180)*0.2/(\mu l$ protein*µg/µl/1000)

nmol/min/UCS = µmol/min/mg x 1000/UCS

4.8. Cytochrome-c oxidase (complex IV)

ferrocytochrome-c:oxygen oxidoreductase, E.C. 1.9.3.1

4.8.1. Reagents

4.8.1.1. * KPi buffer, 0.5 M, pH 7.4. (See 4.5.1.1)
4.8.1.2. * Reduced cytochrome c (CytCred), 500 µM (see Section 4.2);

* Store in aliquots at -80 °C (prepare fresh every three months)

** Prepare fresh

4.8.2. Procedure

4.8.2.1. Switch on the Synergy multiplate reader, switch on the computer, and activate Gen5™ software.
4.8.2.2. Open "Protocols" and in the folder "OXPHOS diagnostiek" select the protocol for complex IV.
4.8.2.3. At the top of the window click on the temperature display and activate the temperature to preheat to 37°C.
4.8.2.4. Thaw mitochondrial samples on ice water and mix well.
4.8.2.5. Prepare CIV master mix, as indicated in Table 4.7.1, and preheat to 40°C.

Table 4.7.1. Complex IV Master mix.

Reagent	1x (µl)	[end]
KPi buffer (0.5 M) – pH 7.4	8	20 mM
Water	112	
*CytCred (500 µM)	28	70 µM
Total	148	

* Add last, just before pre-heating

4.8.2.6. Prepare a diluted buffer as follows (Table 4.7.2):

Table 4.7.2. Diluted KPi Buffer.

Reagent	1x (µl)	[end]
KPi buffer (0.5 M) – pH 7.4	4	10 mM
Water	46	
Total	50	

4.8.2.7. Place 50 µl diluted KPi buffer into each well
4.8.2.8. Add 2 µl 600g mitochondrial sample to each well.

4.8.2.9. Place plate into plate reader tray and initiate reading to incubate for 10 min, after which tray will open.

4.8.2.10. To start the reaction, add 148 µl preheated CIV master mix ([end KPi] = 30 mM) to each well and press enter to continue reading to record linear rate decrease (ν1) at 550 nm for 3 min in 30 sec intervals.

4.8.3. Calculation

Use linear rate calculations from 1 to 2 minutes (reading 2 – 5) – check R^2 values to be more than 0.99 for ν_1 .

For 200 µl reactions: ε_{550} = 4180 Abs/mM

µmol/min/mg = $(\nu_1)/4180)*0.2/(\mu l$ protein*µg/µl/1000)

nmol/min/UCS = µmol/min/mg x 1000/UCS

9. ANNEXURE C: UNTARGETTED LIPID METABOLOMICS SOP

Procedure for the methylation and silylation of bound fatty acids for GC-MS analysis

Reference number		**Revision period**	
Edition	001	**Compiled by**	Dr. Z. Lindeque
Implementation date	2017-01-01	**Previous review date**	
Review date		**pages**	6

Position	Name	Signature	Date
Director HM**	Prof. B.C. Vorster		
TIA Platform Manager	-	-	-
Newborn Screening Laboratory Manager	-	-	-
PLIEM laboratory Manager*	-	-	-
BOSS Laboratory Manager	-	-	-
Infectious Disease Metabolomics Laboratory Manager	-	-	-
Mitochondrial Laboratory Manager	-	-	-
Analytical Platform Manager	-	-	-
Building representative	-	-	-
Molecular biology Manager	-	-	-

O-acyl or glycerol-bound fatty acids (i.e. lipids) are simultaneously stripped and methylated with basic methylation. Hence, this method can be regarded as a lipid profiling method which gives information on the fatty acid chain lengths and ratios found in lipids. Important to know is that basic methylation does not methylate free fatty acids. Post-methylation silylation is performed to derivatize unmethylated compounds (such as cholesterol) to ensure cleaner samples.

Contents

List of Tables

No table of figures entries found.

List of Figures

No table of figures entries found.

List of Equations

No table of figures entries found.

1. PURPOSE

The purpose of this document is to:

- Provide detailed guidelines and procedures for the methylation and silylation of lipid-bound fatty acids before GC-MS analysis

2. SCOPE

Methylation and silylation are essential final steps in sample preparation which should be used prior to GC-MS analysis of FAMEs. This procedure then does not include upstream procedures such as metabolite extraction or lipid fractionation.

3. RESPONSIBILITY

- This procedure shall apply to analysts (staff or students) of HM working in the CHM metabolomics laboratory, who wishes to perform GC-MS analysis of FAMEs.

- It remains the responsibility of the analyst to ensure that appropriate lab safety procedures are followed with the use of hazardous derivatization material.

4. ABBREVIATIONS

- HM Human Metabolomics (include focus area and centre)
- CHM Centre for Human Metabolomics
- BSTFA O-Bis(trimethylsilyl)-trifluoro-acetamide
- TMCS Trimethylchlorosilane
- FAMEs Fatty acid methyl esters
- KOH Potassium hydroxide

5. DEFINITIONS

-

6. REFERENCES

7. MATERIALS AND EQUIPMENT

- Pyridine
- KOH
- Methanol
- Water

- Hexane
- Chloroform
- BSTFA
- TMCS
- Hamilton syringe
- Heating block
- Centrifuge capable of spinning vials at 2 000 x g
- Nitrogen drying block or speed-vac evaporator

8. METHODOLOGY

8.1 Add 100 µl methanol and 100 µl chloroform to the glass vials containing the dried extracts. Vortex properly to re-dissolve sample.

(Note: All extraction and derivatization work should be carried out in a fumehood).

8.2 Add 200 µl methanolic KOH (prepared by dissolving 280 mg KOH in 25 ml dry methanol) to each vial. Vortex sample for 30 seconds and incubate for one hour at 60 °C.

(Note: Ensure that the vials are properly capped to avoid evaporation and possible fatty acid loss).

8.3 Vortex immediate after removing the samples from the heating block and let the samples stand on the bench to reach room temperature before continuing with the next step.

(Note: The volatile short chain FAMEs can be lost if the vials are still at high temperature and pressure when opened).

8.4 Add 400 µl hexane, 200 µl water and 40 µl 1N acetic acid to extract the FAMEs. Vortex for 30 seconds.

8.5 Centrifuge vials for 2 minutes at 2000 x g.

8.6 Transfer the top-hexane phase to a clean vial

(Be careful not to transfer the lower water phase).

8.7 Add another 400 µl hexane to the remaining water phase and vortex for 30 seconds. Repeat step 8.5 – 8.6.

8.8 Dry the combined hexane phases under a gentle stream of nitrogen.

8.9 Add 50 µl pyridine and 50 µl BSTFA (containing 1 % TMCS) to dried extracts and vortex for 30 seconds.

8.10 Incubate samples for another 30 minutes at 45 °C.

8.11 Add 50 µl external standard (30 µg/ml methyl-nonadecanoate or methyl-tricosanoate) and vortex

8.11 Transfer all liquid to a flat bottom insert and put insert in the same vial used for derivatization.

8.7 The sample is now ready for GC-MS analysis. One µl is typically injected onto system.

9. SAFETY

- Any biological samples from plant, animal or human origin must be handled with caution and appropriate lab attire.
- Any (biosafety) workspace must be disinfected with 70% ethanol or isopropanol after use.
- All items that come into contact with biological samples must be disposed of in a Biohazardous Waste bin or washed accordingly when re-used.
- Handling of solvents should be done inside a fumehood or similar extraction unit.
- Cover eyes with goggles when handling corrosive chemicals.
- Dispose of needles and scalpel blades into labeled sharps container.
- Dispose of solvents into designated labeled waste container.
- Dispose of glass into designated and labeled glass waste container.

Procedure for the single-phase extraction of metabolites from mammalian cells (for targeted and untargeted metabolomic screening)

Reference number		**Revision period**	
Edition	001	**Compiled by**	Dr. Z. Lindeque
Implementation date	2017-01-01	**Previous review date**	
Review date		**pages**	10

Position	Name	Signature	Date
Director HM**	Prof. B.C. Vorster		
TIA Platform Manager	-	-	-
Newborn Screening Laboratory Manager	-	-	-
PLIEM laboratory Manager*	-	-	-
BOSS Laboratory Manager	-	-	-
Infectious Disease Metabolomics Laboratory Manager	-	-	-
Mitochondrial Laboratory Manager	-	-	-
Analytical Platform Manager	-	-	-
Building representative	-	-	-
Molecular biology Manager	-	-	-

Foreword/Notes

For tissue and cell samples, homogenization and metabolite extraction are required to get intracellular metabolites out of the cells and into a suspension of choice. This document describes a procedure for homogenizing and extracting intracellular metabolites from mammalian cell cultures using a single-phase extraction method. Polar and apolar metabolites are extracted in a single phase. This method is only recommended for cells containing relatively low amounts of apolar compounds (such as lipids) as high-lipid content will force phase separation and influence extraction efficiency. Metabolites from tissues and cells are considered the endometabolome which can provide localized information.

Contents

List of Tables

No table of figures entries found.

List of Figures

No table of figures entries found.

List of Equations

No table of figures entries found.

1. PURPOSE

The purpose of this document is to:

- Provide detailed guidelines and procedures for the homogenization and single-phase extraction of metabolites from mammalian cell culture samples.

2.. SCOPE

Intracellular metabolite extraction is an essential initial step in sample preparation which can be used prior to additional targeted metabolite extraction procedures, derivatization or untargeted analysis. This procedure then does not include downstream procedures for derivatization and analysis. This procedure is not recommended for lipid-rich tissues as the abundant lipid content will induce phase separation regardless of the solvent ratios.

2. Responsibility

- This procedure shall apply to analysts (staff or students) of HM working in the CHM metabolomics laboratory, as dictated by their downstream procedures.

- This protocol makes use of a post-analytical normalization approach using either the number of cells, protein content or Cyquant values. The choice of normalization method remains the responsibility of the analyst.

3. Abbreviations

- HM Human Metabolomics (include focus area and centre)
- CHM Centre for Human Metabolomics

4. Definitions

-

5. References
6. Materials and equipment

- Water
- Methanol
- Chloroform
- Cell Scrapers (99002, TTP)
- Safe-lock Eppendorf microcentrifuge tubes
- Sub-1 mm Ø glass beads (or powder)
- Vibration mill (or bead beater)

- Microscope (optional)
- Scepter 2.0 cell counter (optional)
- Temperature controlled centrifuge capable of spinning microcentrifuge tubes at 12 000 x g
- Nitrogen drying block or speed-vac evaporator

8. METHODOLOGY

8.1 Pre-cool solvents on ice for at least 15 minutes and methanol (quenching solution) at –80 °C for at least an hour. Two or three containers with ice might be required for this procedure where one is used to incubate the samples and solvents and the other for scraping.

8.2 Count the cells in each well or flask under a light microscope using the Scepter 2.0 automated handheld cell counter and counting grid for normalization purposes.

(Note: With uniform seeding and controlled culturing conditions, one can assume that cells in different wells, and even plates, grow at the same tempo and reach the same % confluency when cultured together. Hence, this step can be omitted when the intervention tested does not influence cell growth significantly).

8.3 Remove culture media from the flasks or wells and put plate on ice to limit metabolic activity.

(Note: Make sure that little or no media remains before further processing. The used media can be collected for analysis to study the exometabolome. Sample preparation procedure for media is the same as for other biofluids).

8.4 Add 1 ml -80 °C cold methanol to each culturing well or flask while on ice.

8.5 Scrape cells from the wells or flask using a cell scraper and transfer the entire solution to a clean Safe-lock Eppendorf microcentrifuge tube.

(Note: Trypsinization of cells is not recommended as it can influence the metabolome).

8.6 Add internal standard solution and water to attain a final volume of 330 µl water. If the internal standards are dissolved in water, then use equation 1 to determine the volume of water to be added. The concentration of the internal standards should not exceed 0.5 µg/1 million cells (equivalent to 1 well of a 6-well plate). The addition of 50 µl internal standard solution with concentration of 100 µg/ml will result in a 25 µg/ml final concentration before analysis.

Volume (µl) water required = 330 µl – volume of internal standard solution (Eq. 1)

(Note: The addition of chloroform at this stage will stiffen the cells and hamper homogenization)

8.7 Add a pellet size amount of glass beads to each tube. Use a spatula or back end of yellow tip to transfer glass beads from container to tube.

8.8 Ensure that all tube caps are properly closed before samples are loaded onto the vibration mill. Shake the samples for 2 minutes at 30 Hz.

8.9 Take a sample (about 100 µl) from the homogenate for protein determination or Cyquant analysis for normalization purposes. The volume of sample is dictated by the method of choice (so see respective SOPs).

8.10 Add 330 µl chloroform and vortex samples for 30 seconds. Leave on ice for 10 minutes.

8.11 Centrifuge samples for 5 minutes at 2 000 x g, 4 °C to pellet proteins, cell debris and glass beads.

8.12 Carefully transfer the supernatant to clean glass vial or microcentrifuge tube as required by downstream procedures and methods.

8.13 Dry sample under nitrogen or vacuum.

8.14 Once dried, the samples can be stored at -80 °C for a limited period or used immediately in downstream procedures.

9. SAFETY

- Any cell culture samples must be handled with caution and appropriate lab attire.
- Any (biosafety) workspace must be disinfected with 70% ethanol or isopropanol after use.
- All items that come into contact with biological samples must be disposed of in a Biohazardous Waste bin or washed appropriately when re-used.
- Handling of solvents should be done inside a fumehood or similar extraction unit.
- Cover eyes with goggles when handling corrosive chemicals.
- Dispose of solvents into designated labeled waste container.
- Dispose of glass into designated and labeled glass waste container.